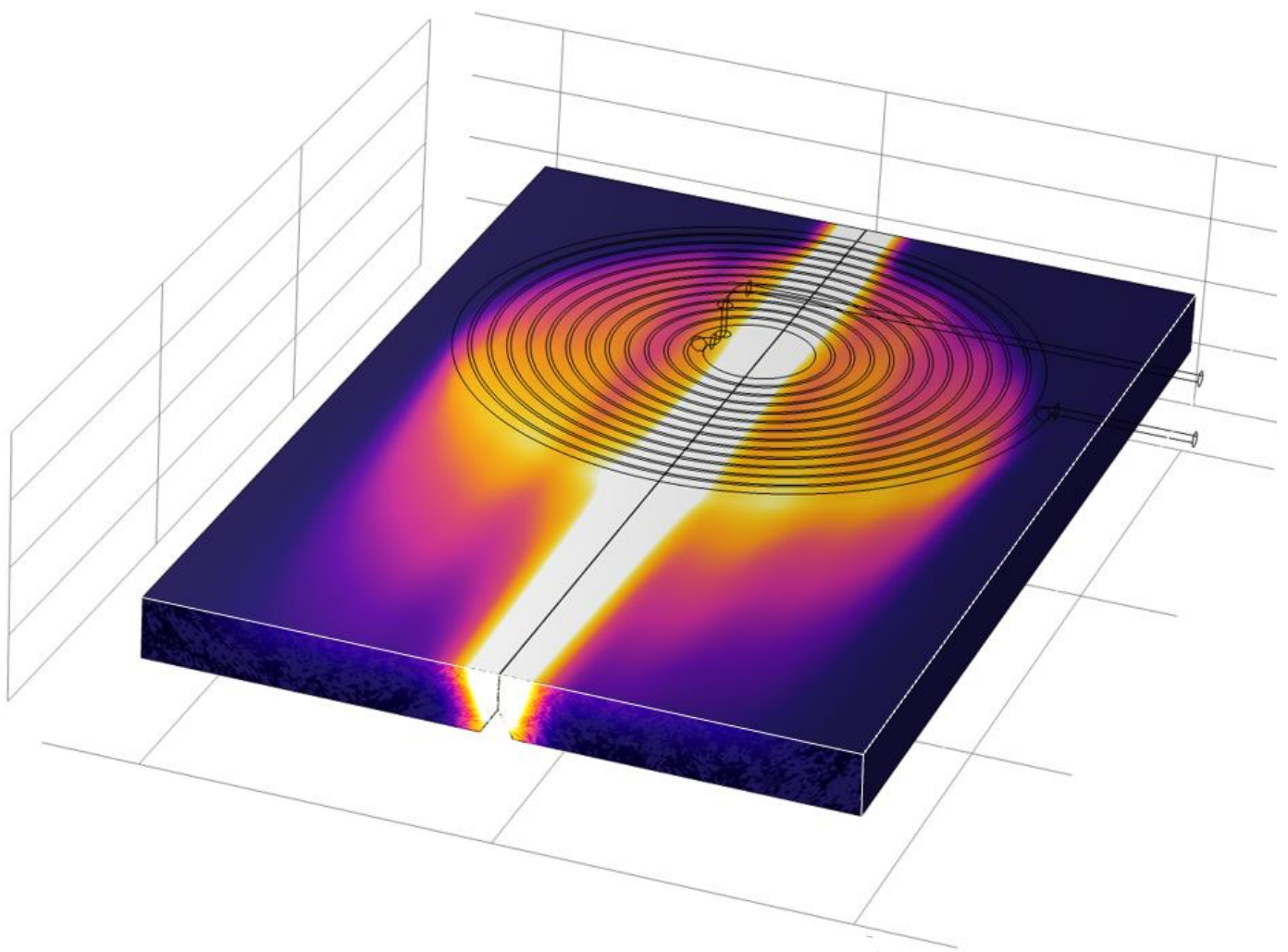


Energy Consumption of Preheating Methods for Thick Section Welds





Materials and Production

Aalborg University

<http://www.aau.dk>

AALBORG UNIVERSITY

STUDENT REPORT

Title:

Energy Consumption of Preheating Methods for Thick Section Welds

Theme:

Procesanalyse og -styring

Project Period:

September 2021 - December 2021

Project Group:

2.024

Participants:

Amran Mahboub
Andreas Hesseldahl Føns
Mads Holm Andersen
Morten Bach
Terkel Føns Dyring
Viktor Bull Kramer

Supervisors:

Christian Buhl Sørensen
Morten Kristiansen

Copies: Online**Page Numbers:** 109**Date of Completion:**

D. 21. December 2021

Abstract:

A significant amount of energy waste and CO₂e is generated by preheating large section welds with gas. It is well established that heating with induction is generally more energy efficient than heating with gas. This study aims to model, using Finite Element Method, how effective inductive heating is on large section welds and compare the energy, CO₂ and price with an already existing solution of using gas. To test the hypothesis that preheating large section welds is also more efficient than gas, experiments were made at Bladt Industries A/S to help calibrate the model in COM-SOL Multiphysics. In these experiments, variables such as distance from coil to steel plate, gap distance between the steel plates, and coil turns were tested and used to validate the model. These validations helped setup a new model that shows how the temperature in the steel plates rises, as they rotate before an induction coil and thereby simulating induction preheating of a circular weld. The final model estimates that it is possible to preheat a circular weld about 37% quicker than using gas. Induction heating has an energy consumption 13 times lower than gas and emits 26 times less CO₂e.

The content of this report is freely available, but publication (with reference) may only be pursued due to agreement with the authors.

Nomenclature

Symbol	Description	Unit
Greek letters		
γ	Density	$\frac{\text{kg}}{\text{m}^3}$
δ	Penetration depth	m
μ	Magnetic permeability	$\frac{\text{H}}{\text{m}}$
μ_r	Nondimensional parameter that indicates the materials ability to conduct the magnetic field better than a vacuum	-
ρ_{coil}	Electric resistivity	$\text{m}\Omega$
ρ_{charge}	Electric charge density	$\frac{\text{C}}{\text{m}^3}$
σ	Electrical conductivity	$\frac{\text{S}}{\text{m}}$
Physics constants		
ϵ_0	Permittivity of free space	$8.854 \cdot 10^{-12} \frac{\text{s}^4 \text{A}^2}{\text{kg m}^3}$
σ_s	Stefan Boltzmann's constant	$5.6696 \cdot 10^{-8} \frac{\text{W}}{\text{m}^2 \text{K}^4}$
μ_0	Permeability of free space	$4\pi \cdot 10^{-7} \frac{\text{H}}{\text{m}}$
Terms		
A	Cross-sectional area of material	m^2
B	Magnetic field	$T = \frac{N}{A \text{m}}$
c	Specific heat	$\frac{\text{J}}{\text{kg} \cdot ^\circ\text{C}}$
e	Emissivity of object	-
f	Frequency	Hz
h	Convective heat coefficient	$\frac{\text{W}}{\text{m}^2 \text{K}}$
H	Magnetic field intensity	A/m
I	Amperage	A
I_{enc}	Current enclosed by the Amperian loop	A
J	Joule	-
k	Thermal conductivity specific to material	$\frac{\text{W}}{\text{m K}}$
l	Length of magnetic circuit	m
m	mass	kg
N	Number of turns in a coil	-

P	Heat transfer rate	W
q	Charge	$C = As$
Q	Thermal energy	J
t	Time	s
ΔT	Change in temperature	K

Vectors

\mathbf{B}	Magnetic field vector	$T = \frac{N}{Am}$
\mathbf{E}	Electric field vector	$\frac{V}{m}$
\mathbf{J}	Electric current density	$\frac{A}{m^2}$

Integrals

\oint_L	Line integral of the closed curve L
$\iint = \int_A$	Area integral of the area A
$\oint\!\iint = \oint_A$	Area integral of the closed area A
$\iiint = \int_V$	Volume integral of the volume V

Abbreviations

1D	One-dimensional
2D	Two-dimensional
3D	Three-dimensional
AC	Alternating current
ATM	Atmospheric pressure
Avg.	Average
CE	Carbon equivalent
CO ₂ e	CO ₂ -equivalent
DKK	Danish kroner (currency)
FEM	Finite Element Method
SI	International System of Units
T _{max}	Highest temperature within observed area
Temp.	Temperature

Preface

This semester project is submitted to the faculty of Engineering and Science at the institute of Materials and Production at Aalborg University. The purpose of this project was to develop a model capable of simulating preheating of thick steel plates using induction and to compare the energy consumption to traditional preheating methods. The approach to this problem was to conduct experiments by heating two steel plates, arranged to mimic a welding situation. These experiments were used to calibrate and validate the model for the simulation. The project is written in cooperation with Bladt Industries A/S. The motivation of this cooperation is to decrease emissions of their monopile construction process, by finding a replacement for preheating using gas.

Acknowledgements

The experiments in this project were made possible by Bladt Industries A/S - special thanks to Nis Hansen, Responsible Welding Engineer at Bladt. Bladt has been helpful in conducting experiments and answering questions regarding preheating and the general workflow of the process. Especially Christian and the welders have been very helpful with the setup of experiments and quick-fixes during the experiments. In addition, we would like to thank Flemming Andersen for helping us during the experiments.

Table of Contents

Title Page	II
Nomenclature	III
Preface	V
Acknowledgements	V
1 Introduction	1
1.1 Preheating	4
1.2 Summary	4
2 Problem Analysis	5
2.1 Weld Cracks	5
2.2 Preheating Methods	6
2.3 Summary	10
2.4 Statement of Intent	10
3 Scope	11
4 Theory	12
4.1 Thermodynamics	12
4.2 Induction Heating	14
4.3 Modeling of the Electromagnetic Field	19
4.4 Finite Element Method	24
5 Methods and Results	27
5.1 Test of Theory - Experiment	27
5.2 Test of Theory - Simulations	38
5.3 Validation of Model	44
5.4 Simulation of a Preheating Situation	52
6 Discussion	62
6.1 Expectations and Results	62
6.2 Methods	65
6.3 Implementation of Model	68
7 Conclusion	70
8 Further Perspectives	72
8.1 Experiments and Models	72
8.2 Applications	73
9 Project Management	74
Bibliography	79
Appendix	

A Meeting with Bladt 15-09-2021	84
B Experiment	85
B.1 Purpose of Experiment	85
B.2 Approach	85
B.3 Equipment	85
C Experiments at Bladt	87
D Ratio - from pixels to mm during experiments	95
E Results	96
F Test of Thermal Camera	97
G Progress of Simulations	98
G.1 Introduction to COMSOL	98
G.2 Simple Heat Source Model	98
G.3 Early Induction Heating Model	98
G.4 Material Properties and Frequency Transient	99
G.5 Validation of Model	100
G.6 Circular Weld	100
H Geometry	101
I Application of EN-1011-2	105
J Maximum Temperature Under Coil	107
K Figure 5.32 Full Size	109

1. Introduction

Meeting renewable energy goals has been a high priority globally, as it is evident that electricity generated from coal and gas is unsustainable. Despite the impressive gains in renewable energy, global CO₂ emissions from energy production still reached a historic high in 2019 due to a rise in the use of coal in the energy sector [1]. Increasing pledges to scale down carbon pollution indicate that there is a shift - the global offshore wind sector is growing at a rapid pace. It grew almost 30% per year from 2010 and 2018 where it benefited from improvements in technology associated with building offshore wind farms [2]. The growth seems to continue as it is expected to grow by 7.3 GW from 34.37 GW in 2021 and further 8.8 GW in 2022 [3] this is illustrated in figure 1.1. In the long term, offshore wind energy is expected to have the biggest share of the the electricity generated in the European Union by 2040 [4].

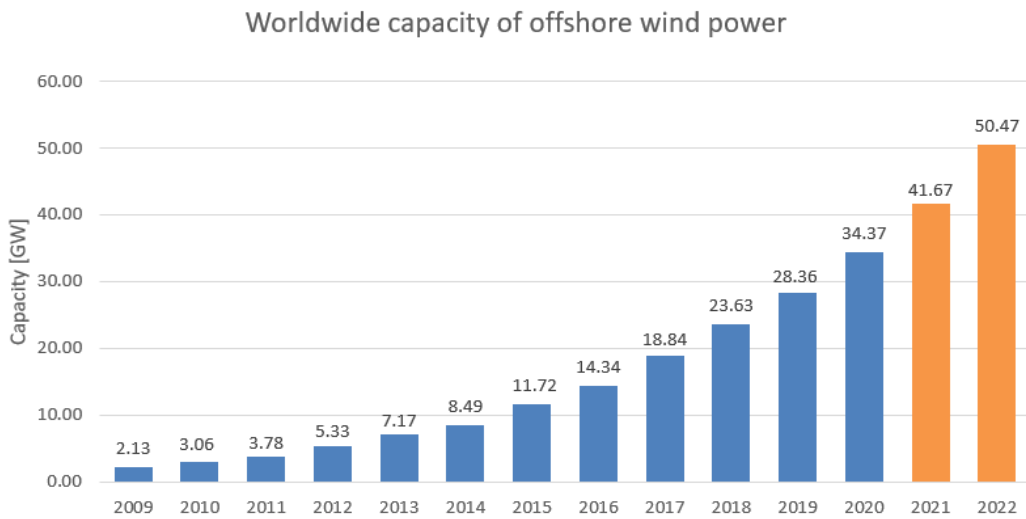


Figure 1.1: Global offshore wind energy capacity from 2009 to 2022. Blue is historic data and orange is the expected values [3][5].

From an economical point of view, the levelised cost of energy, which is a measure of the average net present cost of electricity generated by an energy plant over its lifetime, is more than twice as high for offshore than onshore wind farms [6]. This is partly due to more development and infrastructure being needed for offshore wind farms. The offshore wind farms face a far more difficult and uncertain environment than onshore wind farms. This leads to a high cost of the foundations, as they are designed to withstand the harsh conditions. The foundation accounts for 20-25% of the capital cost, see figure 1.2 [2].

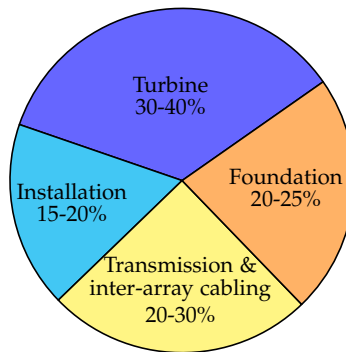


Figure 1.2: Percentage of capital cost.

One way to reduce the cost of the foundations is to minimise the production cost of the large steel segments used for building offshore monopiles. A major part of the offshore monopile construction is the welding of large steel geometries. Metal industries use large amounts of energy when joining these geometries. With increasing environmental concerns, companies aim to become more carbon neutral, which makes them more attractive contractors to their clients. This project therefore aims to study the efficiency and environmental impact of the production.

1.0.1 Bladt Industries A/S

This project and its experiments are performed in cooperation with Bladt Industries A/S. Bladt Industries is a Danish steel contractor specialising in large and complex steel structures for several international markets. One of those is the renewable energy sector, especially the offshore wind industry. Despite the renewable energy sector's relatively new global relevance in the last decades, Bladt Industries's experience in the steel industry dates back to 1965 [7].



Figure 1.3: Wind turbines installed on individual monopiles and transition pieces produced by Bladt Industries. Samsø, Denmark [8].

A major issue when installing large commercial wind turbines offshore, is to provide a sturdy foundation, when anchoring the turbines to the sea floor, such foundations can be seen on figure 1.3. A commonly used method for this, is to set up each turbine on individual steel monopiles¹. The manufacturing process of these large monopiles will be the main focus in this project, as it is one of Bladt Industries's main areas of business.

1.0.2 Manufacturing of Large Monopiles

The monopiles are produced from large plates of steel, the size of the plates are limited to 3 by 12 metres with a thickness of 60 mm to 130 mm. Therefore the plates are combined into appropriate sizes. This process roughly consists of preheating the welding areas, then welding on one side. When the first side is welded, the steel plate is turned and there is milled into the first weld and welded on the other side. The welded plates are rolled into shape and once again preheated and welded to form cylindrical sections. These sections are joined to form monopiles as is shown on figure 1.4. This manufacturing process is illustrated in figure 1.5.



Figure 1.4: A monopile: Hollow cylindrical metal segments assembled with large section welds. The welds can be seen as the white stripes on the monopile [8].

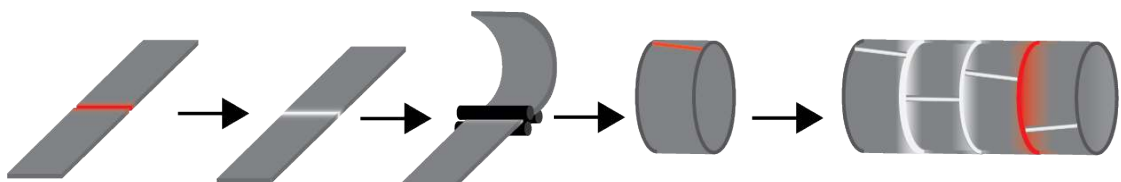


Figure 1.5: Manufacturing process of large monopiles. The red lines illustrates welds and the white lines illustrates finished welds.

¹Monopile: Steel foundation used when anchoring individual wind turbines to the sea floor. Coupled to the turbine tower using a transition piece. The largest monopiles reach bottom diameters between 8 and 13 metres, lengths of up to 120 metres and wall thicknesses up to 150 millimetres. The final weight of such monopiles can reach up to 2,400 tonnes, see figure 1.4 [9].

1.1 Preheating

Of the above steps in the manufacturing of monopiles, the focus in this project will be on the preheating before welding. It is essential to conduct preheating prior to welding to prevent cracks in the welding process [10]. The process of preheating is energy consuming and creates a hot work environment for the welders. Preheating is generally conducted with gas burners and the heat is controlled simply by turning the torches up or down. This will be further explained in chapter 2.

1.2 Summary

This introduction and the cooperation with Bladt Industries leads to the following question to be further analysed:

How can Bladt Industries and other steel contractors make preheating of their welds more energy efficient?

To analyse this, different preheating methods will be reviewed and compared in terms of energy consumption, CO₂e emissions and cost.

2. Problem Analysis

In the analysis, problems with weld cracks, specifically cold cracks, and how they occur will be highlighted. A way to avoid cold cracks is to preheat the steel plates. Some of these preheating methods will be illustrated and explained. Induction heating, which is the preheating method this report focuses on, will be highlighted last before a statement of intent is introduced.

2.1 Weld Cracks

Various types of cracking can occur in welds, but all cracks reduce the strength of the welds and are unwanted. Some cracks are subject to the quality of the weld, however these cracks do not occur in a substantial amount at Bladt Industries. At Bladt Industries, the main focus is now on reducing the occurrence of hydrogen cracks, which is also referred to as cold cracks as they often happen when the metal has cooled to near room temperature. Hydrogen cracks occur due to hydrogen in the material or near proximity to the welded materials, known as the heat affected zone. Hydrogen cracks occur if the steel is rapidly cooled. If the steel is preheated or cooled slowly, hydrogen is allowed to leave the steel, and is thereby not liable to cause cold cracks [11]. An example of a hydrogen crack is illustrated on figure 2.1 where a hydrogen pocket has formed near the weld.

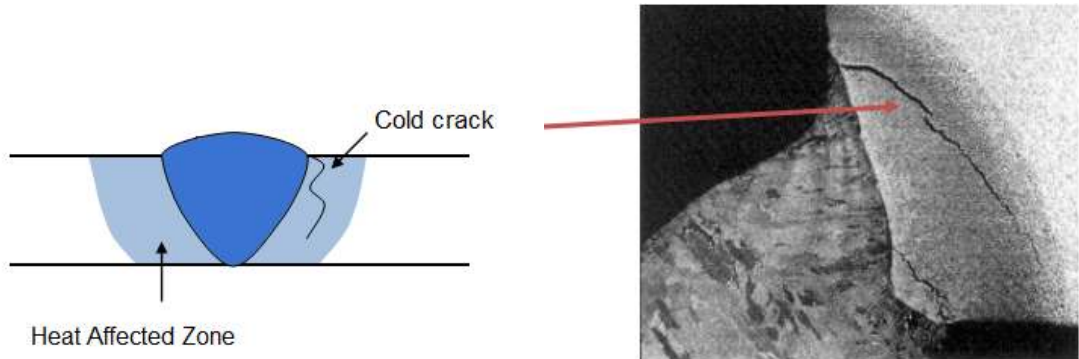


Figure 2.1: Cold cracks in the heat affected zone [11].

In the welding industry a standard (EN-1011-2) is used to prevent hydrogen cracks [12]. This standard uses the carbon equivalent (CE) value of the steel, the dimensions of the welded steel plate, and the hydrogen class of the welding method. The standard uses these values to determine a sufficient preheating temperature. Further explanation and application of EN-1011-2 can be found in appendix I. Example: Two steel plates with a thickness of 90 mm each with a carbon equivalent of 0.65, are welded together using submerged arc welding with EM12K flux and a diffusible hydrogen content of 3-5 ml. In this case, it

is classified as class D, which can be used to determine the preheating temperature when the input of the welder is known [13].

One of the main issues with hydrogen cracks is that they are detected after the final weld has been applied, with ultra sound examination. If hydrogen cracks are detected, the weld needs to be milled and redone. This extra process delays the manufacturing and adds to the total costs, therefore hydrogen cracks are unwanted in the welds, thus preheating is applied.

2.2 Preheating Methods

Preheating is a method to prevent cold cracks. Preheating a material such as steel can be done in several different ways. Heating blankets, gas and induction heating are some of the most common ways to preheat a steel part before a welding process [14]. In order to get a better understanding of the different problems surrounding various preheating methods, this section will make a comparison between three different methods. The different subsections compare the differences in energy consumption, their environmental impact, and an assessment of their cost, as well as providing a basic understanding of the different technologies.

2.2.1 Heating Blankets

Heating blankets is a technology primarily used in stationary preheating of short and flat welds. The technology uses direct resistance heating to heat up the blankets. Direct resistance heating, also know as Joule heating, is based on the flow of electrical current through a high resistance body [15]. In practice, the heated body is the blanket that lies directly on the steel. Above the blanket is thermal insulation that insures that most of the heat gets transferred to the steel below. The blanket is held tight to the steel with magnets. This is illustrated in figure 2.2, where several blankets are connected.

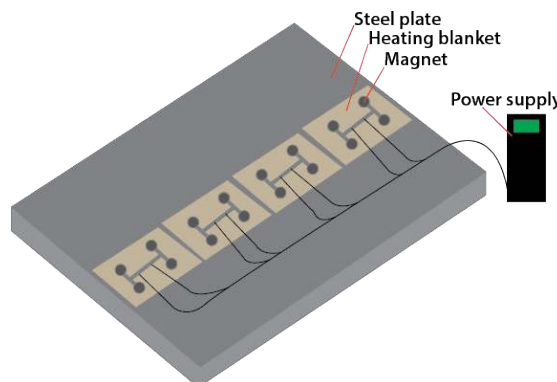


Figure 2.2: Heating blankets on a steel plate.

The power of each heating blanket used by Bladt Industries is 2.7 kW. For the heating of the stationary segment, several blankets are used for 2 hours as described in appendix A. The blankets have a length of one metre. The energy used to heat a metre can therefore be calculated:

$$\frac{2.7 \text{ kW} \cdot 2 \text{ h}}{1 \text{ m}} = 5.4 \frac{\text{kWh}}{\text{m}} \quad (2.1)$$

Knowing each heating blanket consumes 2.7 kW of power over 2 hours, the energy consumption and environmental impact of this preheating method can be estimated to 5.4 kWh per heating blanket. Producing one kWh of electricity in Denmark in 2020 emitted an average of 0.125 kg CO₂e, which includes the conversion of other green house gasses to the amount of CO₂ with an equivalent environmental impact [16]. The amount of CO₂e emitted per metre heated steel section can with these values be calculated as:

$$5.4 \frac{\text{kWh}}{\text{m}} \cdot 0.125 \frac{\text{kg CO}_2\text{e}}{\text{kWh}} = 0.675 \frac{\text{kg CO}_2\text{e}}{\text{m}} \quad (2.2)$$

In terms of costs, the price for heating one metre of material using heat blankets can be calculated as the product of the energy consumption and the average price per kWh:

$$5.4 \frac{\text{kWh}}{\text{m}} \cdot 1.08 \frac{\text{DKK}}{\text{kWh}} = 5.83 \frac{\text{DKK}}{\text{m}} \quad (2.3)$$

The cost of using heating blankets is estimated as 5.83 DKK per metre.

2.2.2 Gas

Gas is a more traditional method of preheating. The advantages and the reason that it is still used is the simplicity, flexibility and reliability of the technology. Unlike heating blankets, gas can be used to preheat objects in motion since direct contact is not needed. This makes it possible to preheat simultaneously with the welding to save time. The technology is illustrated in figure 2.3.

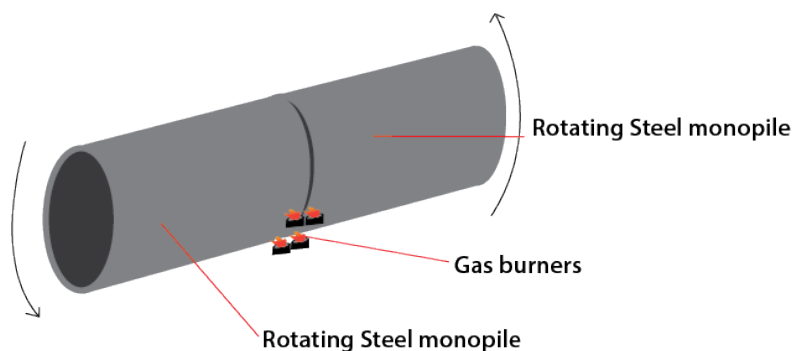


Figure 2.3: Preheating using gas on a monopile.

A commonly used gas for this preheating method is natural gas which has an CO₂e emission of 242.65 $\frac{\text{g CO}_2\text{e}}{\text{kWh}}$ [17]. When burning natural gas, CO₂ is not

the only greenhouse gas emitted. Another significant pollutant is methane gas which make up 60-90% of natural gas [18]. Burning gas also heats up a lot of the surrounding area making the workplace more uncomfortable for the workers. Lastly, the large gas tanks is a potential fire hazard.

It is difficult to control the amount of energy used due to the many variables affecting preheating such as wind, air temperature and humidity. Bladt Industries uses a system of 4 gas burners that each uses 8 kilograms per hour. Gas from Station Aalborg has an energy content of $11.280 \frac{\text{kWh}}{\text{m}^3}$ and a density of $0.746 \frac{\text{kg}}{\text{m}^3}$ [19]. This preheating takes about 2 hours - followed by some additional heating during welding [20]. The total volume of gas used to preheat a circular weld can therefore be calculated to:

$$4 \cdot 8 \frac{\text{kg}}{\text{h}} \cdot 2 \text{ h} \cdot \left(0.746 \frac{\text{kg}}{\text{m}^3} \right)^{-1} = 86 \text{ m}^3 \quad (2.4)$$

This equates to the following energy consumption per metre:

$$\frac{86 \text{ m}^3 \cdot 11.280 \frac{\text{kWh}}{\text{m}^3}}{8\pi \cdot \text{m}} = 38.5 \frac{\text{kWh}}{\text{m}} \quad (2.5)$$

The CO₂e emission per metre around the circumference of the segment is:

$$38.5 \frac{\text{kWh}}{\text{m}} \cdot 0.243 \frac{\text{kg CO}_2\text{e}}{\text{kWh}} = 9.36 \frac{\text{kg CO}_2\text{e}}{\text{m}} \quad (2.6)$$

The cost of heating with gas per metre depends on the circumference of the monopile as well as the price for gas. In the previous calculations the diameter is set to 8 metres.

From April 2017 to October 2021 the prices per m³ gas varied from 0.87 DKK to 8.18 DKK [21]. According to Bladt, a fair indication of their total cost of gas, is to use a gas price of 5 DKK per m³ of natural gas [20]:

$$\frac{86 \text{ m}^3}{8\pi \cdot \text{m}} \cdot 5 \frac{\text{DKK}}{\text{m}^3} = 17.07 \frac{\text{DKK}}{\text{m}} \quad (2.7)$$

These calculations for both the heating blankets and the gas are only relevant for a steel plate with a thickness of 90 mm.

2.2.3 Induction

Induction heating is a method of preheating that is not widely used in the welding industry today. The technology makes use of an AC magnetic field generated by a coil (often copper) to induce current in an electrically conductive object such as a steel plate [15]. An illustration of this technology can be seen in figure 2.4.

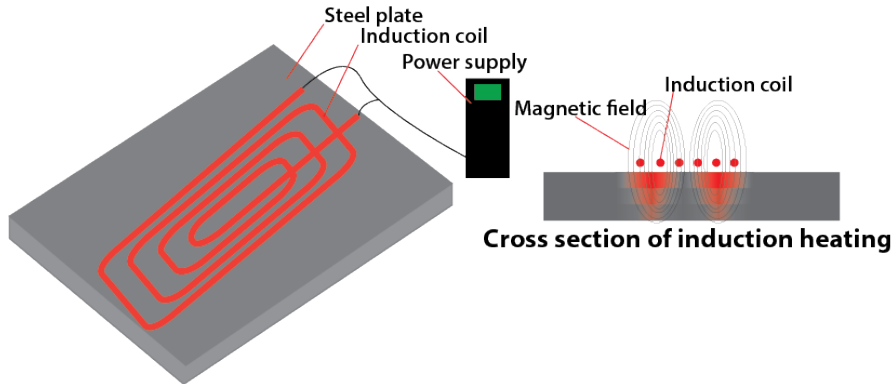


Figure 2.4: Induction coil heating a steel plate.

Due to the above, the coil does not need to be in direct contact with the steel. This means that it has the potential to replace gas as a preheating method, since the object does not need to be stationary. Provided that the AC power is generated from renewable energy, an induction coil would reduce the overall CO₂e emissions compared to gas heating, as it is not burning fossil fuel to heat up the object. Bladt Industries has conducted an experiment using a 35 kW AC power supply running at 13.7 kHz through an induction cable by Miller¹, but this has not led to an implementation of the technology in the manufacturing of monopiles [23].

There are a number of reasons that this technology is not more used in the industry of large steel construction today². Mostly it has to do with the lack of experience with the technology which causes unacceptable inconsistencies in the preheating. The lack of experience with the technology also leads to a lack of an economical strategy for implementing the technology. These problems were described by Bladt Industries in the initial meeting with them as described in appendix A. To get a better understanding of the technology and how it can be implemented, a model needs to be developed. This model should express how the heat spreads through the steel and how much energy the induction consumes. This could make it possible to make a guideline for using the induction preheating method and make a more accurate estimate of the cost of using the technology.

¹Miller is a manufacturer of arc welding products, including products capable of preheating metals prior to welding [22].

²Miller's product is mostly used as a preheating method for smaller constructions.

2.3 Summary

Preheating is essential to prevent process- and quality errors like hydrogen cracks when welding large plates. There are several different methods used for preheating. One is electric heating blankets which suffer from the disadvantage of having to be in direct contact with the heated object. In the case of Bladt Industries, the objects are large, cylindrical and in rotational motion, which is why they utilise gas burners instead of heating blankets. When preheating using gas burners, the process consumes large amounts of energy, which is only delivered to the surface of the steel plates and to the surrounding environment. It is therefore relevant to study whether gas can be replaced with induction. Induction could potentially lower production time, cost and CO₂e emissions. To examine these possibilities of induction heating, it is useful to set up a model. An optimisation process is possible with such a model. Finally, the optimised setup will allow for both an economical and environmental comparison between different heating methods.

2.4 Statement of Intent

In order to fully understand induction heating and develop its applications in regards to preheating, it is necessary to develop a model of induction heating in steel plates. The problem is well suited for finite element method (FEM) modelling using COMSOL Multiphysics, as it can be formulated without phase transitions and nonlinear effects. The statement of intent in this study is therefore:

How is an FEM-model set up in COMSOL Multiphysics, which accurately simulates induction heating of steel plates with thick section weld geometries?

- *How can the model be used to compare the energy efficiencies of induction heating, gas heating, and resistance heating?*
- *How is the model best validated by experiments?*
- *How can the model be modified to fit the preheating process of a rotating monopile section?*
- *How can this model be used to make a suggestion to set up an induction preheating method for Bladt Industries?*

3. Scope

The scope of the project is to develop a model that enables a comparison of the energy consumption of different preheating methods, and therefore a finished solution for Bladt Industries to implement the technology in their production will not be devised. During the next step in the production process (the welding), the metal needs to be maintained at a correct temperature. Today, this is done by adjusting the gas burners. This can also be done with an induction heater. Despite this, this study will focus only on the preheating process prior to welding.

The final model is used on two flat plates moving continuously to simulate the rotation of the monopile, instead of simulating the entire monopile. This means that the geometry of the steel plate will differ from reality, since it is not slightly curved like the monopile. The model will replicate the preheating process prior to the welding of the inside of the monopile and not the heating during the welding. The simulation will be using the weld gap geometry provided by Bladt.

To validate the legitimacy of the model, an experiment will be conducted. Performing an induction heating experiment on a monopile pipe section will require many resources. The experiment is instead done on a flat, thinner steel plate. The assumption is that an FEM model, which is accurate on the flat and thinner plate, can be scaled up to the size and geometry of a monopile section and still be accurate.

There are three variables in the experiment: gap distance between the plates, number of turns in the coil and the distance between the coil and the steel plates. These variables will be adjusted in the experiment. Additional variables would lead to more iterations of the experiment. This is not possible due to the time constraints of the project, as well as being unnecessary to validate the accuracy of the model. The induction heating power supply did not allow manual control of parameters such as the power, current, and frequency, as these were automatically set according to how much of the induction cable was in close contact with the steel plates.

4. Theory

To better understand the physics of induction preheating of a thick section welding geometry, an understanding of several formulas and principles of physics is necessary. The physics that will be presented in this chapter are thermodynamics, electromagnetism and induction. This is to examine how heat transfers inside steel and into the surrounding air, how the magnetic field generated by the coil can be described and what formulas are used to calculate the energy transfer in induction. This chapter also examines how the FEM used in COMSOL Multiphysics is utilised to simulate induction heating.

4.1 Thermodynamics

4.1.1 Heat Capacity

The heat capacity of a material is measure of how much energy it takes to heat a 1 kilogram of material 1 °C. The heat capacity has the symbol Q and is measured in joules. A material with a low heat capacity can hold less energy than a material with a relatively high heat capacity. The heat capacity given by:

$$Q = m c \Delta T \quad (4.1)$$

Where m is the mass of the object, c is the specific heat capacity of the material measured in $\frac{\text{J}}{\text{kg}^\circ\text{C}}$ and ΔT is the change in temperature. For steel S235 the specific heat capacity is $470 \frac{\text{J}}{\text{kg}^\circ\text{C}}$ at 1 atm and 20 °C [24]. The specific heat capacity is temperature dependent, the higher temperature the more energy it takes to raise the temperature a given ΔT . In the FEM model the heat capacity is kept at a constant to minimise computation time.

4.1.2 Heat Transfer

Heat transfer describes different mechanisms of transferring heat. These different mechanisms needs to be taken into account when setting up boundary conditions in COMSOL Multiphysics.

The transfer of heat happens when there is a temperature difference in a system. The three basic principles of heat transfer is conduction, convection and radiation. These three methods will be described in the sections below.

Heat transfer rate is commonly represented by the letter P . It refers to the quantity of thermal energy transferred from one object to another - or simply through one medium. The unit for thermal energy transferred per unit of time is watt. It is a measure of energy per unit time.

When FEM software is simulating heat transfer it is calculated with heat flux, which is the measure of energy per unit time per area.

Conduction

Thermal conduction describes the transfer of heat energy through solids. Heat transfer through conduction is, on an atomic scale, an exchange of kinetic energy between microscopic particles, such as molecules, atoms and free electrons. Here the particles with lower energy gains energy by colliding with other particles with greater energy. If the end of a metal rod is inserted in a heat source, the other end will also slowly heat up, as the particles near the heat source will vibrate around their equilibrium point and start to collide with neighbouring particles and thereby transfer some of their energy in the collisions. This will slowly make the amplitudes of the atoms and electrons farther from the heat source increase and therefore raise the temperature in the other end of the rod as well.

Material properties of the heated substance have an influence on the rate of thermal conduction. This property is called thermal conductivity. Metals hold a large numbers of electrons that are relatively free to move and are therefore able to carry energy over large distances. This property makes them good thermal conductors, whereas gases, asbestos, and glass are poor conductors as the distance between the particles are greater. Conduction occurs if there is a temperature difference between two materials in contact or between two parts of one subject. The heat transfer rate, P , is proportional to the temperature difference ΔT and inversely to the thickness Δx . The law of thermal conduction is therefore:

$$P = k A \frac{\Delta T}{\Delta x} \quad (4.2)$$

Where the constant k is thermal conductivity and is specified by the material. A is the cross-sectional area of the observed material [25].

Convection

Heat transfer by convection is the transfer of heat between two bodies by currents of moving gas or fluid. When air is heated and travels away from the heating source, it carries thermal energy. The molecules expand when they are introduced to thermal energy. When the temperature of the fluid (air) increases, the volume expands by the same factor. This will cause a displacement in the fluid, as the hot air rises, the colder and therefore denser air is pushed downwards. This cold air is then heated and will also expand as the temperature is increased. This series of events represent convection currents. It is important to note that when convection occurs, there is a transfer of both energy and matter. There are two types of convection heat transfer. The first is

called free or natural convection. Natural convection is when the heat transfer results from differences in density within a fluid. The other is called forced convection. This when a heated substance is moved by force for example a pump or a fan [25]. Newtons law of cooling is a basic equation for convection heat transfer:

$$P = h A \Delta T \quad (4.3)$$

Where P is convective heat transfer rate, h is the convective heat coefficient with units $\frac{W}{m^2 K}$, A is surface area of the heated subject [26].

Radiation

Heat transfer by radiation is heat transferred by electromagnetic waves. The amount of energy transferred by radiation depends on three constants, the emissivity (e) of the object, the surface area (A) and Stefan Boltzmann's constant $\sigma_s = 5.6696 \cdot 10^{-8} \frac{W}{m^2 K^4}$. It is proportional with the difference in temperature of the object and its surroundings raised to the power of four [25].

$$P = \sigma A e (\Delta T)^4 \quad (4.4)$$

The emissivity of an object is a dimensionless value varying from 0 to 1. 1 meaning the object is able to absorb all energy radiated towards it, also known as a perfect black body. Steel typically has an emissivity of 0.8, but strongly depend on the surface finish. If highly-polished to a reflective surface, it can have an emissivity as low as 0.07 [27].

4.2 Induction Heating

Induction heating works by placing an electrically conducting material within a magnetic field generated by applying AC through a coil. The material tries to oppose the magnetic field, by producing an electric current, which opposes the electric current applied in the coil. This phenomenon is known as Lenz's law that states, that an induced electric current flows in a direction such that the current opposes the change that induced it [28]. These internal currents in the material are called eddy currents and can be seen in figure 4.1. When these currents pass through the material, the material's resistance causes a voltage drop. This voltage drop causes electrical energy to convert to thermal energy, generating heat in a process called Joule heating [29]. Joule heating is the sole heating mechanism in non-magnetic materials. In ferromagnetic materials, another type of heat generation is hysteresis losses. Small magnetic dipoles in the material turn with every reversal of the magnetic field. The energy required to turn the dipoles is dissipated as heat [29]. Understanding of induction has a relevance when defining different material properties and understanding the necessary boundary conditions when simulating induction.

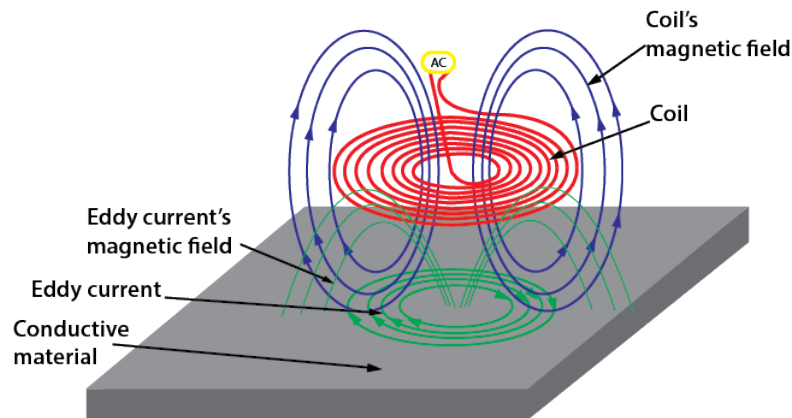


Figure 4.1: Eddy currents induced in a conductive material with a pancake (flat) coil.

4.2.1 Magnetic Field Intensity

The intensity of a magnetic field can be used to describe the strength of the magnetic field generated by a flat circular coil (sometimes called a pancake coil). It is described with the SI-Unit $\frac{A}{m}$. This means that a flat circular coil of 1 turn with a diameter of 1 metre carrying a current of 1 ampere has a magnetic field intensity of $1 \frac{A}{m}$ [30].

The magnetic field intensity (H) can be calculated as:

$$H = \frac{NI}{l} \quad (4.5)$$

Where N is the number of turns in the coil, I is the current, and l is the length of the magnetic circuit in metres. This equation therefore states that the magnetic field intensity H increases when increasing the number of turns in a coil N or when increasing the current I . This equation is intended to be used on a helical coil, but is assumed to be similar for a pancake coil[31].

4.2.2 Magnetic Permeability and Relative Permeability

Relative permeability written as μ_r is a nondimensional parameter that indicates the material's ability to conduct the magnetic field better than a vacuum. The permeability of a vacuum is written as μ_0 and is a constant with a value of $4\pi \cdot 10^{-7} \frac{H}{m}$. The product of these two are called magnetic permeability and is written as [30]:

$$\mu = \mu_r \mu_0 \quad (4.6)$$

All materials can be divided into three categories based on their relative permeability: paramagnetic, diamagnetic and ferromagnetic. Diamagnetic materials have a relative permeability less than 1 ($\mu_r < 1$). Paramagnetic materials have a relative permeability slightly greater than 1 ($\mu_r > 1$). When working with

induction heating both dia- and paramagnetic materials are classified as non-magnetic materials, such as aluminium, titanium and copper. A ferromagnetic material in contrast to dia- and paramagnetic has a higher magnetic permeability ($\mu_r >> 1$) and can therefore be magnetised and heated using induction. These materials include all carbon steels and also a large number of alloy steels.

The ferromagnetic property of the material is determined by its structure, chemical composition, grain size and other prior treatments¹. The ferromagnetic property is also effected by the intensity and frequency of the magnetic field and the temperature of the material. The relative permeability (μ_r) can vary from 2 to more than 200,000 depending on the magnetic field intensity H , the steel alloy and its material properties[32]. The magnetization curve which describes the nonlinear relation between H and magnetic flux density B is given by $\mu_r = \frac{B}{H\mu_0}$ for a typical steel. This can be graphed by the following curves:

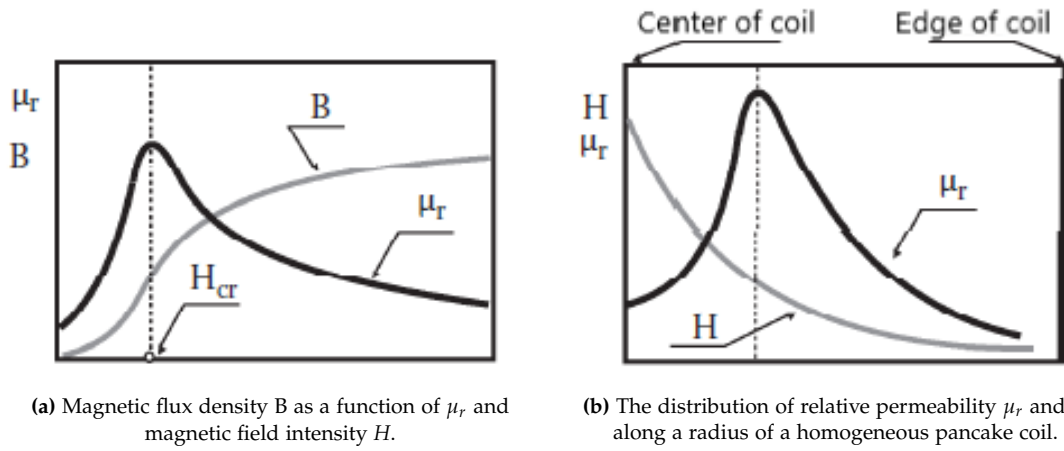


Figure 4.2: Nonlinear relation between B and H [30].

As seen on figure 4.2a the maximum value of μ_r occur at a critical point of H (H_{cr}) and when H exceeds this value, the relative magnetic permeability starts to decrease. When looking at the magnetic field around a pancake coil on top of a steel plate, the relative permeability has the highest value close to the center of the coil as seen on figure 4.2b. The relative permeability drops when moving towards the edge of the pancake coil.

All ferromagnetic materials have a temperature at which it loses its magnetic properties and becomes paramagnetic. This temperature is called the Curie point. For this study the main focus is on carbon steel which Curie point is dependent on the carbon content of the steel. As can be seen in figure 4.3 the highest Curie point is 768 °C from 0-0.45% carbon content, with its lowest Curie point at 724 °C for carbon content higher than 0.76%.

¹E.g. work hardening or annealing.

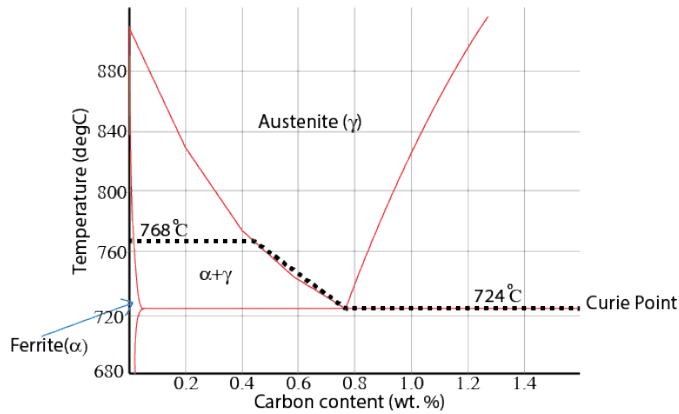


Figure 4.3: Phase diagram for carbon steel, the dotted line illustrates how the Curie point of the steel is dependent on the carbon content of the steel [30].

4.2.3 Electrical Resistivity

A material's ability to conduct electric current is specified as a material's electrical conductivity (σ) and has an SI-unit of $\frac{S}{m}$, another unit which is often used is $m \cdot \Omega^{-1}$, the latter unit is used in the calculation of skin effect. The electrical resistivity (ρ_{coil}) is given by the conductivity of a material and has an SI-unit of $m \cdot \Omega$ [33].

4.2.4 Skin Effect

The induced current in a workpiece reduces exponentially in the depth of the material from the surface closest to the coil. Therefore, most of the heat is generated close to the surface of the workpiece. This is known as the skin effect, which can be used to calculate the current density at a given depth of the workpiece, using the exponential law:

$$J = J_e e^{-\frac{y}{\delta}} \quad (4.7)$$

Where J is the current density at the distance y , J_e is the current density at the surface of the conductor, and δ is the penetration depth of the electromagnetic wave. Lower frequencies lead to greater penetration depths of the electromagnetic waves, this effect is illustrated in figure 4.4. The penetration depth is defined as the distance from the surface, where the current density is $\frac{1}{e}$ of the current density at the surface of the conductor. The penetration depth, δ , is defined as:

$$\delta = 503 \sqrt{\frac{\rho_{coil}}{\mu_r f}} \quad (4.8)$$

Where ρ_{coil} is the electrical resistivity of the material, μ_r is the relative permeability, and f is the frequency [34].

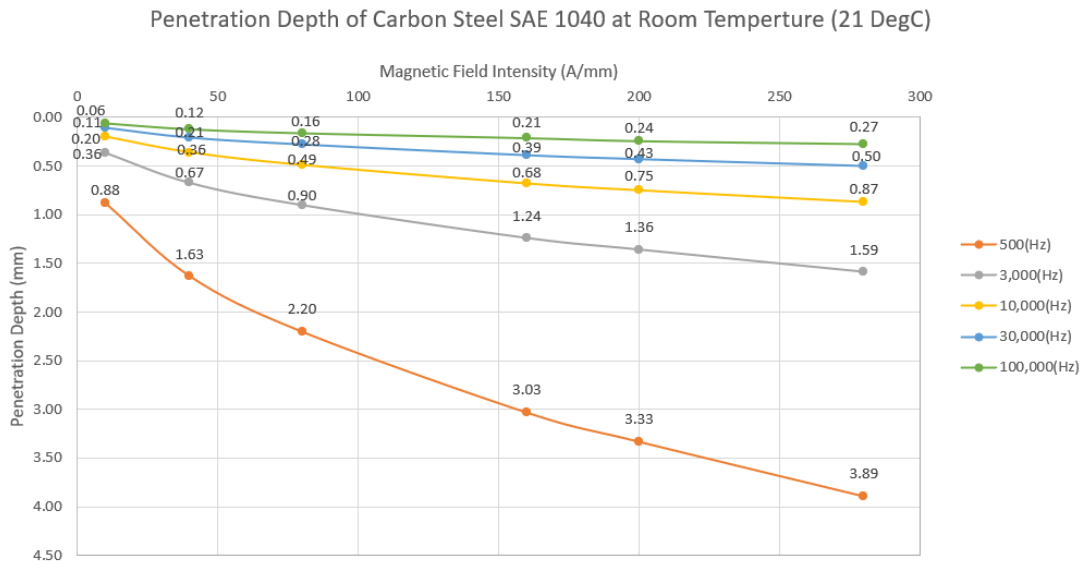


Figure 4.4: Different frequencies effect on the penetration depth of the magnetic field in steel SAE 1040 [35].

The penetration depth of a pancake coil is smaller than that of a traditional induction coil, as the eddy currents induced by the pancake coil diffuse with increasing depth. Additionally, eddy currents induced by wires, symmetrical about the center axis of the coil, cancel each other out in pancake coils [36].

4.2.5 Proximity Effect

There are multiple surrounding factors affecting the conductor² and the magnetic field surrounding the coil. Multiple conductors are often in the proximity and they have their own magnetic fields. These magnetic fields interact differently with nearby fields thus affecting the power density distributions and the current flow. When analysing the magnetic field of two different scenarios, the first scenario having only one conductor and the other scenario having two conductors, the magnetic field is more dense between the two conductors. This is represented in figure 4.5.

²The object affected by the magnetic field.

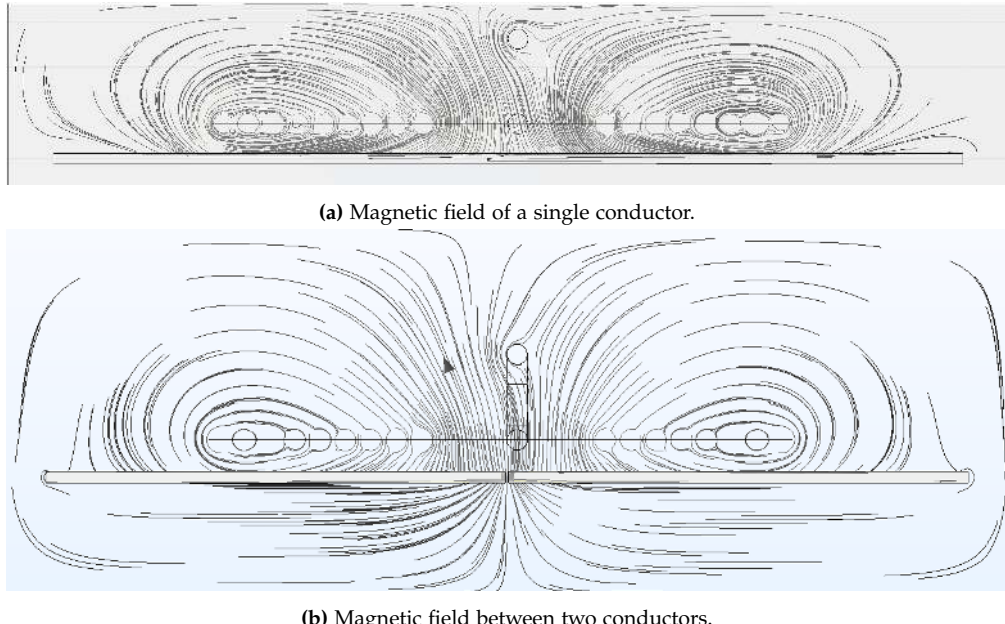


Figure 4.5: Magnetic field between a single (a) and two conductors (b).

When a conductor is near another conductor, their currents will redistribute. If their currents are flowing in the opposite direction of each other, both currents will be concentrated in the areas facing each other, resulting in a strong magnetic field between them. Now, because the magnetic field is stronger between the two conductors, the external magnetic field will instead be weaker than it would with only one conductor present. Here the conductor's magnetic field will often cancel each other out and thereby make them weaker. If the currents of the two conductors have the same direction, the opposite is true: a weaker magnetic field between them and a stronger one around them.

If two conductors with opposing currents are placed near each other, the strength of the electromagnetic proximity effect is increased. As this distance increases the strength decreases [37].

4.3 Modeling of the Electromagnetic Field

Maxwell's four equations can be used to describe the electromagnetic phenomena. The input from the energy source to an induction coil is an AC, that generates an alternating magnetic field around the coil. This magnetic field induces an electrical field in the workpiece, and thereby generating heat in the workpiece. If the electromagnetic field is set to be time-varying, the differential form of Maxwell's equations can be written as:

$$\nabla \cdot \mathbf{E} = \frac{\rho_{charge}}{\epsilon_0} \quad (4.9)$$

$$\nabla \cdot \mathbf{B} = 0 \quad (4.10)$$

$$\nabla \times \mathbf{E} = -\frac{\partial \mathbf{B}}{\partial t} \quad (4.11)$$

$$\nabla \times \mathbf{B} = \mu_0 \mathbf{J} + \mu_0 \epsilon_0 \frac{\partial \mathbf{E}}{\partial t} \quad (4.12)$$

Here \mathbf{E} is the electric field vector, \mathbf{B} is the magnetic field vector, ρ_{charge} is the electric charge density, ϵ_0 is the permittivity of free space, \mathbf{J} is the electric current density, μ_0 is the magnetic field constant, and t is time [38].

The first Maxwell equation can also be written in the integral form:

$$\oint_A \mathbf{E} d\mathbf{a} = \frac{q}{\epsilon_0} \quad (4.13)$$

The left-hand side of the equation is a surface integral of area A , representing the electric flux, and measures how much of the electric field gets in or out of the area [39]. The equation can be replaced by the volume integral through the divergence integral theorem which states that [40]:

$$\oint_A \mathbf{F} d\mathbf{a} = \int_V (\nabla \cdot \mathbf{F}) dv \quad (4.14)$$

Therefore the following is given:

$$\int_V (\nabla \cdot \mathbf{E}) dv = \frac{1}{\epsilon_0} q \quad (4.15)$$

q can be rewritten such that:

$$\rho_{charge} = \frac{q}{V} \Rightarrow V \rho_{charge} = \int_V \rho_{charge} dv \quad (4.16)$$

This integral can now be inserted instead of q and the differential form of the equation can be expressed:

$$\int_V (\nabla \cdot \mathbf{E}) dv = \frac{1}{\epsilon_0} \int_V \rho_{charge} dv \Rightarrow \nabla \cdot \mathbf{E} = \frac{\rho_{charge}}{\epsilon_0} \quad (4.17)$$

The first equation 4.9 tells whether the electric field is a source or a sink in the given spot. If the divergence is positive, then the charge density is positive, and thus the charge q is also positive. In this point of space there is therefore a positive charge which is a source of the electric field. See figure 4.6a. Conversely it is a sink of the electric field if the divergence is less than 0 and thus the charge is negative. Lastly if the divergence equals 0 the charge density is also 0. In this point there is either no charge, or a positive and negative charge which cancel each other out. The first Maxwell equation therefore states that charges generate electric fields.

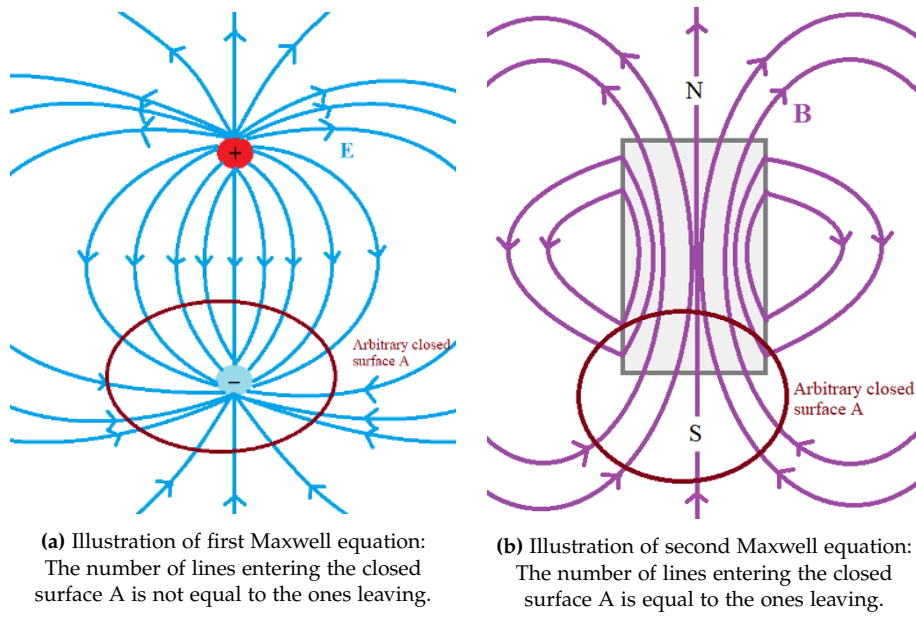


Figure 4.6: Divergence of the electric and the magnetic field.

The second Maxwell equation in integral form can be written as:

$$\oint_A \mathbf{B} \cdot d\mathbf{a} = 0 \quad (4.18)$$

It states that the magnetic flux, through the closed surface A , is always 0. The equation can be replaced through the divergence integral theorem like before and a new integral is presented:

$$\oint_A \mathbf{B} \cdot d\mathbf{a} = \int_V (\nabla \cdot \mathbf{B}) dv = 0 \quad (4.19)$$

If the integral equals 0, the integrand also have to be 0. And thus the differential form is expressed as:

$$\nabla \cdot \mathbf{B} = 0 \quad (4.20)$$

Since the divergence of the magnetic field equals 0 at any point in space, there is no magnetic charges (also called monopoles). Another possibility is that there is an equal amount of positive and negative magnetic charges, so the total charge at the given point cancels out. An ideal magnetic dipole is an example of this as seen on figure 4.6b. The north pole represents a positive magnetic charge and the south pole represents the negative magnetic charge. Summarised, this equation states that a magnetic field is not generated with magnetic monopoles, hence only magnetic dipoles are possible.

The third Maxwell equation, also called the Faraday's Law of Induction, is expressed as following in the integral form:

$$\oint_L \mathbf{E} \cdot d\mathbf{l} = -\frac{\partial}{\partial t} \int_A \mathbf{B} \cdot d\mathbf{a} \quad (4.21)$$

The left-hand side of the equation is an electric field integrated over a closed line. This integral is a summation of the electric field that rotates along the line L . This is called the voltage along L . On the other side is a differentiation of an integral through surface A that represents the magnetic flux. This side therefore equals the change in magnetic flux over time t . Because of the negative sign on the right-hand side, the change in magnetic flux and the electric voltage behave opposite of each other. By using Stokes's theorem which states:

$$\oint_L \mathbf{F} \cdot d\mathbf{l} = \int_A (\nabla \times \mathbf{F}) \cdot d\mathbf{a} \quad (4.22)$$

The closed integral can be written as [40]:

$$\oint_L \mathbf{E} \cdot d\mathbf{l} = \int_A (\nabla \times \mathbf{E}) \cdot d\mathbf{a} \quad (4.23)$$

Now the differential form can be shown by moving the time derivative inside the integral. Because of the integral on both sides applies to the same surface A , the integrands are equal to each other.

$$\begin{aligned} \int_A (\nabla \times \mathbf{E}) \cdot d\mathbf{a} &= - \int_A \frac{\partial \mathbf{B}}{\partial t} \cdot d\mathbf{a} \\ &\Downarrow \\ \nabla \times \mathbf{E} &= -\frac{\partial \mathbf{B}}{\partial t} \end{aligned} \quad (4.24)$$

The third Maxwell equation therefore says that the change in magnetic field \mathbf{B} gives a rotating electric field \mathbf{E} and vice versa. See figure 4.7a for a visual representation of this.

The fourth Maxwell equation, also called Ampere's Law, in integral form is given by:

$$\oint_L \mathbf{B} \cdot d\mathbf{l} = \mu_0 I_{\text{enc}} + \mu_0 \epsilon_0 \frac{\partial}{\partial t} \int_A \mathbf{E} \cdot d\mathbf{a} \quad (4.25)$$

Where I_{enc} is the electric current. It can also be described as an electric current density \mathbf{J} by taking the integral of \mathbf{J} over the surface A . Like the third equation, the integral form can now be written in differential form by using Stokes's theorem and moving the time derivative inside the integral.

$$\begin{aligned} \int_A (\nabla \times \mathbf{B}) \cdot d\mathbf{a} &= \mu_0 \int_A \mathbf{J} \cdot d\mathbf{a} + \mu_0 \epsilon_0 \int_A \frac{\partial \mathbf{E}}{\partial t} \cdot d\mathbf{a} \\ &\Downarrow \\ \nabla \times \mathbf{B} &= \mu_0 \mathbf{J} + \mu_0 \epsilon_0 \frac{\partial \mathbf{E}}{\partial t} \end{aligned} \quad (4.26)$$

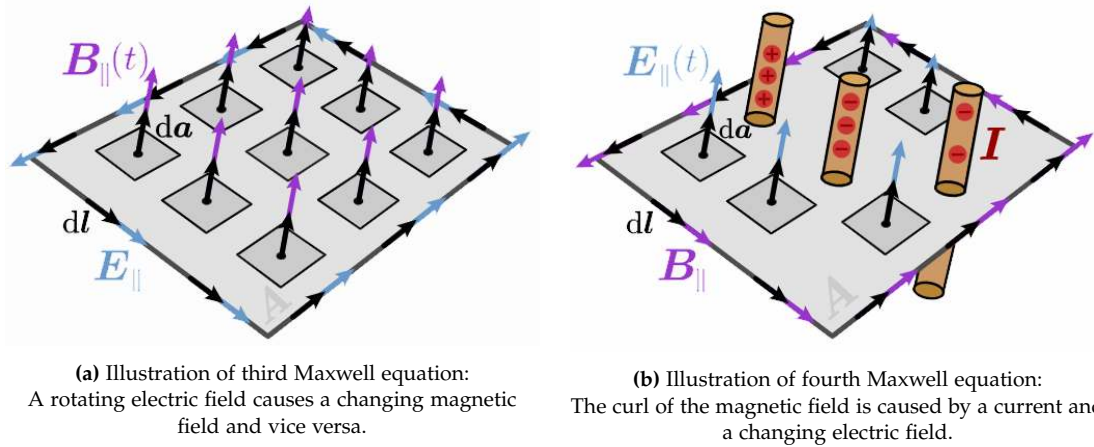


Figure 4.7: Curl of the electric field and the magnetic field [39].

The fourth equation therefore states that an electric current and change in the electric field generates a magnetic field [38][39]. See figure 4.7b for a visual representation of this.

These parameters satisfies the equation for Ohm's law:

$$\mathbf{J} = \sigma \mathbf{E} \quad (4.27)$$

Now the thermal energy Q can be modelled by the formulas above and by theory of heat transfers from section 4.1.2.

The Joule heat power density in an induction heating process is given by [41]:

$$Q = \frac{|\mathbf{J}|^2}{\sigma} \quad (4.28)$$

The thermal energy Q also called heat generation is associated with induced eddy currents per second in a volume. Generally, the time dependent heat transfer in a metallic workpiece can be described by the Fourier equation 4.29, where the thermal heat Q is taken as the internal heat source. When boundary conditions of convective and radiative heat transfer are taken into account, the heat conduction equation is then obtained:

$$Q = c \gamma \frac{\partial T}{\partial t} + \nabla \cdot (-k \nabla T) \quad (4.29)$$

Where c is the specific heat capacity of the metal and ρ is the density of the metal. The Fourier equation 4.29 and appropriate boundary and initial conditions constitute the temperature distribution in 3D at any time and point in the workpiece. This equation is therefore used for mathematical modeling of a heat transfer processes of induction heating [42].

4.4 Finite Element Method

Finite Element Method (FEM) is a numerical model used to compute approximated solutions for different engineering problems, including heat transfer and electromagnetic analysis. This is done by splitting the geometry of the simulated bodies into a finite number of small elements connected in nodes. These connected elements are called the mesh. The mesh is beneficial to avoid calculating the values for the entire body but instead the values for the specific nodes. From this, the values for the individual element can be approximated, and thereafter combined to approximate the values for the entire body [43]. The calculations in this method can be done using different software. For this specific study the software used is COMSOL Multiphysics.

4.4.1 Implementation of FEM

Implementing FEM to solve a problem follows a general model that can be seen in figure 4.8.

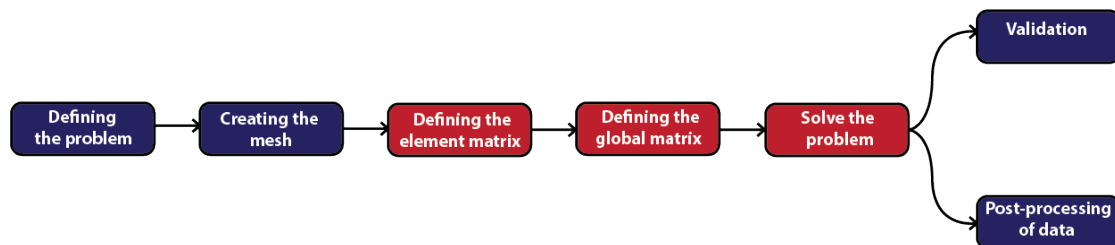


Figure 4.8: General model for implementing FEM to solve a problem. The blue boxes are the steps taken by the engineer and the red boxes are the steps taken using software.

Defining the Problem

Defining the problem starts with defining the geometry of the bodies that will be analysed, the space they are in, and the materials the different bodies are constructed from. Then the physics, needed to be calculated in the nodes, is defined. For this study, the physics that will be calculated are thermodynamics and electromagnetism. Lastly, the boundary conditions of the model are set such as the boundaries of the space, room temperature and, in the case of electromagnetism, magnetic insulation along the space boundaries called Dirichlet condition [42].

Creating the Mesh

The mesh can be constructed on the basis of four different geometries. The geometry in the 2D plane can be based on triangles or squares. A mesh based on squares tends to give more accurate results, but is unfit to create more

complex geometries. The geometry in the 3D plane can be based on pyramids or boxes. A mesh based on boxes also tends to give more accurate results, but has the same problem as squares of being unfit to create more complex geometries [43]. Another thing to consider, when constructing a mesh, is the sizes of the individual elements of the mesh. Smaller elements mean that more elements can be fitted in each object, which leads to more accurate results. The consequence is that more elements need greater computational power. It is therefore important to build a mesh with a fine structure for the areas, where there is a lot of development, and a coarser mesh, where values are more stable. For the modelling of induction, it is important to have a finer mesh, where the concentration of magnetic flux is highest.

Defining the Element Matrix

The computer defines a set of values that are calculated in each node in the element. These definitions combine into an element matrix describing how the values of the different node impact one another. This is illustrated in figure 4.9 where four nodes are heated to a given temperature. Node 1 and 3 are warmer than nodes 2 and 4. From this, the temperature of the element can be estimated.

Defining the Global Matrix

After the element matrix is defined, all the different matrices from the different elements are combined into a global matrix. This is illustrated in figure 4.10a, where the first element A is combined with all the surrounding elements. This is possible since all the elements share nodes with its surrounding elements. For instance, element A is sharing nodes 2 and 4 with element E. An illustration of how this looks in FEM software can be seen on figure 4.10b.

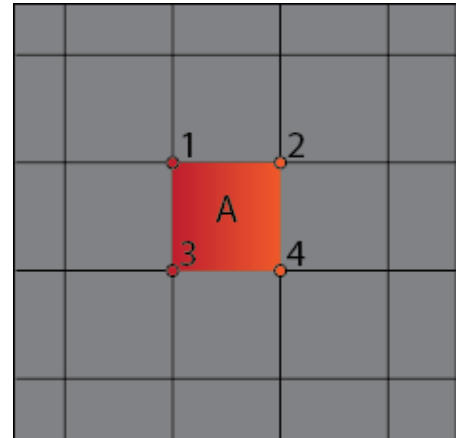
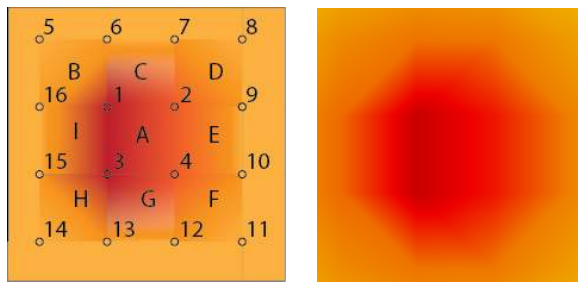


Figure 4.9: An element in the model defined by four nodes with a set high temperature at node 1 and 3 and a lower temperature at node 2 and 4.



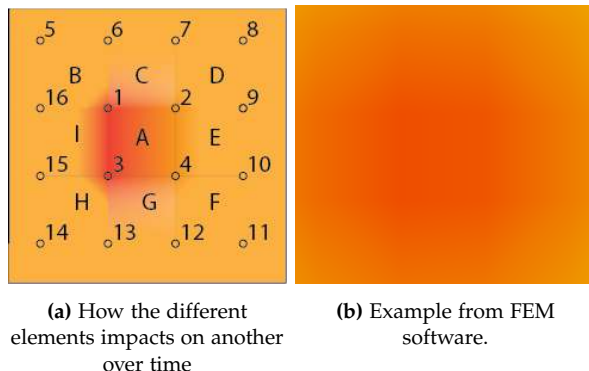
(a) Full geometry split into nine elements with sixteen nodes. Nodes 1 and 3 are warmer than 2 and 4. Nodes 5 to 16 are coldest.

(b) Example from FEM software.

Figure 4.10: The global matrix is constructed from the nodes (a) with a representation from FEM software (b).

Solving the Problem

After everything is defined, the software solves the matrix according to what information is wanted by the engineer. The solution could be obtained, when a certain temperature is reached, or after a time period, as is illustrated in figure 4.11.



(a) How the different elements impacts on another over time

(b) Example from FEM software.

Figure 4.11: The development of temperature over time (a) with a representation from FEM software (b).

Post-processing of Data

When the simulation is done, it is the job of the engineer to derive the relevant data from the solved matrix. This could be a certain temperature and a specific time in a point of the element.

Validation

The last step is validating the results. This step can be done in different ways. For this study, it is done by conducting experiments using induction heating, and by comparing the results with the results from the FEM model.

5. Methods and Results

To get an understanding of how the experiment should be conducted - and how much time should be devoted, some initial simulations were conducted before the experiments (see appendix G). Simulations and theory combined gave a rough estimate of how the experiment should be carried out.

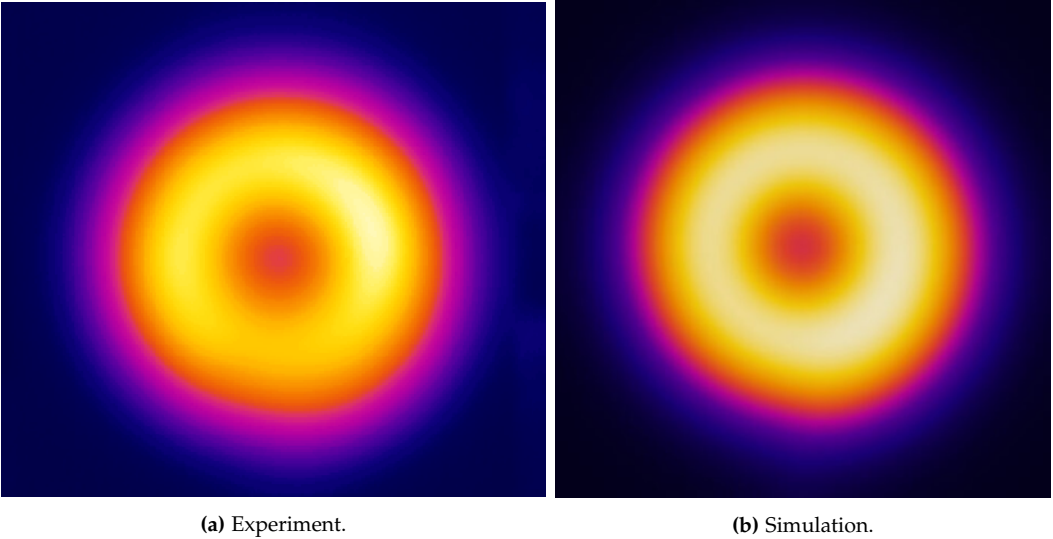


Figure 5.1: Visual comparison between experiment (a) and an early model of induction heating (b).

5.1 Test of Theory - Experiment

In order to test the theory and in order to have empirical data on induction heating of steel, an experiment will be conducted to test how a single steel plate and two steel plates with a gap in between them are affected by an induction coil. The subsequent cooling will also be observed. The experiment will test what the optimal distance is between the coil and steel plate, how a gap between two plates affects the heating, and lastly, the effect of the coil geometry.

5.1.1 Expectations

From the theory in chapter 4, some important parameters and results can be predicted. These predictions and expectations will be compared to the data from the experiments.

Due to the proximity effect, the closer the distance between the inductor and the workpiece (coil to steel), the higher the magnetic flux density and therefore higher temperature. The proximity effect will again have an effect on the heat generated when conducting the experiment with two steel plates placed near each other. The closer the gap between the steel plates, the higher the magnetic

flux density and therefore higher temperatures at the edges between the plates. This will reduce the required time needed to heat the area near a gap. These predictions need to be proven by conducting experiments, where they will later be used to validate the model in COMSOL. Likewise, it was expected that more turns in the coil, leads to a shorter heating time. This is caused by the proportionality between magnetic field intensity H and number of turns in the coil N , from formula 4.5. On the other hand, it was expected that the heat distribution of the plate would be more even, with fewer turns in the coil. This was expected due to the longer heating time, caused by lower power input in the plate. With longer heating time, the heat in the steel plate has more time to transfer, causing a more even heat distribution. As for the cooling (conduction, convection and radiation) it was expected that the plate(s) would cool slower as the temperature drops in the plate(s).

5.1.2 Approach

The experiment was divided into two days. The first day was used to determine the optimal distance between the coil and the steel plate, using a single steel plate. Once this factor was determined, the second day was used to study the cooling, to vary the size of the gap between two plates, and to determine the effect of different coil geometries.

It was originally planned that the power output and frequency should be varied during different experiments. However, this was not possible on the Miller Proheat 35, as these parameters were automatically controlled by the power supply. A detailed plan of the experiment and bill of materials can be seen in appendix B.

Day 1 - Setup

As can be seen on figure 5.2, the induction coil was strapped to a sheet of plywood with zip ties to secure that the geometry of the coil was constant. The plywood and the coil were then placed parallel to the steel plate. On the other side of the steel plate, a thermal camera was placed on a tripod to measure plate temperatures. The distance between steel plate and thermal camera was 3 metres. From the centre of the plate and to the edge, thermocouples were placed to measure the heat gradient of the metal. The red colouring of the steel plate illustrates the expected heat gradient and is not the actual colour of the metal.

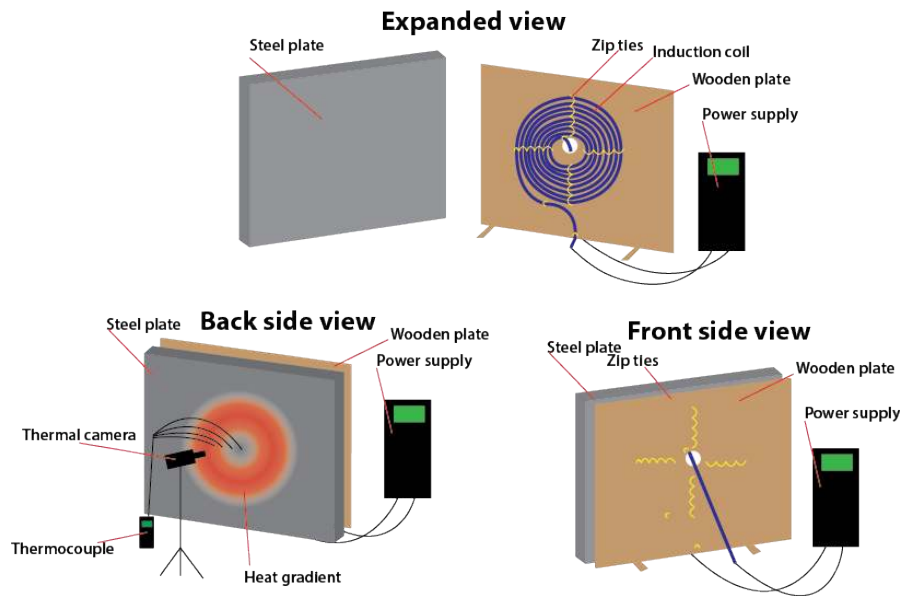


Figure 5.2: Illustration of the setup of the experiment the first day.

The approach of the first day of the experiment was to conduct six experiments where everything except for the distance between the coil and the steel plate was held constant. The distance between the coil and the steel plate is measured from the centre of the cable cross section, to the closest surface of the steel plate, see figure 5.3. All measurements during experiments were sketched and noted, see appendix C.



Figure 5.3: How coil-steel distance is measured - from centre of cable to surface of steel plate.

Day 1 - Results of the Experiments

To compare the effect of different coil distances, the time from 30°C to 200°C was extracted from the data recorded with the thermal camera.

The coil was kept at 8.5 turns throughout the experiments of day 1, due to the size of the steel plate. It was decided that the diameter of the coil should be smaller than the width of the plate, to allow for some amount of conduction to occur during the experiment. Additionally, the magnetic field exceeds the diameter of the coil, which would also heat the rest of the plate. The inner diameter was defined by how sharply the cable was allowed to turn, see figure 5.8b.

CHAPTER 5. METHODS AND RESULTS

Variable	Experiment	Power	Current	Voltage	Frequency	Distance coil-steel	30 to 200°C
Coil-steel distance	6	9.4 kW	154 A	695 V	6.4 kHz	13.0 mm	371.0 s
	1	8.0 kW	154 A	695 V	6.4 kHz	31.0 mm	423.5 s
	5	8.3 kW	153 A	695 V	6.3 kHz	31.0 mm	423.5 s
	2	8.0 kW	153 A	693 V	6.3 kHz	36.0 mm	423.5 s
	3	7.1 kW	152 A	693 V	6.3 kHz	42.0 mm	595.0 s
	4	6.8 kW	150 A	691 V	6.3 kHz	59.0 mm	644.0 s

Table 5.1: Experiments from day one sorted by coil-steel distance.

The experiments conducted show that decreasing the distance between the coil and steel plates results in a faster heating, see table 5.1. The shorter distance the better. Even though a distance of 13 mm during experiment #6 resulted in the shortest heating time, it was not used on the second day to protect the induction cable and to avoid melting the zip ties.

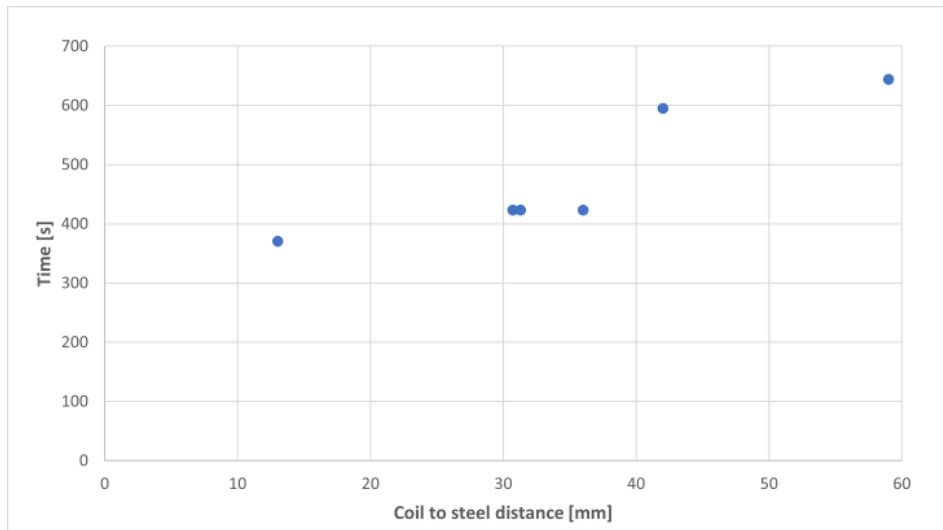


Figure 5.4: Heating for 30 °C to 200 °C.

Experiment #1 and #5 were both performed at a distance of 30.0 mm. To make both data points visible, they are displayed ± 0.3 mm from the actual data point.

The variation in time duration from 30 °C to 200 °C results from the coil power level, which is dependant on the distance between the coil and steel plate. See figure 5.5.

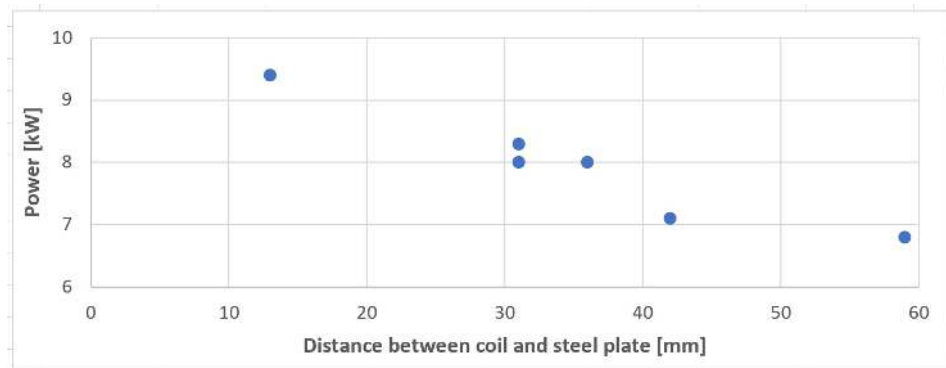


Figure 5.5: The relation between coil power and distance between coil and steel.
Note that the y-axis starts at 6 kW to visually clarify the relation.

The above, only focuses on the maximum temperature on the plate. It is important to note, that the heat distribution on the plate's surface is affected by the fact that the plate was induction heated with a pancake coil - not an even heat source. To compare the heat distribution on the plate, a horizontal cut line of the left side of the centre (unaffected by tape and thermocouples) was extracted from the thermal pictures. All images were extracted after 406 seconds of heating, as this was the heating time from cold to a little more than 200 °C in the shortest experiment (#6). Initial temperatures are between 13 and 21 °C. Graphing the temperatures at 406 seconds as a function of distance from the coil centre, supports figures 5.4 and 5.5. Higher temperatures are reached in the experiments with the shortest distance between coil and steel. The thermal pictures and graph in figure 5.6 also manifests a warm circular ring similar to the coil geometry surrounding a colder centre.

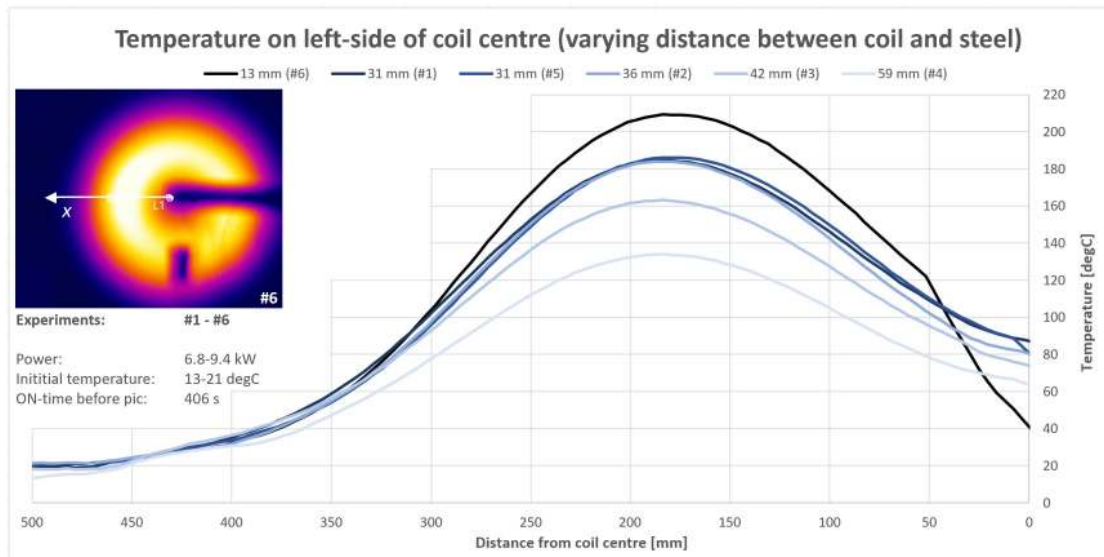


Figure 5.6: Varying distance between coil and steel: Temperature-position graph illustrating temperatures on a horizontal cut line from coil centre. Areas appearing cold on the image is caused by thermocouples and the tape holding it.

Day 2 - Setup

The setup for the experiments on the second day (shown on figure 5.7 and 5.9) was very similar to the first day. The difference was the implementation of a gap by using two steel plates - resembling a welding geometry. The gap was centred in regards to the coil and thermal camera. Distance between the thermal camera and the plates was 3 metres.

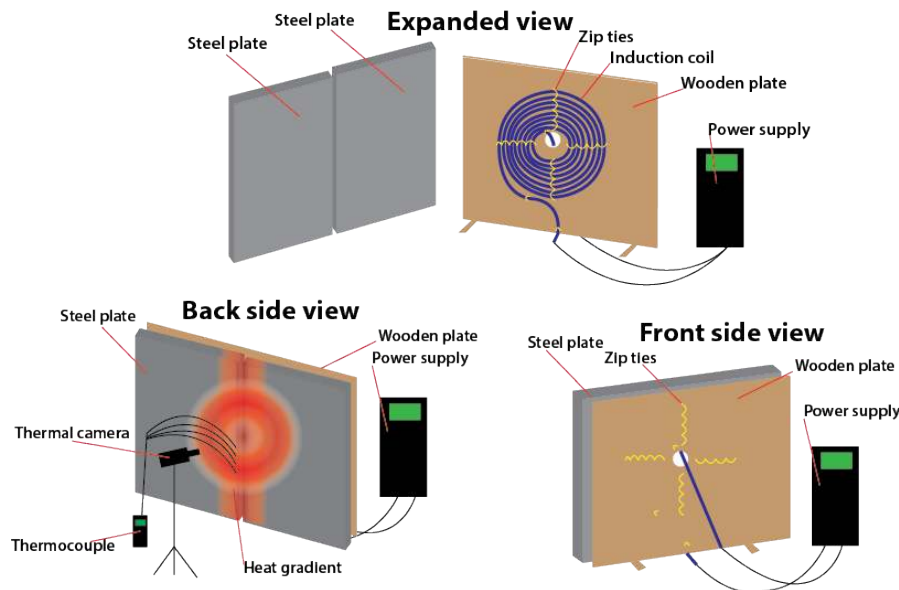


Figure 5.7: The setup of the experiment the second day.

The two plates were set up in such a way to study how the magnetic field and the induction heating is influenced by a gap.

The approach of the second day was to first conduct five experiments with the same coil as the day before. The coil was placed at a distance of 34 mm (close to the optimal distance, but without the risk of melting zip ties). The only parameter was the size of the gap. The steel plates were then heated until a maximum temperature of 300 °C was logged by the thermal camera. During the heating - and following cooling - process, the thermal camera was set up to take a picture every 7 seconds while the thermocouples simultaneously measured the temperature of the steel near the gap.

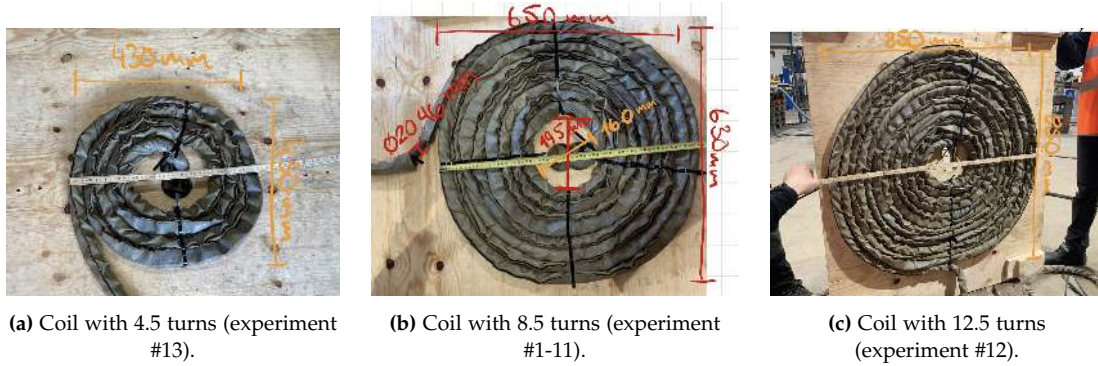


Figure 5.8: The three coils with dimensions used throughout the experiments.

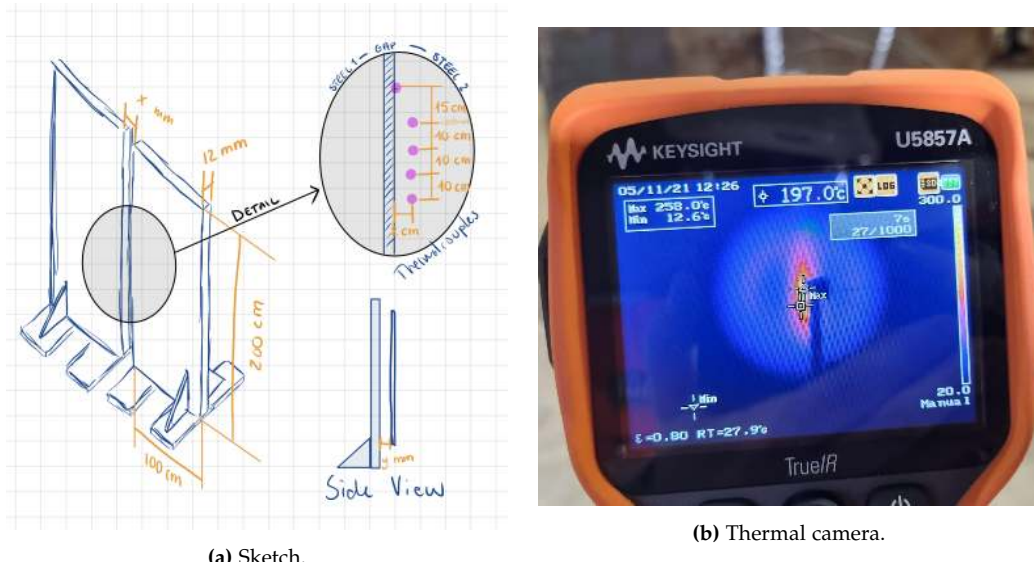


Figure 5.9: Sketch of the actual setup at Bladt (a). In the detailed view pink dots illustrate the thermocouples. Image of the thermal camera (b). Note how the tape, holding the thermocouples, blocks the heat radiation and appears cold on the image.

Two more experiments were conducted, where the only changing parameter was the geometry of the coil itself. All experiments prior to this were conducted with a coil geometry of 8.5 turns. The last two experiments were conducted with geometries of 12.5 and 4.5 turns, respectively.

Day 2 - Results

As on day one, the heating time from 30 °C to 200 °C was recorded for comparison, but with a fixed coil centre to steel distance of 34 mm, equivalent to 23 mm from steel to coil. Additionally, heating times from 30 °C to 300 °C were also noted.

CHAPTER 5. METHODS AND RESULTS

Variable	Experiment	Power	Current	Voltage	Frequency	Gap	Turns	30 to 200 °C	30 to 300 °C
Gap	10	7.7 kW	144 A	693 V	6.0 kHz	1.88 mm	8.5	77.0 s	206.5 s
	7	7.5 kW	145 A	694 V	6.0 kHz	2.8 mm	8.5	161.0 s	350.0 s
	8	7.8 kW	146 A	694 V	6.1 kHz	2.8 mm	8.5	129.5 s	283.5 s
	9	7.8 kW	147 A	694 V	6.1 kHz	5.6 mm	8.5	129.5 s	290.5 s
Close ups	11	8.1 kW	146 A	696 V	6.1 kHz	1.88 mm	8.5	52.5 s	140.0 s
Turns in coil	13	6.2 kW	200 A	673 V	8.5 kHz	2.8 mm	4.5	185.5 s	416.5 s
	7	7.5 kW	145 A	694 V	6.0 kHz	2.8 mm	8.5	168.0 s	350.0 s
	8	7.8 kW	146 A	694 V	6.1 kHz	2.8 mm	8.5	129.5 s	283.5 s
	12	22.9 kW	170 A	701 V	6.8 kHz	2.8 mm	12.5	23.1 s	47.6 s

Table 5.2: Note that experiment #7 and #8 are used both in the experiment where the gap and where the turns are varied, as they both use a number of coils between experiment #12 and #13 and have the same gap as #12 and #13.

The heating time during the experiments on the second day, shown on table 5.2, is much shorter than on the first day. This was also expected because of the proximity effect and the skin effect.

In experiments #7-10, the gap was varied and all other variables were held at a constant. There is a link between gap size and the heating characteristics. There is a significantly shorter heating time, when the gap distance was 1.88 mm compared to 2.8 mm and 5.6 mm. In experiments #7 and #8, the gap is the same - therefore the heating time was expected to be equal, however experiment #7 was heated in 161 seconds and experiment #8 was heated in only 129.5 seconds. In experiment #7 the power is lower at 7.5 kW compared to 7.7 and 7.8 kW in the three other gap distance experiments. This has an influence on the heating time and may be due to the coil being a bit farther from the steel plate. This may be caused by the steel plate being farther from the coil due to deformation as a result from thermal stresses. As the coil is farther from the steel plate, less power is delivered by the Miller Proheat - resulting in a longer heating time. Nevertheless, it can be concluded that the shortest heating time was achieved with the smallest gap of 1.88 mm.

As the measured heating times are only observed using the temperatures within the gap, it is also relevant to observe the temperatures farther from the gap. Therefore, cut lines from the three comparable experiments (#8, #9 and #10) were created and temperatures were plotted. Only the left side of the gap was analysed due to thermal (reflective) tape on the right plate. All three thermal pictures used are captured after 210 seconds of heating - at this point experiment #10 reached 300 °C and heating was shut off. See figure 5.10.

CHAPTER 5. METHODS AND RESULTS

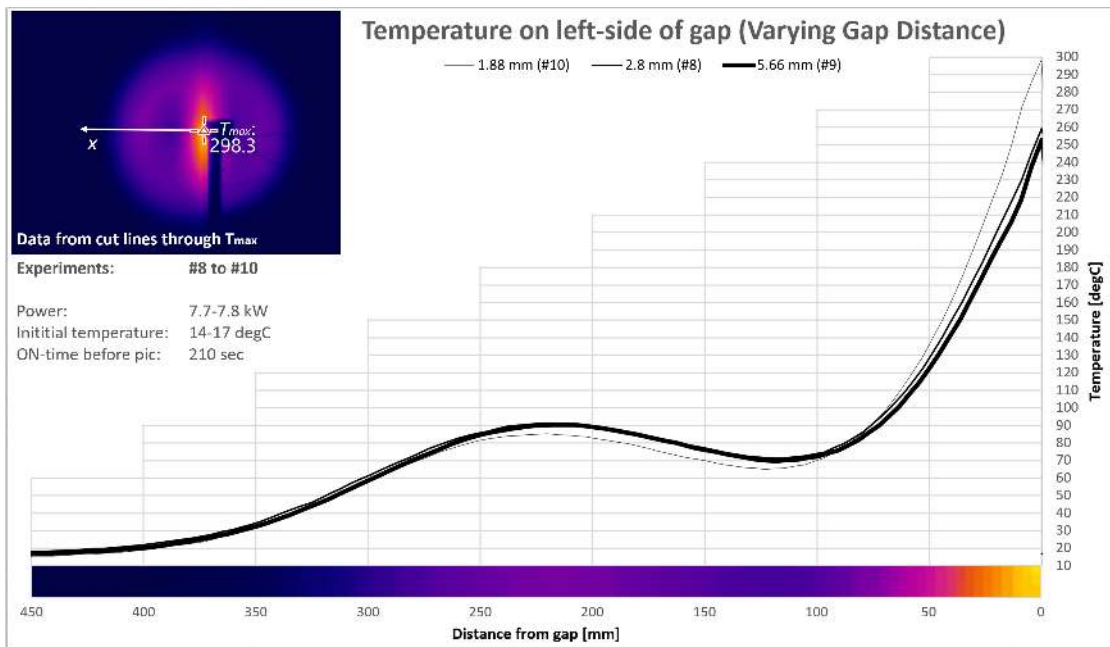


Figure 5.10: Varying gap distances: Temperature-position graph illustrating temperatures on a horizontal cut line from T_{\max} .

On figure 5.10 it is clear that smaller gap distances will result in higher temperatures within the gap. Interestingly, as the magnetic field is concentrated in the gap due to the proximity effect, the temperatures farther from the gap are lower than the experiments conducted with larger gap distances.

In experiments #12 and #13, the coil geometry was changed - influencing the power output of the Miller Proheat, as can be seen in the bottom of table 5.2. The increased power also meant that the heating time for a coil with 12.5 turns was five times shorter than a coil geometry of 8.5 turns, see figure 5.11.

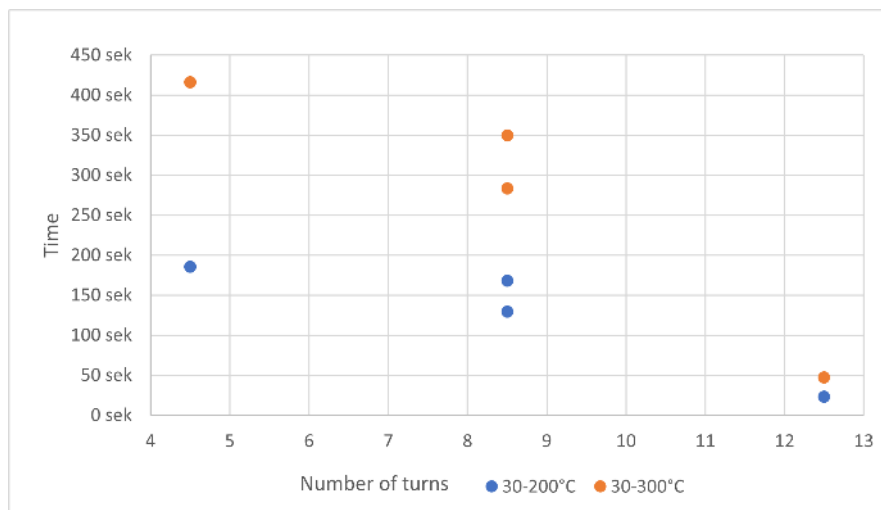


Figure 5.11: Number of coil turns and their corresponding heating times.

The above temperatures are only observed in the gap. A temperature-position graph is made to better understand the temperature distribution. The three experiments used are #8, #12 and #13. The three pictures are captured after 56 seconds - as the experiment with the largest coil (#12) was stopped at this point. See figure 5.12

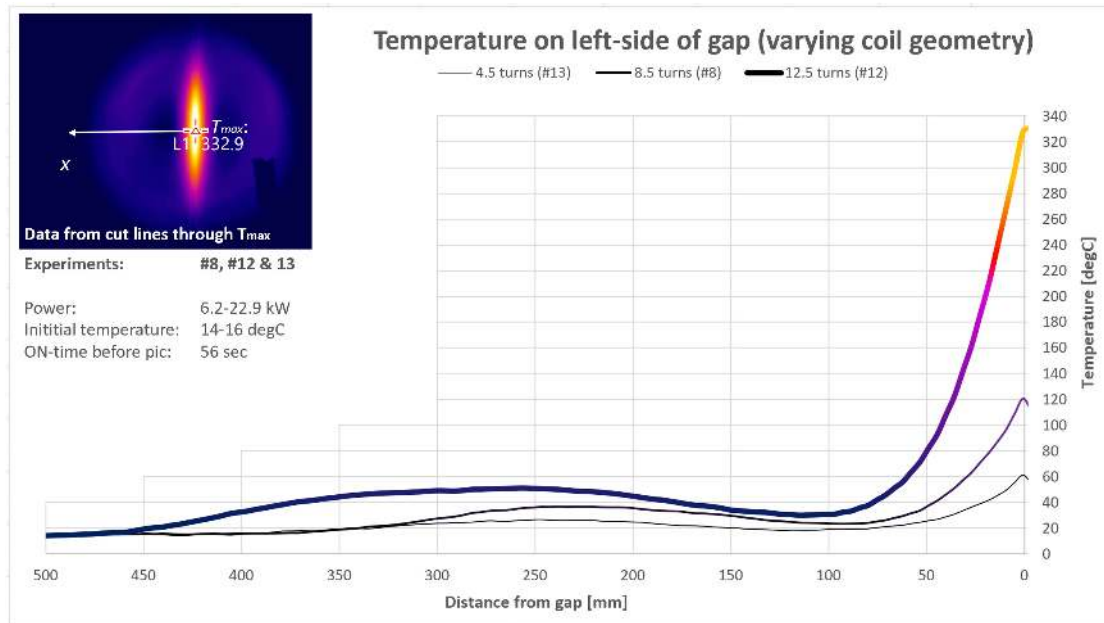


Figure 5.12: Varying coil geometries:
Temperature-position graph illustrating temperatures on a horizontal cut line from T_{\max} .

In conclusion, a larger number of turns in the coil will generally increase the temperatures of the steel at all distances from the gap. The temperature is at its highest near the gap. Furthermore, a warm ring similar to the ones seen on day 1 (experiments without gaps) can be seen.

Cooling Data

Experiment #3 and #8 were also used to collect data from the cooling process after the induction cable was turned off. This data will be compared with the simulations in COMSOL to validate the boundary conditions.

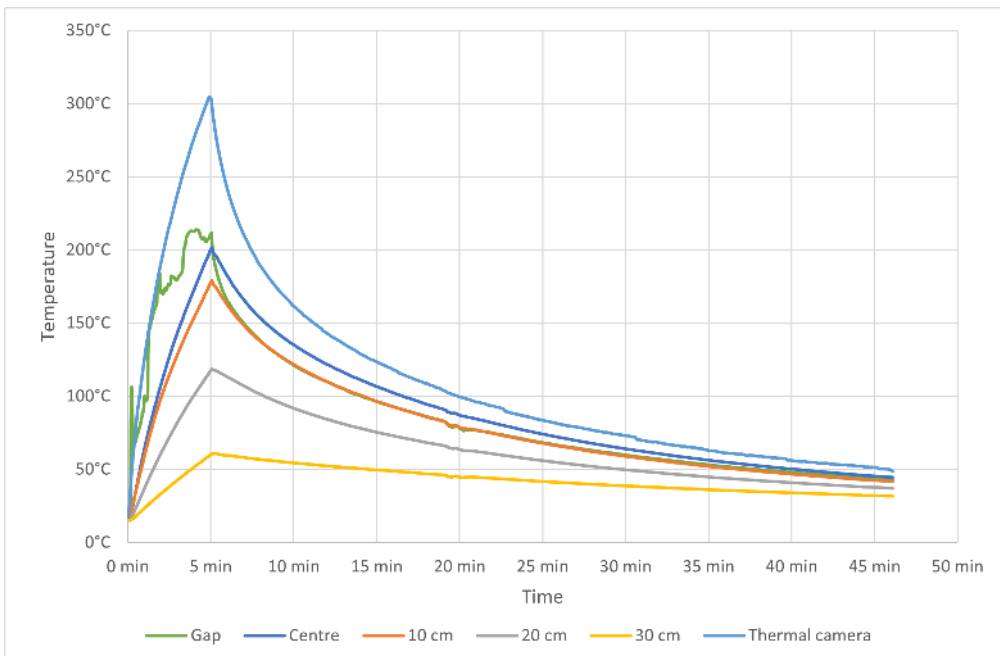


Figure 5.13: Heating and cooling of experiment #8 logged by thermocouples and thermal camera. Note that the graph illustrating the temperature in the gap (green) is unstable during heating, due to disturbance from the induction coil.

The graphs on figure 5.13 show that a large difference in temperature between the heated plate and the ambient air, gives a fast cooling rate, as described in section 4.1. The graph of the thermal camera plots the temperature in the point of the maximum temperature, of the final thermal image before the power was shut off. This point lies right next to the gap at the centre of the coil.

5.1.3 Sources of Error

The experiments cannot be replicated completely because of small, sometimes inevitable, errors. One source of error could be imprecise positioning of the coil, both the distance and centre alignment. This error occurred because the coil was mounted on plywood with cable ties, and when heating metal it will expand and deform (see pictures from experiments #1 and #2 in Appendix C). This deformation could not be restrained due to the stresses acting in the steel. When heating two steel plates, and the proximity effect occurs, impurities in the surface along the edge of the gap might have resulted in local extreme temperature.

5.1.4 Conclusions

Besides the empirical data, the experiments on day 1 resulted in a better understanding of the effects of the coil-steel distance. As expected a shorter coil-steel distance, resulted in reduced heating times.

Day 2 gave an insight on two different parameters. It was clear that a (welding) gap between two steel plates affected the heating process. A small gap will result in higher temperatures within the gap. Also, it was proven that the number of coil turns had an effect on heating time. More turns resulted in a shorter heating time.

Lastly, cooling rates were recorded in order to check and calibrate boundary conditions in the model. As expected, the cooling rates were greatest at the beginning of each cooling process, as the steel temperatures were at their highest at this point.

All of the above empirical data will be used to setup a correct model of induction heating and cooling of steel plates with and without welding gaps.

5.2 Test of Theory - Simulations

In this section the results from the experiments will be used to validate a model of induction heating. This is done by first comparing the cooling rate of the metal plate in the test with the model to confirm that the boundary conditions regarding thermodynamics are correct. Once the thermodynamic boundary conditions are confirmed, the magnetic boundaries and the magnetic properties of the material can be set. Once the problem is fully defined and the mesh is created, the simulations are run for every experiment to determine the validity of the model.

5.2.1 Defining the problem

The following needs to be defined:

- The physics calculated in the nodes
- The geometry of the model with the properties of the materials
- The boundary conditions of the simulations

Physics

When setting up the model in COMSOL Multiphysics, the physics and multiphysics are defined. The physics used in the model are *Magnetic Fields* and *Heat Transfer in Solids* and the multiphysics is *Electromagnetic Heating*. *Electromagnetic Heating* calculates the resistive and magnetic losses in the plate. *Magnetic Fields* defines the coil, and computes the electromagnetic field distribution in the air and in the plate using Ampéres Law. *Heat Transfer in Solids* computes conduction, convection and surface-to-ambient radiation for the steel plate. For more

information on the model setup and the learning curve of using COMSOL, see appendix G.

Geometry

The "one plate" model contains three domains: The steel plate, the induction coil, and an air box surrounding the other two domains. While the "two plate" model contains four domains, because of the extra plate. In the "one plate" model, the dimensions of the plate is 1000 mm x 1000 mm x 12 mm, while in the "two plate" model the dimensions of each plate is 500 mm x 1000 mm x 12 mm, as can be seen in figure 5.14. The coil is designed to match the overall geometry of the coil set up for the experiments at Bladt.

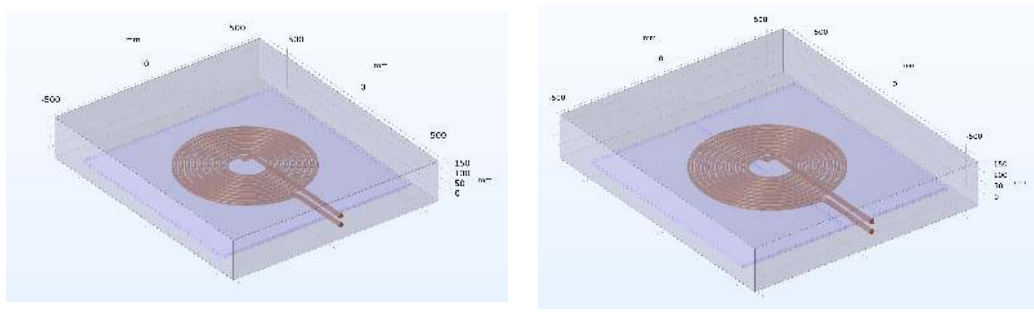


Figure 5.14: The geometry of the two different models that are used in the simulations.

The steel plates used in the model are smaller than the ones used in the experiments. This is because the heat is only present under the coil, and the heat does not have time to diffuse outwards. Using this geometry reduces the computation time of the simulation and does not influence the results significantly. It will have a small effect on the heat transfer in the plate, however it is deemed small enough that it does not justify the extra computational time.

Material Properties

S235

S235 is not a built-in material in COMSOL. Therefore the material properties had to be set manually to achieve results matching the experiments. The material properties for S235 depend on parameters such as temperature and magnetic field strength. Specifically, density, electrical conductivity, and thermal conductivity decrease with increasing temperatures, and the specific heat capacity at constant pressure also varies with temperature. The permeability of steel varies with the magnetic field strength and intensity, and because of its ferromagnetic abilities described in section 4.2.2. Instead of using the relative permeability in the magnetisation model calculations, a B-H curve of the material can be used to get a more accurate simulation which is dependent on the

magnetic field strength and intensity. An effective B-H curve material model can be used to study and analyse nonlinear magnetic materials in frequency transient simulations. This can be done by plotting data for the B-H curve. The COMSOL application "effective nonlinear magnetic curves" computes the effective B-H curves from imported data for B-H curves. COMSOL can only process data from a B-H curve in the first quadrant and starting from origin [44]. This B-H curve is therefore plotted using data from literature as seen on figure 5.15 [45].

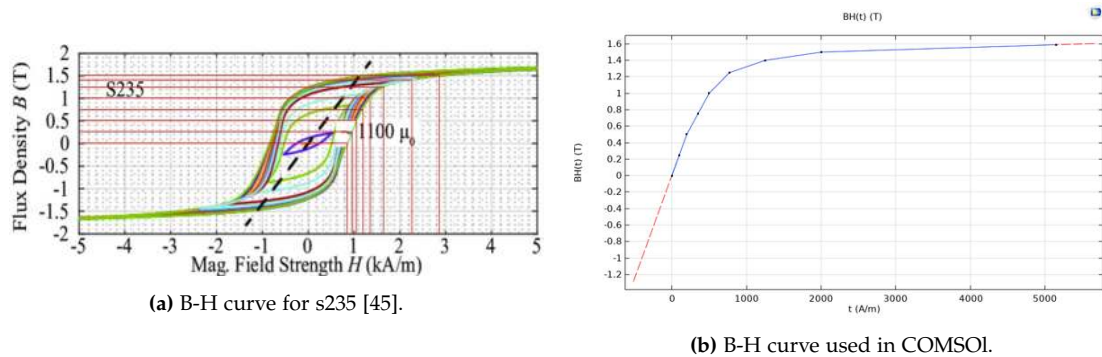


Figure 5.15: Figure (b) illustrates the data points taken from figure (a).

The computed data for the effective curve can then be exported as a "material library" which can then be used in the simulations.

The most accurate model would use variable parameters. When using these variable material parameters, it is necessary to use the *frequency transient* study-step, which combines the computation of temperature changes over time with the distribution of the electromagnetic field in the frequency domain. This allows the temperature changes to affect the electromagnetic field distribution. However, the downside of using *frequency transient* is that the computational time is significantly longer than that of *frequency domain*. A comparison between the two study strategies was made, to investigate how much of a difference the variable parameters would make.

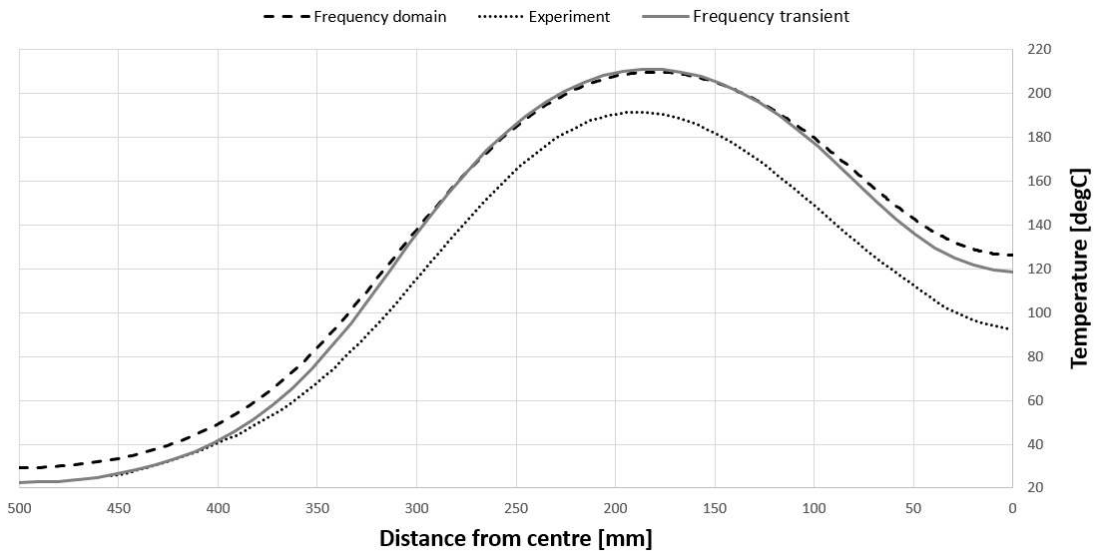


Figure 5.16: Comparison of temperature cut lines between *frequency domain* and *frequency transient* study steps, using the values of experiment #1. The model using *frequency domain* has constant material parameters, while *frequency transient* uses an effective B-H curve and linearised resistivity.

In figure 5.16 it can be seen that the results of *frequency transient* are closer to the temperatures of experiment #1, than the results of *frequency domain*. While the max temperatures are the same, both 210 °C, the temperatures at the centre and edge of the plate are, respectively, 7 °C and 6 °C lower in the *frequency transient* simulation, which better matches the results of experiment #1. However, because of the significantly longer simulation time, this difference does not warrant running all simulations in *frequency transient*, due to the time constraint of this project. Especially because calibration of coil power would require several, multihour runs of each simulation. The material properties can be seen in table 5.3.

Property	Value	Unit
Relative permeability [45]	1100	-
Electrical conductivity [24]	$4.32 \cdot 10^6$	$\frac{\text{S}}{\text{m}}$
Relative permittivity	1	-
Specific heat capacity at constant pressure [24]	470	$\frac{\text{J}}{\text{kg K}}$
Density [24]	7800	$\frac{\text{kg}}{\text{m}^3}$
Thermal conductivity [24]	49	$\frac{\text{W}}{\text{m K}}$

Table 5.3: Constant material properties for S235 used in the model.
As recommended by COMSOL the relative permittivity is set to 1.

Copper

The material properties of copper used in the COMSOL model, are set as the built-in values from the material library in COMSOL. The electrical conductivity is $5.998 \cdot 10^7 \frac{\text{S}}{\text{m}}$. The values of the relative permeability and permittivity are both 1. The material properties of copper can be seen in table 5.4

Property	Value	Unit
Relative permeability	1	-
Electrical conductivity	$5.998 \cdot 10^7$	$\frac{\text{S}}{\text{m}}$
Relative permittivity	1	-

Table 5.4: Material properties for copper used in the model.

Air

The material properties of the air domain are set to the built-in material properties from the material library in COMSOL. However, note that in table 5.5, the electrical conductivity of air is changed from 0 to $1 \frac{\text{S}}{\text{m}}$. This is done to prevent computational errors in the simulations, because division by 0 is impossible. This happens as either the resistivity or the length the conductivity is measured over, has to be 0. Such a scenario does not exist in the real world.

Property	Value	Unit
Relative permeability	1	-
Electrical conductivity	1	$\frac{\text{S}}{\text{m}}$
Relative permittivity	1	-

Table 5.5: Material properties for air used in the model.

Boundary Conditions

To replicate the experiments in the COMSOL simulations, the ambient temperature and emissivity need to correspond to the experiments. To validate the boundary conditions regarding conduction, convection, and radiation, the cooling of an experiment is compared to a simulation.

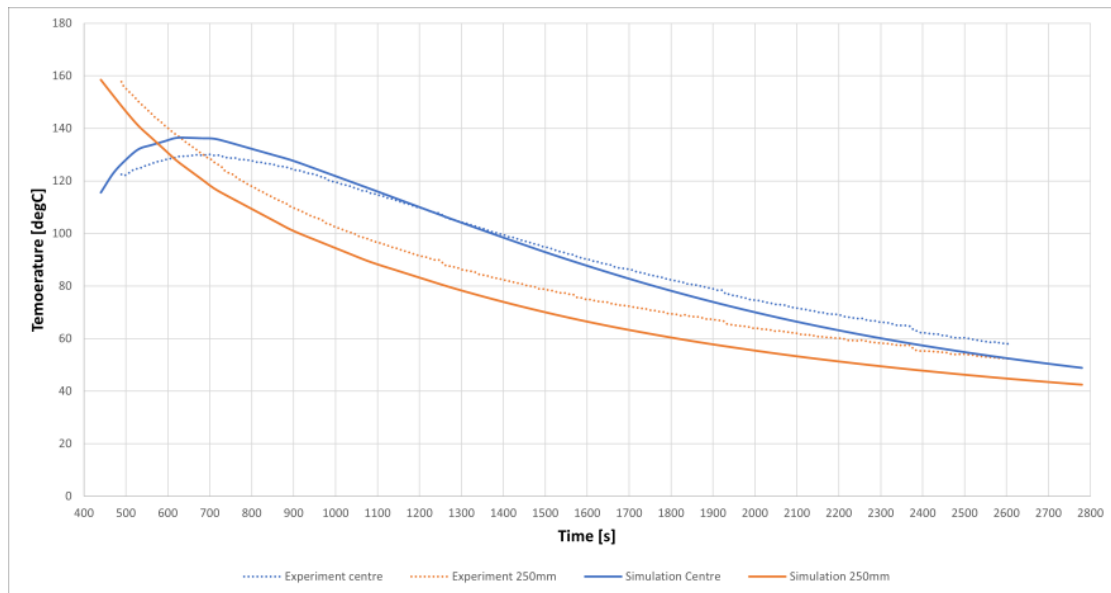


Figure 5.17: Comparison between simulation and experiment #3 in two different positions.
Note, the time starts at 440 seconds when the coil is turned off.

The graphs on figure 5.17 shows the temperature over time of two different positions on the steel plate. The slope of the graphs shows the cooling rate of these positions. When comparing the slopes of the experiment and the simulation, it shows that the cooling rate is similar. This indicates that the boundary conditions, regarding heat transfer, are set correctly. The temperature deviates with 10 °C. The misalignment of the graphs along the x-axis might be due to inaccurate time measurements.

The induction cable used in the experiments was water cooled and malleable, while the induction coil in the simulations is modelled as solid copper. To mimic the water cooling and thermal isolation of the induction cable, the coil is not included in the heat transfer computation in COMSOL, which means that it does not affect the temperature of the plate. Because of the approximation of the coil being solid, the resistance in the coil and the cross sectional area is not an accurate representation of the cable used in the experiment. The voltage and current from the experiment can therefore not be implemented in the model, as the power the coil delivers will be too low. In the simulations, the current is therefore adjusted so that the power is equal to that of the experiments, see appendix G.

5.2.2 Creating the Mesh

The simulation is built on a 3D model. Therefore the mesh is built of 3D shapes, like boxes and pyramids. The mesh is different in the three geometries, as can be seen in figure 5.18.

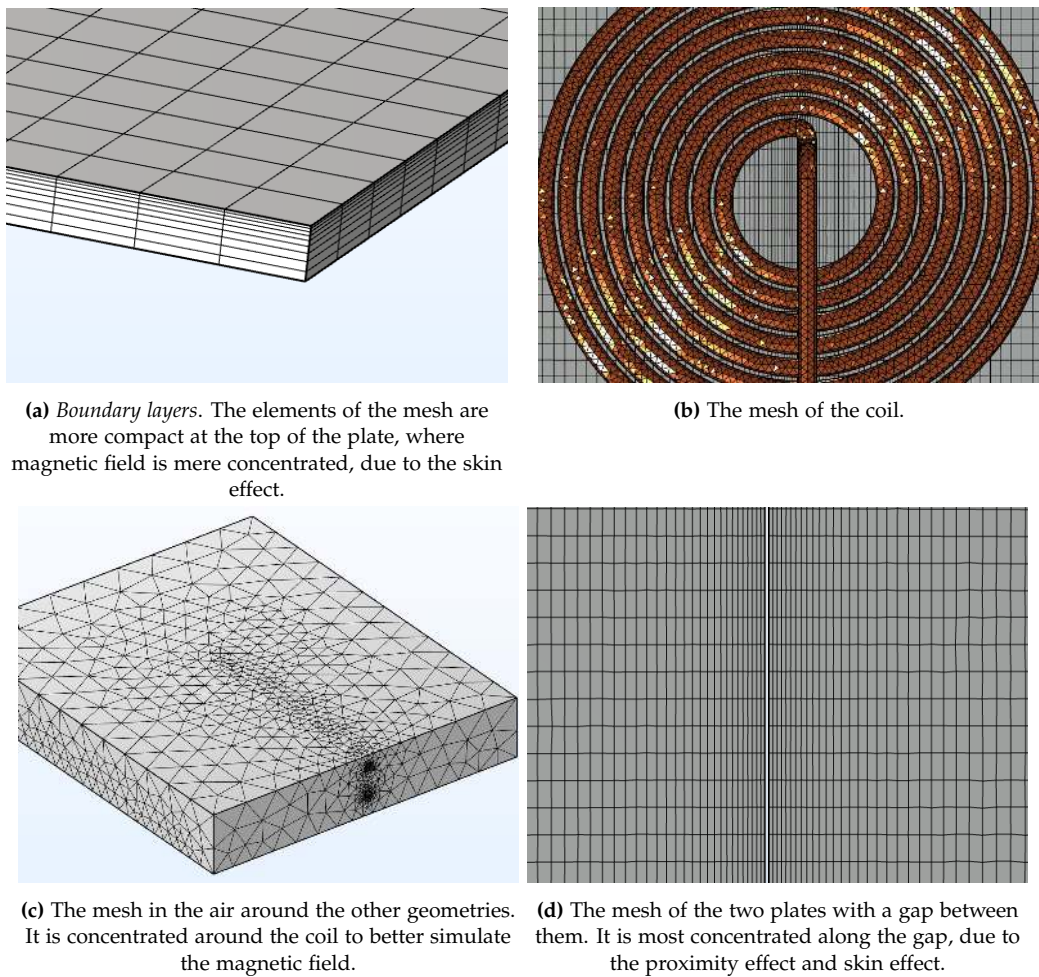


Figure 5.18: The mesh in the different parts of the geometry.

5.3 Validation of Model

In this section, specific experiments will be compared to simulations, with the purpose of validating the FEM-model. For each experiment a comparison of thermal images from both the experiment and the simulation, as well as a graph showing a comparison between cut lines¹, are presented.

When choosing the experiments to use for validating the model, three "single plate" experiments, three "two plate" experiments, and one experiment with a bigger coil geometry were picked, to limit the amount of simulations that had to be computed. The chosen experiments represent a spectrum of the relevant variables, coil-steel distance for the single plate, and gap distance for the two plate experiments.

¹The cut line is a line drawn on the surface of the plate, on the opposite side of the coil. The line is drawn from the centre of the coil to the left side of the plate. An example of how such a cut line is placed can be seen in figure 5.10.

While the temperature color tables of COMSOL and the thermal camera are very similar, there are slight differences, especially at the maximum and minimum of the color ranges. The maximum temperature of the thermal camera is white and brighter than COMSOL's maximum color, which is a very light yellow. The minimum color of the thermal camera is a slightly lighter blue than the minimum color in COMSOL.

5.3.1 Single plate

The "single plate" experiments allow comparison between simulation and experiments, without the added complexity of a gap. In these three experiments, only the distance between the coil and plate was varied manually. In all "single plate" thermal images, the color range is set from 20 °C to 240 °C.

Experiment #1

Coil-steel distance: 31 mm | Frequency: 6.4 kHz | Coil Power: 8.0 kW

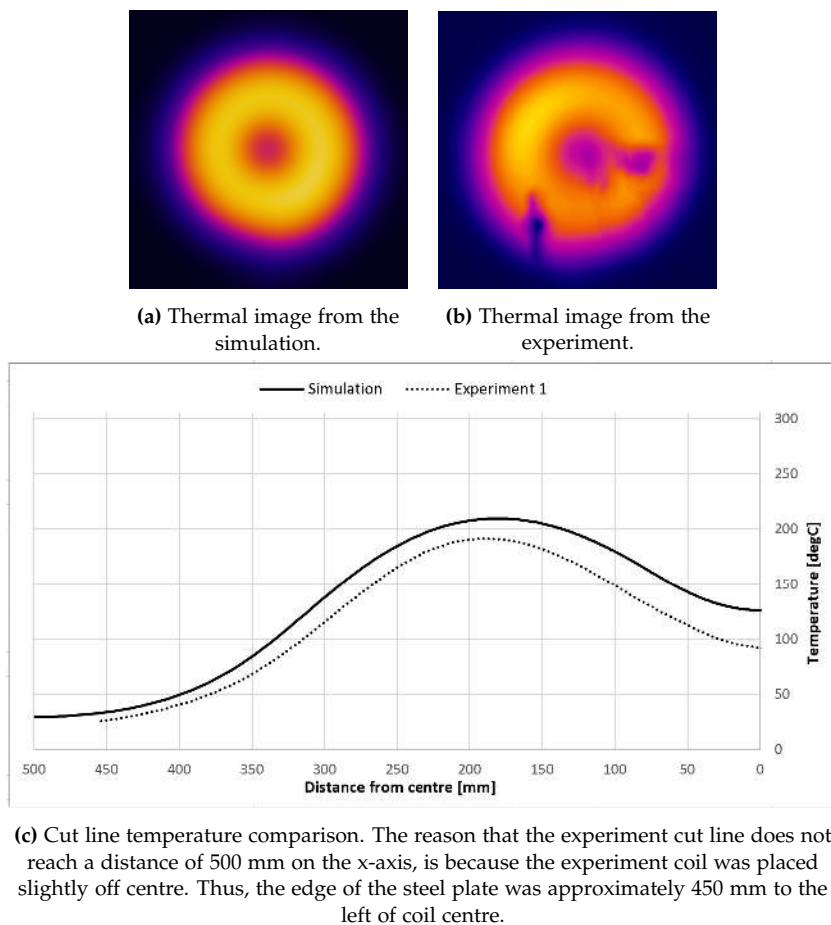


Figure 5.19: Comparison between the simulation and experiment after 440 seconds of heating, when a maximum temperature of 200 °C was measured in the experiment.

The simulation reaches higher temperatures than the experiment. The maximum temperature of the simulation cut line is 212 °C, while the maximum temperature of the experiment cut line is 190 °C. In figure 5.19c, it can be seen that the biggest difference in temperature occurs at the centre of the coil, which could be partly due to small differences between the CAD-designed coil model, and the actual induction cable used in the experiments.

Experiment #3

Coil-steel distance: 53 mm | Frequency: 6.3 kHz | Coil Power: 7.1 kW

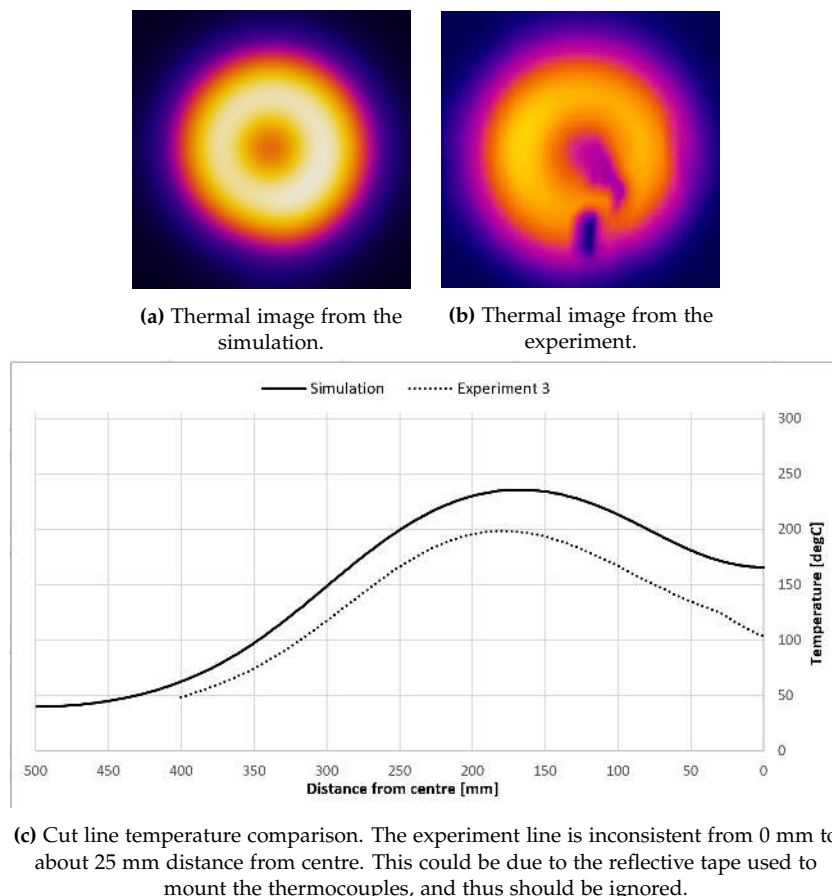


Figure 5.20: Comparison between the simulation and experiment at 613 seconds, when a maximum temperature of 200 °C was measured in the experiment.

In figure 5.20 the maximum temperature of the cut line is 236 °C for the simulation and 199 °C for the experiment. The simulation is more accurate towards the edge of the plate, than at the maximum temperature and the centre.

Experiment #4

Coil-steel distance: 59 mm | Frequency: 6.3 kHz | Coil Power: 6.8 kW

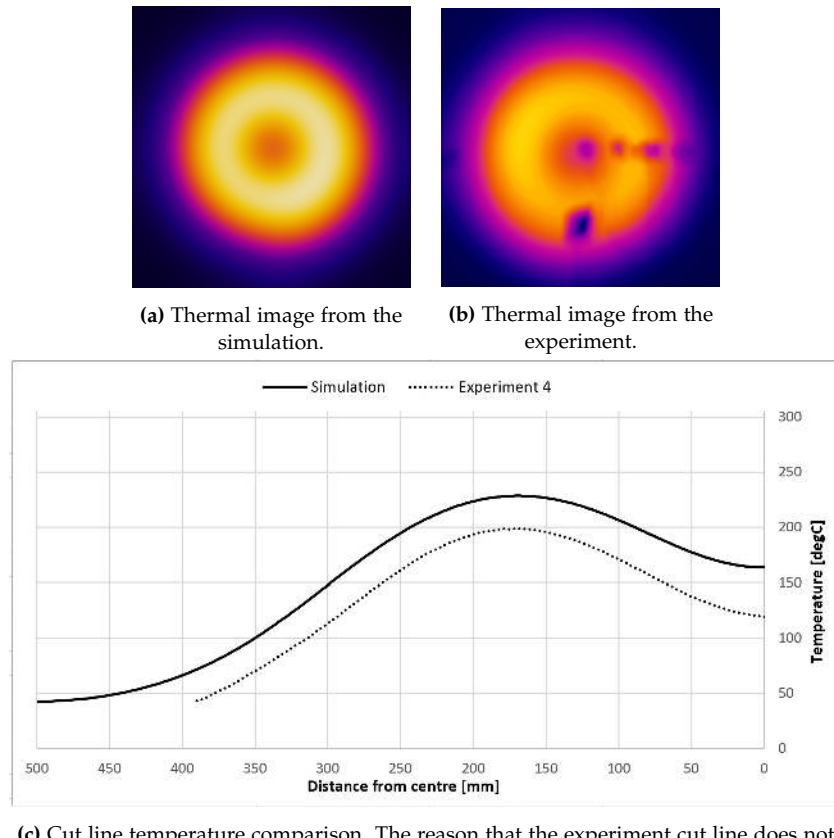


Figure 5.21: Comparison between the simulation and experiment at 657 seconds, when a maximum temperature of 200 °C was measured in the experiment.

In figure 5.21 the maximum cut line temperature is 228 °C for the simulation and 200 °C for the experiment. The curvature of the cut line temperatures of this experiment are similar, but generally the simulation is about 30 °C higher than the experiment.

Comparisons of the "Single Plate" Experiments

The simulation with the shortest coil-steel distance and the shortest running time is the most accurate of the three. Simulation #3 and #4 have similar inaccuracies, however simulation #3 is more accurate towards the edge of the plate. All three simulations reached higher temperatures than the experiments they were based on.

The cut line max temperature is 190 °C in experiment #1, and about 200 °C in both experiment #3 and #4. This is because the experiments were stopped

whenever any point on the plate reached 200 °C, and this point does not coincide with the horizontal cut line in experiment #1. The reason that the maximum temperature is more localised in this experiment, could be due to part of the induction cable not being sufficiently held in place by the zip ties, and thus hanging closer to the steel plate. This is noticeable in figure 5.19b. This would be accentuated in the experiment with the shorter coil-steel distance, which could explain why the maximum temperatures of experiments #3 and #4 are less localised.

5.3.2 Two Plates

To validate the model's ability to simulate the skin effect and proximity effect in the gap, a simulation is done to recreate the results from experiment #8, #9 and #10.

Experiment #8

Gap distance: 2.8 mm | Frequency: 6.1 kHz | Coil Power: 7.8 kW

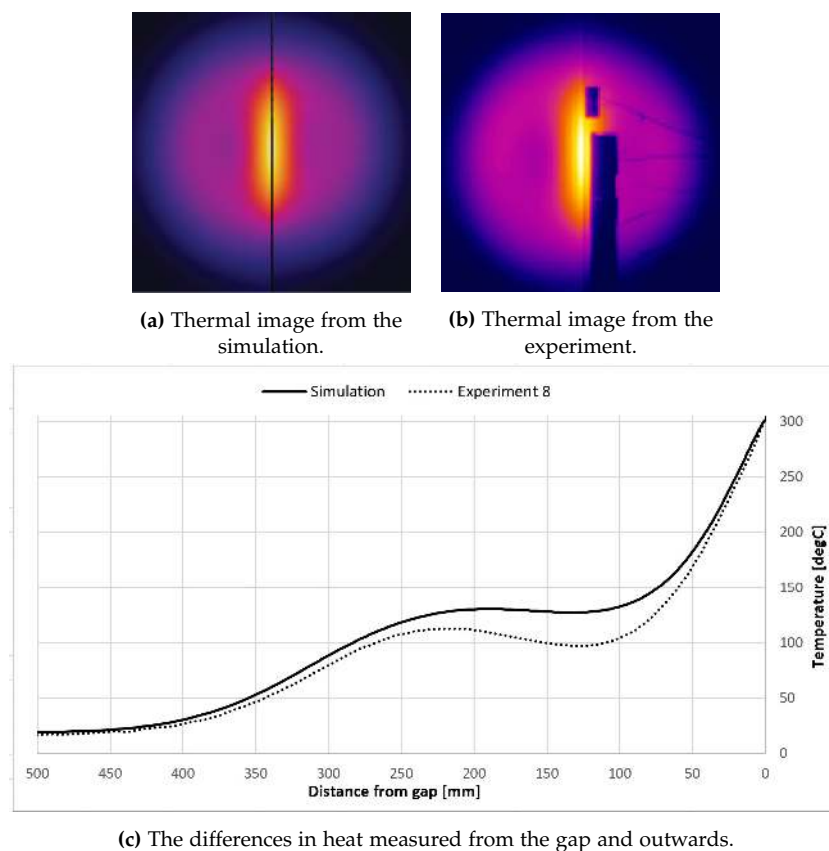


Figure 5.22: Comparison between the simulation and experiment at 294 seconds, when a maximum temperature of 300 °C was measured in the experiment. The colour range of the thermal image ranges from 20 °C to 310 °C

As can be seen in figure 5.22a and 5.22b, the thermal image from the simulation looks similar to the thermal image of the experiment. There are some inconsistencies such as the heat of the gap in the simulation is more evenly spread along the middle where in the experiment the heat is more concentrated in the centre of the gap. As can be seen in graph 5.22c, the model reaches too high temperatures in the cold spots next to the gap. This temperature difference in the cold spots is always less than 30 °C. In other areas, the simulation is behaving the same way as the experiment, and it is reaching the right maximum temperatures.

Experiment #9

Gap distance: 5.6 mm | Frequency: 6.1 kHz | Coil Power: 7.8 kW

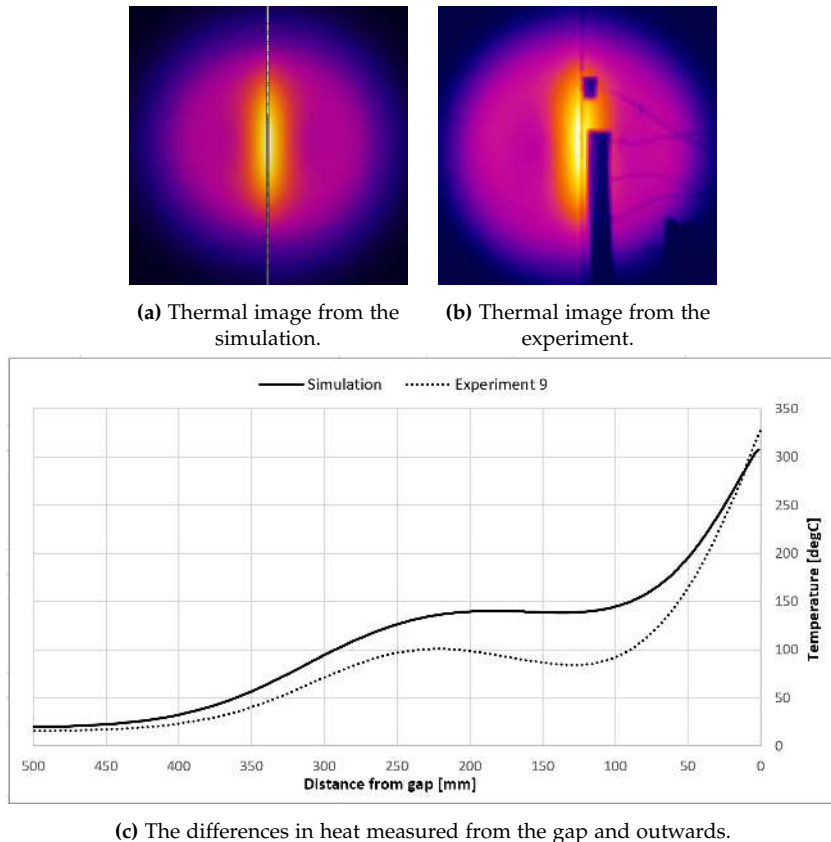


Figure 5.23: Comparison between the simulation and experiment at 327 seconds, when a maximum temperature of 325 °C was measured in the experiment. The colour range of the thermal image ranges from 20 °C to 300 °C.

In the comparison images of experiment #9 and the associated simulation (figure 5.23a and 5.23b) it is clear to see that the simulation is behaving as the experiment. In both the simulation and experiment, the most intensive heat is generated near the vertical centre of the gap. The heat is more evenly spread

out over the middle in the simulation. When looking at the graph 5.23c it can be observed that the model has bigger problems simulating the wider gap. The model is simulating a temperature difference of 60 °C in the colder spot beside the gap. This could be explained by the permeability of the steel being modelled as a constant and not a variable. This will likely not cause substantial problems for the final simulation of a preheating situation, since the gap will be smaller than the 5.8 mm of experiment #9, but it is worth noting that the model has a problem simulating wider gaps.

Experiment #10

Gap distance: 1.88 mm | Frequency: 6.0 kHz | Coil Power: 7.7 kW

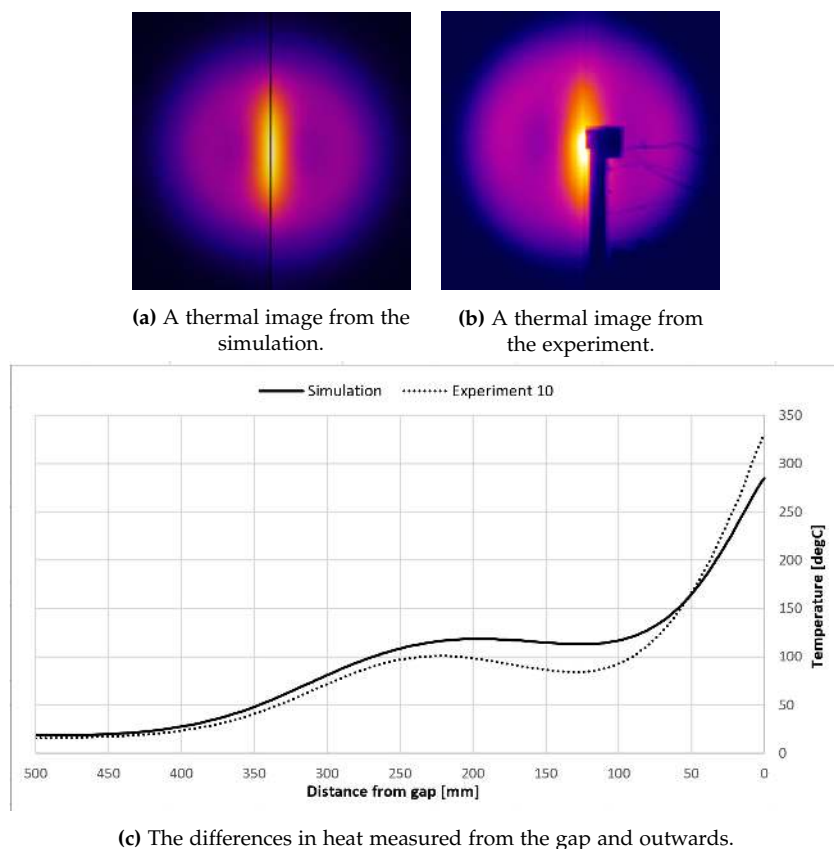


Figure 5.24: Comparison between the simulation and experiment at 260 seconds, when a maximum temperature of 325 °C was measured in the experiment. The colour range of the thermal image ranges from 20 °C to 280 °C

In the comparison of experiment #10 and the associated simulation, the same problem occurs with most of the heat being generated in the centre of the gap instead of being more evenly divided along the gap, as can be seen in figure 5.24a and 5.24b. As previously discussed in section 5.1.3, this error of local high temperatures in the centre can possibly be explained by inconsistencies in the gap. This can also be observed in graph 5.24c, where the maximum

temperature of the simulation is around 40 °C lower than in the experiment. From the graph 5.24c it can also be observed that the temperature in the cold spot beside the gap is the closest of all three comparisons with a maximum temperature difference of around 25 °C. From this, it can be concluded that the model generates more accurate results simulating a smaller gap, but at the cost of a less accurate maximum temperature.

5.3.3 Different Coil Geometry

To validate the model's ability to simulate different coil geometries, a simulation comparing experiment #12 is set up. This is done since the experiments resulted in a higher power using a larger 12.5-turn coil. This higher power may be necessary in the final simulation of a preheating situation.

Experiment #12

Gap distance: 2.8 mm | Frequency: 6.8 kHz | Coil Power: 22.9 kW

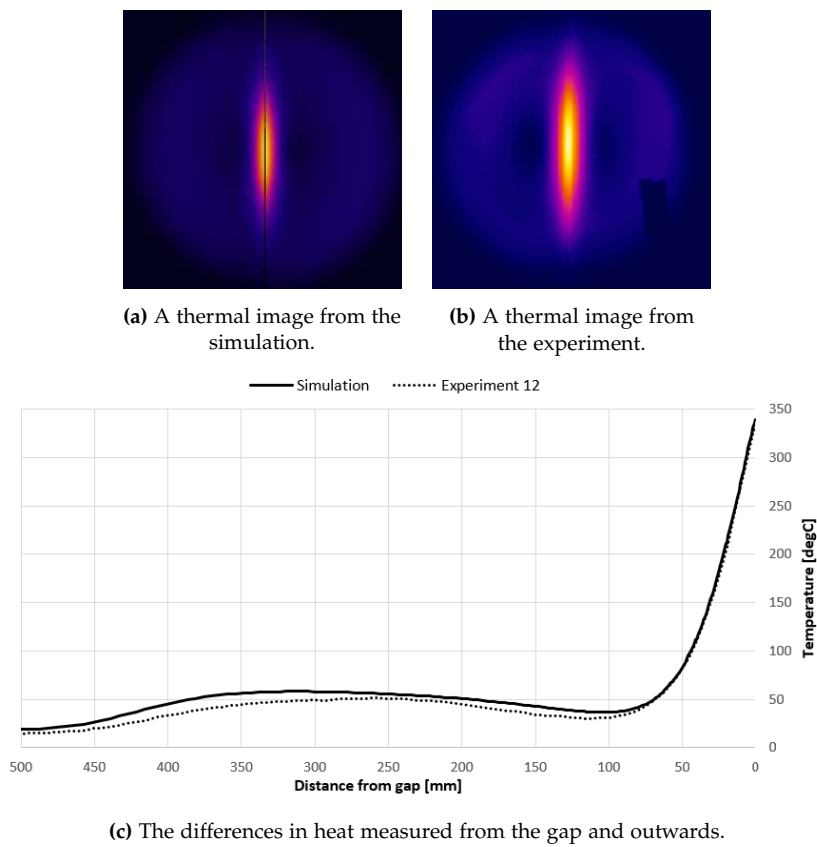


Figure 5.25: Comparison between the simulation and experiment at 59 seconds, when a maximum temperature of 340 °C was measured in the experiment. The colour range of the thermal image ranges from 20 °C to 350 °C.

When comparing the simulation with the experiment it can be observed that the larger coil does not make the model more inconsistent with reality. This

can be seen in figure 5.25a and 5.25b, where the thermal images show how the model concentrates the heat in the same locations as in the experiment. In graph 5.25c, it can be observed that the highest difference in temperature is no bigger than 15 °C with most of the simulations following the experiment. This simulation is the most accurate of the seven.

5.3.4 Results of Validation

To summarise the results of the validation, the average temperatures from the different data set used in the graph of this section is compared in table 5.6. This is done to get an estimation of how accurate the model in general is.

	Single plate			Two plates			12.5-turn coil
Experiment	#1	#3	#4	#8	#9	#10	#12
Avg. temp. experiment	119.05	142.55	143.78	90.01	85.61	86.24	53.79
Avg. temp. simulation	140.87	177.63	176.00	103.31	109.93	93.45	60.01
Difference	21.82	35.08	32.22	13.30	24.31	7.22	6.22
Avg. temp. difference	29.71			14.94			6.22
				Combined avg. difference			16.96

Table 5.6: The average temperatures (°C) from the cut line data and the difference between the simulations and the experiments.

In table 5.6 it can be seen, that the average temperatures of the three comparisons, are respectively 29.71 °C, 14.94 °C and 6.22 °C. The combined average temperature difference between the experiments and the simulations is 16.96 °C, where the simulation is always the highest. This number is in not conclusive of the accuracy of the model, but gives an idea of the accuracy of the model. From this it can be generalised that the model simulates higher temperatures than reality. Another tendency that can be seen in the comparisons is that greater distances in both the gap between the plates and the steel-coil distance, create bigger differences in the average temperature. The reason for this could be partly due the longer running time. With longer running times, inconsistencies could be allowed to develop. It could also be a general problem with the model's ability to simulate larger gaps. None of these problems with the model create a problem in the final simulation of a preheating situation, since the gap in this simulation is so small. Likewise in the final simulation, the running time to simulate induction heating is short. The only factor of importance from the validation is therefore the higher average temperatures, which will be taken into account in the final simulation.

5.4 Simulation of a Preheating Situation

This model builds on the experience gained in the previous section. The model is split into two steps to simplify the model and reduce computation time.

The first step is a 3D model, where the two steel plates under the coil move horizontally to mimic a preheating situation. The second step is a 2D model where a heat input - corresponding to the temperatures from the cross section of the 3D model - will be added. The 2D model is a simple time dependent simulation which only simulates the conduction and radiation of heat in the plane and therefore it requires low computing power to solve. In short, the end result will be to observe a 2D cross section over time, which in turns is heated using thermal data gained from a 3D study of induction heating. See figure 5.26.

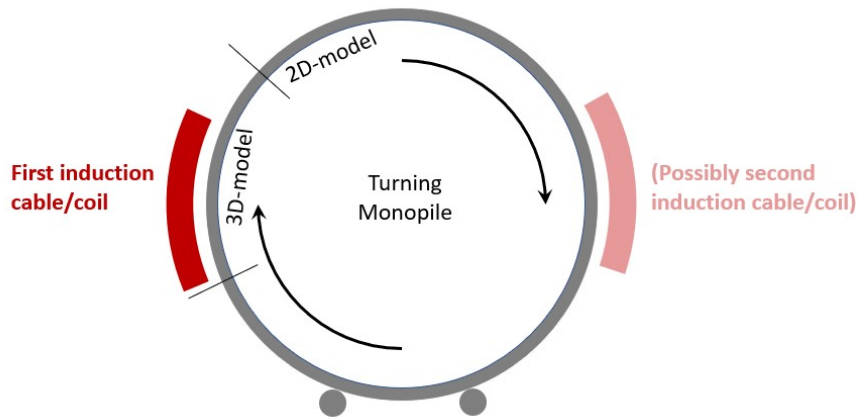


Figure 5.26: When welding, the circumference is rotated. The ability to rotate the monopile is utilized in the preheating process. This way, the induction coil(s) can remain stationary. The 3D simulated section is marked. After this, the simulation is modelled in 2D.

5.4.1 Step 1 - 3D

The first step of the simulation is a 3D simulation, where the steel plates are heated by the induction coil, this can be seen in figure 5.27. The difference between this simulation and previous simulations, is that the model is no longer stationary. In order to reflect the rotation of the monopile, the material under the coil in this simulation is fed/moved with a speed of 1 m/min, which equates to a rotation time of 25.1 min/rev. This speed is also used for welding, and the equipment at Bladt Industries is already capable of rotating the monopiles in this manner. The duration of the 3D simulation is set to one minute - equating to a distance of one metre. After this distance, the magnetic field, and thus the heating, becomes negligible. Because of this, a 2D map of the temperature at the end of the steel plates can be moved to a simpler 2D model to simulate conduction, convection, and radiation of heat only. The product of the 3D simulation, the 2D map of temperatures, will be used at every heating instance in the next step.

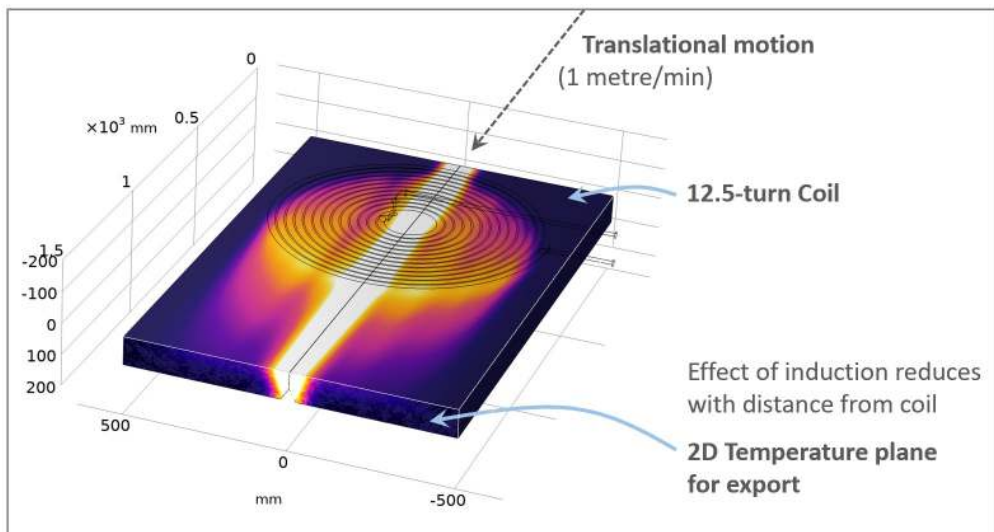


Figure 5.27: The geometry of the 3D model in the first step. Color scale only for visualisation. Exact export temperatures from 2D plane can be read in figure 5.34

5.4.2 Step 2 - 2D

The second step of the simulation is a 2D simulation, which can be seen in figure 5.28. In the second step, the temperatures taken from the first step (3D) is used to determine a heat input in the cross-sectional 2D plane. This can be done because the change in temperatures on the 3D cross section are proportional to the energy added in each mesh element, cf. section 4.1.1, where the mass and specific heat capacity are constants (important that mesh is similar). This heat input is added as a fabricated power for the duration of one time step (60 ms). This instant of heating power is calculated to result in a temperature profile in the cross section similar to the temperatures derived by the 3D simulation. The simulation (cooling only) then runs for a given amount of time, calculated to be the time of one rotation, before the same heat input is added to the plates during each rotation. This process of adding heat, repeats until a satisfactory temperature, given by the EN-1011-2 standard, is reached. Using this standard to set a goal temperature for the preheating process, a heat input must be determined. Using the calculations from appendix I, and assuming a weld heat input of 6-8 kJ/mm, gives a preheating temperature of 100 °C. The temperature is measured 75 mm from the weld gap as given by the standard.

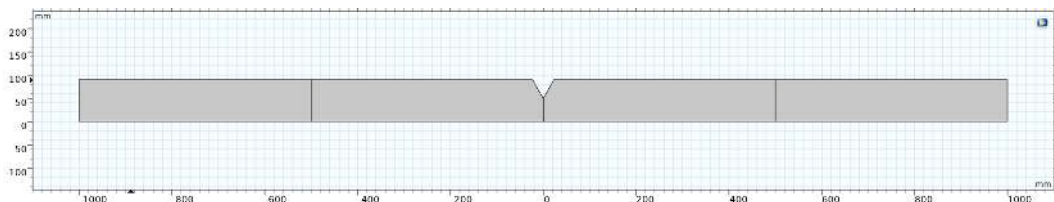


Figure 5.28: The geometry of the 2D model in the second step.

Physics

The physics used in the first step of the simulation are the same as defined in chapter 4 and in section 5.2.1. The model in the second part of the simulation uses only the physics of thermodynamics since the heat from the induction heating is simulated as a simple heat input. Rotation, as mentioned in subsection 5.4.2, is reflected by implementing translational motion in the model.

Geometry

The weld geometry of the plates in the model are similar to the weld geometry provided by Bladt. A cross section of this geometry can be seen figure 5.29.

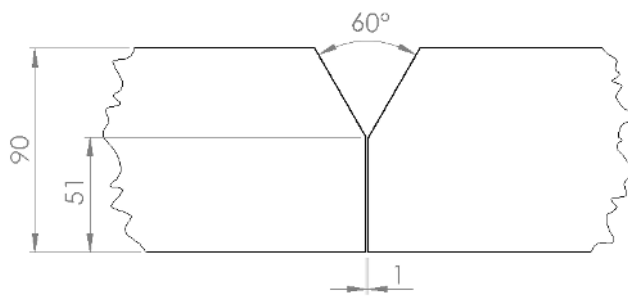


Figure 5.29: The geometry of the weld section. All measurements of lengths are in mm.

In the first step of the simulation, there are four different domains which can be seen in figure 5.27:

Domain 1 and 2: The two steel plates with the weld section milled into the middle. Each of the plates measures 1.5 metres in length and 0.5 metres wide.

Domain 3: The 12.5-turn coil with a diameter of 0.9 metres and is placed underneath the plates where the gap is smallest.

Domain 4: The box of air surrounding the geometry measures 1.5 metres in length, 1 metre wide and 0.4 metres high. The geometry in the second step of the simulation is a 2D geometry of the two plates, where each plate has a width of 1 metre.

In the second step (2D), domain 3, the coil, is negligible. This means that the 2D simulation only contains three domains.

Mesh

The mesh of the different domains are illustrated on figure 5.30. The mesh is as the previous simulations built up of squares, and concentrated towards the gap and surface facing the coil. This gives more accurate results, as it takes account for the proximity- and skin effect described in chapter 4.

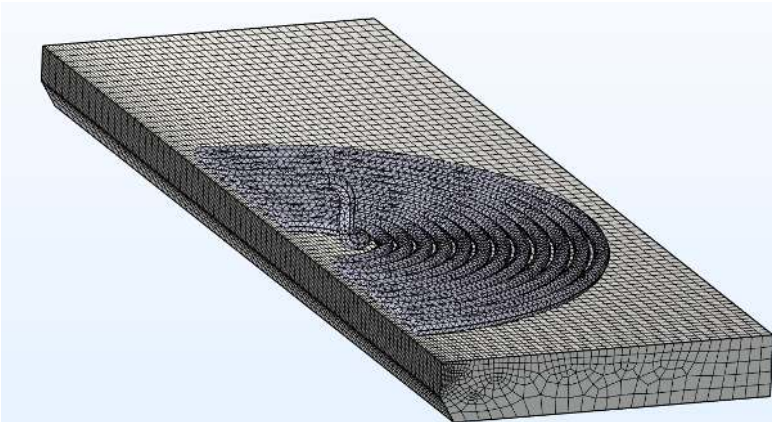


Figure 5.30: The mesh of the 3D simulation. Note the model is cut in half to show the mesh in the gap.

Materials

S355

S355 is a fine grain thermomechanically weldable steel [46]. As opposed to the first model, this model uses S355 steel. The first model uses S235 because it was the same steel used to conduct the experiments. However the monopiles at Bladt are constructed from S355 steel and therefore the latter model uses this type of steel. The material properties regarding thermodynamics and electromagnetism of both steel types are very similar. Meaning most properties are the same as in the previous models, see table 5.3 and table 5.7.

Property	Value	Unit
Specific heat capacity at constant pressure [47]	475	$\frac{\text{J}}{\text{kg K}}$
Density [47]	7850	$\frac{\text{kg}}{\text{m}^3}$
Thermal conductivity [47]	40	$\frac{\text{W}}{\text{m K}}$

Table 5.7: Constant material properties for S355 used in the model.

Air and Copper

The properties for air and copper are the exact same as used in the first model, see subsection 5.2.1.

5.4.3 Results of Simulation

To evaluate the results of the final 2D simulations, two points in the cross section will be the primary focus. It is known that both maximum and minimum temperatures during welding and preheating have to be monitored. This will be done in two different locations. The maximum temperature is expected within the gap, on the surface closest to the coil, which in this case is the

opposite side of the welding geometry (the blue point on figure 5.31). The minimum temperature needs to be monitored on the surface 75 mm from the gap, according to EN-1011-2. The temperature is measured on the same side as the welding geometry (green point on figure 5.31).

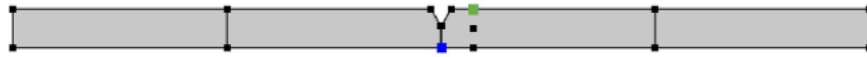


Figure 5.31: Illustration of the points used to measure temperature. Green is 75 mm from the welding gap. Blue is in the gap where the temperature is highest. Similar colour identifications are used in figure 5.32.

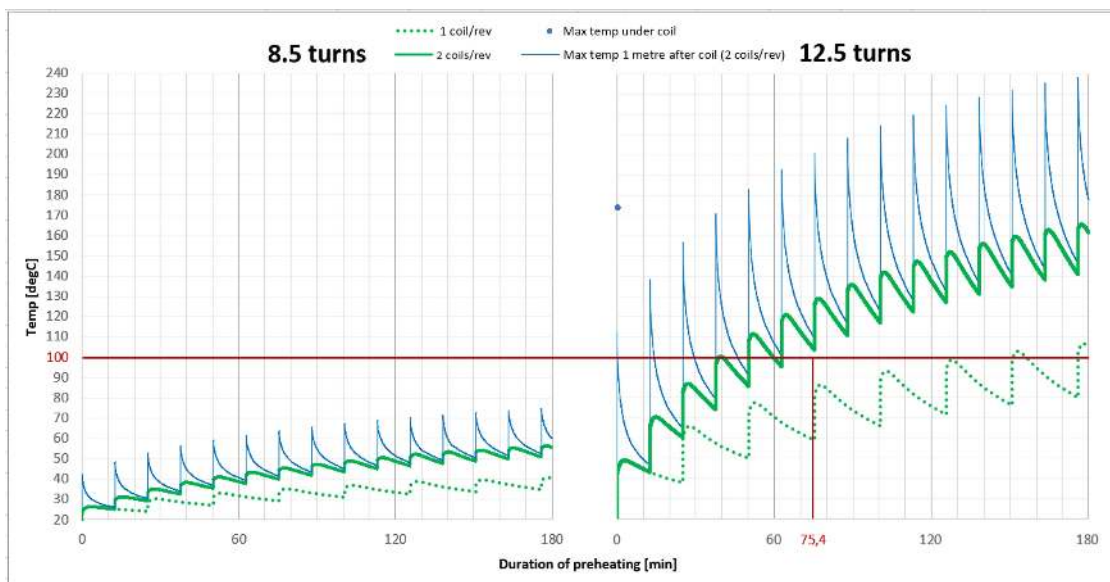


Figure 5.32: Final simulations with a revolving monopile heated by a 8.5-turn coil and 12.5-turn coil, respectively. Red is the time to reach desired temperature 75 mm from welding gap using two large 12.5-turn coils. Full-page view in appendix K.

One 8.5-turn coil

First, an induction preheating process is simulated with the coil of 8.5 turns. It was experienced that it did not reach the desired temperature at the green measurement point (75 mm from the gap, dotted green line on the left half of figure 5.32) within a realistic time duration. This is plausible as the steel cools for about 25 minutes between each encounter with the coil.

Two 8.5-turn coils

Adding an extra coil of similar power level and geometry reduces the cooling time between each encounter with a coil. Additionally, the total power added to the system doubles. Despite this, two coils of 8.5 turns did not reach desired minimum temperatures 75 mm from the gap (solid green line on the left half of figure 5.32) within a reasonable time. The maximum temperature is not an issue (blue line on the left half of figure 5.32).

One 12.5-turn coil

During section 5.3, it was validated that an accurate model of the larger 12.5-turn coil had been set up. Furthermore, this coil provided a focused heat input near the gap. Placing one such coil around the circumference of a monopile results in higher temperatures (the dotted green line on the right half of figure 5.32). After 3 hours, the temperature is near the target temperature of the preheating process ($100\text{ }^{\circ}\text{C}$, according to EN-1011-2). This is slower than pre-heating using gas, which takes about two hours. As with one 8.5-turn coil, the steel is cooled for about 25 minutes between each encounter with the coil.

Two 12.5-turn coils

With two larger coils, the cooling time is reduced. Furthermore, the heat input is doubled. The green point of the steel surface (see figure 5.31 and green solid line on the right half of figure 5.32), located 75 mm from the gap, now reaches proper temperatures above the desired $100\text{ }^{\circ}\text{C}$. This happens after 75.4 minutes, which equates to three full revolutions of the monopile.

With temperatures and heat inputs of this magnitude, it is important to monitor the maximum temperatures. The maximum temperature in the slice, 1 metre after the coil, is shown as the blue line on the right half side of figure 5.32. At this point, the steel reaches a maximum temperatures of less than $200\text{ }^{\circ}\text{C}$ at the turn-off point at 75.4 minutes. Here, the steel has already moved 1 metre from the coil centre. Because of this, higher temperatures are expected. Experience from the 3D simulation can be drawn to approximate a maximum temperature at coil encounter from known values. After 75.4 minutes, only the temperature one metre after the coil is known, as the model is never converted back to 3D. The 2D simulation never analyses the area under the coil, but adds a heat input after 1 metre - equivalent to temperatures from the 3D simulation after 1 minute of cooling/translational motion. In the 3D simulation, the maximum temperature after 1 metre is $116\text{ }^{\circ}\text{C}$ at the time $t=0$. The highest temperature recorded under the coil is $173\text{ }^{\circ}\text{C}$. At the temperature under the coil during this first heating instance in 3D (at $t=-1\text{ min}$), temperature data from 2, 3, 4, and 5 min after the heating, can be gathered from the 2D simulation. Using this temperature data, the maximum temperature under the coil after the sixth heating instance can be calculated to approximately $255\text{ }^{\circ}\text{C}$ (see figure 5.33 and calculations in appendix J). This is below the specified maximum temperature of $550\text{--}650\text{ }^{\circ}\text{C}$, specified by Bladt in appendix H.

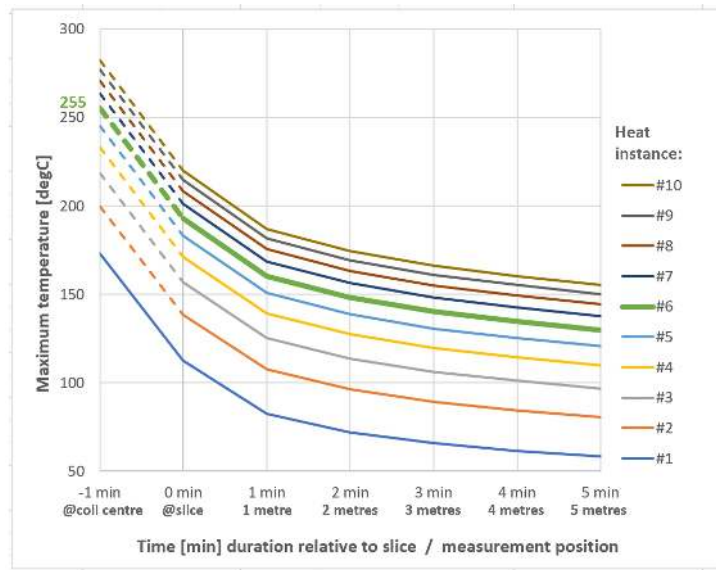


Figure 5.33: Maximum temperatures during each heating instance and the following six minutes. The calculations can be found in appendix J.

5.4.4 Verification of Simulation

Temperatures from the cross-sectional plane from the 3D simulation is used to verify the power input that was designed to be a fabricated heat source in 2D. The temperatures are all drawn from a cut line located at the surface nearest the coil. The temperatures from 3D are measured at the last frame, whereas the temperatures from 2D are drawn from a similar cut line 60 ms into the 2D simulation (after the designed power input has been applied). The cut line temperatures match, thus the method of applying a designed power input in 2D to convert from 3D has been verified (see figure 5.34).

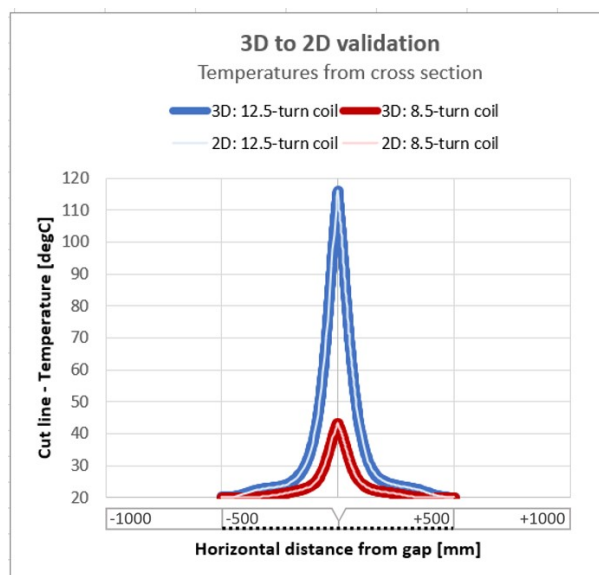


Figure 5.34: Temperatures from end of first step (3D) and beginning of second step (2D).

5.4.5 Energy Consumption of the Final Model

The energy consumption and costs of induction preheating is calculated based on the power and time data extracted from the COMSOL Multiphysics model. The coil power is 22.3 kW, and from this, the total power consumption can be estimated following the model illustrated on figure 5.35. The model is based on realistic and tested assumptions regarding efficiency and power loss in induction heating.

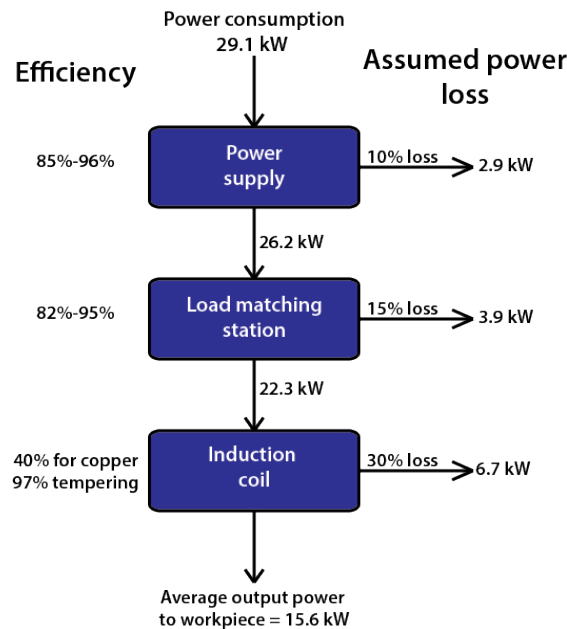


Figure 5.35: The power efficiency of induction heating and the assumed losses of energy of both the heating and the generating of high frequency current [48].

Following the model on figure 5.35, the power draw of each 12.5-turn coil, is estimated to be 29.1 kW. In the preheating situation where two coils are used, the drawn power is therefore 58.2 kW. The induction coils heat the monopile sections for a total of four revolutions before reaching the desired temperature of 100 °C, which takes 75.4 minutes.

$$\frac{58.2 \text{ kW} \cdot 75.4 \text{ min}}{8\text{m} \cdot \pi} = 2.91 \frac{\text{kWh}}{\text{m}} \quad (5.1)$$

The energy consumption per metre, preheated monopile section, is calculated to be $2.91 \frac{\text{kWh}}{\text{m}}$. Therefore the cost of induction as a preheating method can be calculated to:

$$2.91 \frac{\text{kWh}}{\text{m}} \cdot 1.08 \frac{\text{DKK}}{\text{kWh}} = 3.14 \frac{\text{DKK}}{\text{m}} \quad (5.2)$$

The CO₂e emission of induction is calculated to be:

$$2.91 \frac{\text{kWh}}{\text{m}} \cdot 0.125 \frac{\text{kg CO}_2\text{e}}{\text{kWh}} = 0.36 \frac{\text{kg CO}_2\text{e}}{\text{m}} \quad (5.3)$$

5.4.6 Partial Conclusion

It can be concluded that using induction to preheat thick steel plates instead of gas, is significantly cheaper, both economically and environmentally. Comparing the two methods, induction consumes about 13 times less $\frac{\text{kWh}}{\text{m}}$, emits about 26 times less $\frac{\text{kg CO}_2\text{e}}{\text{m}}$ and is about 5 times cheaper in energy costs, assuming that Bladt preheats to 100 °C. However, the final results of this simulation are a rough estimate, since the model in general overshoots the reality by around 17 °C, and the power consumption is based on an estimate of efficiency and power losses.

6. Discussion

In this chapter the results of the experiments, simulations and the general approach of this study will be discussed. The main focus of this discussion will be the possible sources of error, their impact, and why they occurred. This chapter will also present the expectations prior to the study and how they compared to reality. Finally the approach to the final simulation of a preheating situation will be discussed.

6.1 Expectations and Results

After first visiting Bladt Industries and hearing how the gas preheating affects the temperature in the room, it was assumed that there would be a lot of energy waste. The expectation was therefore that preheating using induction would be more energy effective as a high rise in the room temperature indicates energy waste.

Preheating large steel plates was tested by simulating using COMSOL and gave the following results:

	Energy consumption
Induction heating	2.91 $\frac{\text{kWh}}{\text{m}}$
Heating blanket	5.4 $\frac{\text{kWh}}{\text{m}}$
Gas heating	38.5 $\frac{\text{kWh}}{\text{m}}$

Table 6.1: Results of simulation of induction heating compared to heating blankets and gas heating.

As can be seen in table 6.1 the energy waste of gas heating is very high. This becomes most apparent when comparing it directly to induction heating which uses around 13 times less energy. Induction heating also performs better than the heating blankets in the comparisons. The energy consumption of induction heating is about half that of the heating blankets. The expectations at the start of the project was that the efficiency of the heating blankets and induction would be relatively similar. It is important to note that these are directly compared, even though the two technologies are not used in the same process step, when manufacturing monopiles. Heating blankets are used in a stationary and flat situation, whereas gas burners is used in a curved and dynamic station.

6.1.1 Experiments

To validate and set up a more precise model, experiments with steel plates and an induction heater were conducted over two days at Bladt Industries. A

model that is a good depiction of reality needs to be validated with multiple experiments. A better model can be set up with more experiments where multiple variables are tested. Due to limitations of resources and time, thirteen experiments were conducted where only three different parameters were studied. The setup of the experiments will be discussed and assessed in the following section.

Setup of Experiments

Plate Size

The setup was first and foremost limited by the time constraints from Aalborg University, and the fact that this is a semester project of limited time. It was therefore necessary to choose which experiments would give the best data to validate the model. Because of these limitations it was determined to only experiment on steel plates with a thickness of 12 mm. This was due to the fact that the steel plates at 90 mm thickness weigh around 1400 kg each ($1 \text{ m} \cdot 2 \text{ m} \cdot 0.09 \text{ m} \cdot 7800 \frac{\text{kg}}{\text{m}^3} \approx 1400 \text{ kg}$), which would make it difficult to move the plates. The plates in the experiments weigh only around 190 kg ($1 \text{ m} \cdot 2 \text{ m} \cdot 0.018 \text{ m} \cdot 7800 \frac{\text{kg}}{\text{m}^3} \approx 190 \text{ kg}$), making them easier to deal with and it would take even longer to heat and cool the plates. Therefore, thinner plates and more time to do more experiments was prioritised.

Steel Type

Steel plates of type S235 were used, instead of S355, in the experiments as they were the only available steel type in the desired dimensions. Furthermore, it was not possible to get an accurate welding geometry of the relative thin steel plates. It was agreed that this more simple geometry could be allowed because it would also be easier to replicate in COMSOL as well as a more simple example of the proximity effect. The limitations regarding steel geometry, welding geometry and steel type should not have a significant impact on the simulations as these are the parameters that can be changed in COMSOL once the model was validated.

Water Cooling Between Experiments

Due to the limited time and plates available, it was not an option to let the plates air cool to room temperature after every experiment. The plates were air-cooled followed by water cooling until they reached a temperature of around 20 °C. Because of differing initial temperatures of the steel plates, only thermal images with a maximum temperature above 30 °C were included in the data set. This was done to get a more direct comparison of the experiments to better discover tendencies regarding induction heating. Using water to cool the plates created some problems with tension in the steel. This resulted from the rapid heating, causing the plates to become slightly bent after each experiment. The bent plates caused inaccuracy in the distance between the coil and

the plate causing more localised hot spots. On the second day, it caused the gap between the plates to become more uneven.

Coil Management

The induction cable was fixed to a plywood plate with cable ties. Plywood was chosen to have as little magnetic material within the magnetic field as possible. Likewise, it was an easy solution when the coil size needed to be changed. However, due to the limited space between the turns of the cable, it was not fixed all along the cable but only in a horizontal and vertical line. It was expected that this would be sufficient, however it was not. This resulted in segments of the cable being slightly loose and able to tilt forward towards the steel plate.

Distance Between Edge and Coil

The fact that the induction coil was not precisely placed at the centre of the steel plate, and that the distance between them varied gave some irregularities in the data set. It was therefore difficult to compare the data from the experiments and the simulations because these imperfect setups can cause differences in temperature in the steel plate.

Limited Experiments with Varying Coil Geometries

Only one experiment was conducted with a larger coil geometry. More experiments with differing coil geometries could have been beneficial, as it could have shown a system in how the coil geometry affects the heating of a steel plate. The simulation run for the experiment turned out very accurate, but since only one experiment was conducted for a bigger coil, it is not possible to say if it is generally better.

Measuring Equipment

To measure the temperature throughout the steel plate while heating it, two main methods of measuring were used: A thermal camera and thermocouples. Besides the two main methods of measuring, a handheld laser thermometer and heat chalk were used.

Handheld Thermometer and Heat Chalk

The handheld thermometer could give an idea of the temperature before the more accurate thermal camera was moved from its stationary position. Likewise, the heat chalk gave a reference point of the temperature. However, because the heat chalk did not instantly melt, when the temperature reached the right temperature, it was difficult to use the heat chalk as a reference during the heating process. The chalk is designed to quickly verify if an object is above a given temperature.

It became clear during the experiments that the different means of measuring

temperature all gave slightly different results. The heat chalk and the handheld thermometer were ruled out as the most inaccurate means of measuring. However, the thermocouples and the thermal camera also gave differing results, in the range of 20-30 °C.

Thermocouples

One of the issues with the thermocouples was keeping good contact between the end of the cables and the steel. It was preferred to have the cable welded to the steel plate, however the heat from the welding equipment, melted the cables and was not a liable solution. A potential solution could have been to drill small holes in the surface, which could have allowed welding the cables to the plate. However, this would have meant that the measurements would not be taken on the surface of the plate, and would have caused difficulty when moving or cooling the plate. Subsequently, heat resistant tape was used to hold the cables in place. The heat resistant tape was unable to stick to the rough surface of the oxidised steel plates, especially when the plate became hot. It was not always clear when the cables lost contact with the steel plates and as a result not clear when the thermocouples were reading correctly. Heat resistant aluminium tape turned out to be a better way of keeping the cables in place, however its reflective surface blocked part of the view of the camera, which meant that the view of one half of the plate could not be used for analysis. This was considered sufficient due to the symmetry of the coil. However, if a second round of experiments were to be conducted, it would be preferred not to have anything blocking the view of the plate. Another cause of imprecision in the thermocouples, is the disturbance from the magnetic field generated by the coil. This is seen clearly on figure 5.13, where the thermocouple closest to the coil measured false values, and returned to normal when the coil was turned off. This happens because the magnetic field induces electricity in the wire, also described by Faraday's law [49].

Thermal Camera

A test of the thermal camera was conducted. The test consisted of heating a steel bar in an oven, to a given temperature and measuring it with the thermal camera. Based on this test, it was decided that the thermal camera was the most accurate equipment for measuring the temperature of the steel plates. The thermal camera measured within 0.2 °C of the oven, see appendix F.

6.2 Methods

When conducting experiments and setting up the model, many choices were made, both in regards to data processing, defining the model, and validating the models. In this section, the different choices and their consequences on the model, will be explained.

6.2.1 Data Processing

Empirical Data: Thermal Images and Camera Placement

All data used in the model building and validation of the model was from the thermal camera. The reasoning for not utilising the data from the thermocouples were the large inconsistencies in the data sets and the fact that they logged lower temperatures than the thermal camera, which had been proven to be accurate. The thermal camera also had the advantage of including more data, since every pixel of the thermal image could be analysed. One problem with using the thermal camera was the lack of length measurements in the picture, since both edges were not always within the camera's vision, especially in the two plate experiments. This length measurement was necessary to compare the experiments with the simulations. The length of a pixel in the thermal image was estimated from experiment #12 (see appendix D), where the height and width of the camera's view had been measured. This estimation could be a source of inconsistency in the data processing, since small changes in camera placement could make a difference.

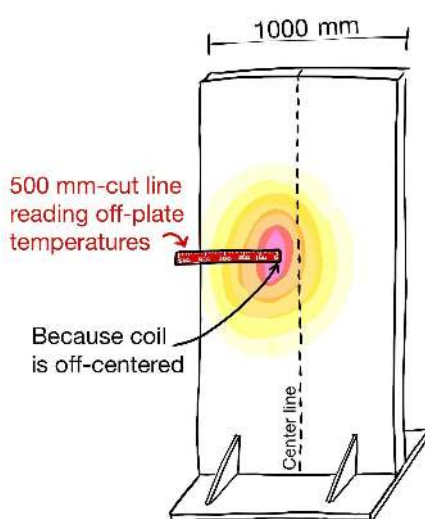


Figure 6.1: Some temperature values are measured off the plate, when the coil is not centred on "single plate".

"Single Plate" Experiments: Cut Lines from Coil Centre

In the "single plate" simulations, the cut lines from which the temperatures are measured are placed with a starting point in the centre of the coil and then measures the temperatures outwards to the left in a horizontal line 500 mm long. However, when placing the cut lines in the thermal images, the coil was not always perfectly centred on the steel plates. This meant that if the starting point of a cut line was placed in the centre of the heated circle made by an uncentred coil, then the end point of the cut line would sometimes end outside of the plate, measuring ambient temperatures. Such temperatures was removed from graphs. See figure 6.1.

"Two plate" experiments: Cut Lines from Gap

In the experiments with two plates and their associated simulations, the starting point of the cut line is at the maximum temperature located in the gap, at the edge of the left plate. All cut lines measured the temperatures on the surface opposite side from the coil. These cut lines were primarily used in the

validation of the model, in comparisons of the experiment and simulation. This position was chosen, since it was the only way of making sure they were measuring comparable sets of data given the difficulties placing the data point from the thermal camera. 1D temperature cut lines were chosen, because using 2D temperature images would result in 3D comparison diagrams (x,y,temp). Comparing two planes in a 3D diagram would not be as comprehensive as a 2D comparison diagram.

6.2.2 Model and Simulation

The decision to use constant material properties in separate *frequency domain* and *time dependent* study steps, instead of variable material properties in the *frequency transient* study step, acted as a compromise between the accuracy, simulation time, and computational requirements. This decision allowed for more simulations with finer mesh to be run within the time restraints of the project. Based on the test, seen in figure 5.16, *frequency transient* simulations would have been slightly more accurate, but the margin of error was deemed acceptable given the other advantages of using constant material properties. Especially, the calibration of coil power, would have taken significantly longer using *frequency transient*, as it usually took around four times of changing the current to get within an acceptable range of the coil power in the given experiment, and for each change in current a simulation including at least one time step had to be run.

The CAD-model of the coil has an Ø22 cross sectional diameter. This diameter is based on a measurement of the induction cable used in the experiments. However, the Ø22 diameter includes the 1 mm thickness of the isolation layer in which the induction cable was wrapped. COMSOL runs its simulations with the assumption that the coil is made of solid copper with an Ø22 diameter. This differentiates from the actual cross-sectional geometry of the induction cable used in the experiments, which is not solid copper, has water running through it for cooling, and includes layers of thermal isolation and protection. This means that the distance between copper and plate is shorter in the simulations than in the experiments, which could be a small part of the reason that the simulations generally achieve higher temperatures than the experiments.

6.2.3 Validation of Model and Method of Comparison

A combined average temperature difference was calculated between the cut lines from the experiments and simulations. This combined average temperature difference was used as a generalisation of the accuracy of the model. This number can not be used to predict what the temperatures of a future simulation is going to be, but can generally predict that a future simulation is going to be hotter than reality by some degree. The individual differences were calculated as well, which can give an indication of where the issues are in the

model. This is not conclusive, since only one experiment was conducted with 12.5 turns and in general a low number of experiments were conducted. The main focus of this validation was to see if what happened in the simulation compared to the experiment by comparing the temperatures of the cut lines. This method of comparison is not flawless since it only compares two different data sets. In the "single plate" validation, the cut line from the simulations went through the maximum temperature, where in the experiment the maximum temperature was a little above the cut line, due to flaws in the setup of the experiment. It could have lowered the average temperature differences of the "single plate" validation if all cut lines had been going through the maximum temperature. However, this would have worsened the credibility of the comparisons, as it would have utilised a source of error, to achieve temperatures closer to those of the simulation.

To get a more accurate validation of how well the model simulated the proximity effect, a comparison of the temperatures along the gap could have been made. This might have revealed a more evenly spread heat in the middle of the gap due to the lack of roughness in the gap of the simulation. This would have given a larger difference in the average temperature, but a more accurate validation.

6.3 Implementation of Model

The model created as a product of this project has the purpose of simulating a preheating situation and to give an estimation of the preheating duration and power consumption. It can therefore be helpful for companies wishing to restructure their production process, by replacing their current heat source with induction or optimise their existing induction heating solution. Additionally, the model could save a company the time and money it takes to conduct experiments with induction heating, by running a simulation instead, which could provide an estimate of how a given geometry would be heated.

The approach of constructing the model was to try to keep it simple both mathematically, so the model is verifiable and computable, and also possible to comprehend and visualise. This was done by splitting the model into the two steps: 3D and 2D. This method will be more imprecise than modelling it exclusively in 3D like the rotating cylinder on figure 5.26. For example, the 2D simulation does not take variable ambient temperature into account. This will occur when heating a large pipe like a monopile, where the inside temperature will rise while the outside will not.

The comparison of energy consumption, costs, and emissions is based on information provided by Bladt. This information only states how much gas is

consumed during the preheating process in general, not the ambient situation which this statement is correct in. The preheating model created in COMSOL assumes that the ambient temperature is 20 °C and no wind is present. If the temperatures in both situations are different, the comparison is not truly valid. However, this is easy to accommodate by altering the model in COMSOL. Furthermore, information on gas usage, target temperatures, and monopile diameters provided by Bladt were either values that vary depending on markets and Bladt's costumers, or estimates with few significant figures.

Although this model is a good indicator for how the heat is transferred in a circular weld, some limitations exist due to the assumptions made to make this model possible. This model is based on the previous models and the assumptions made for them applies for this model as well. Variables such as permeability found for S235 is assumed to be the same for S355, and that may give some margin of error.

7. Conclusion

The metal industry seek greener solutions to combat climate change and to become more attractive suppliers. In the case of Bladt Industries, an alternative is sought for the preheating of monopiles. Their current solution for preheating circular welds, gas burners, is neither environmentally friendly or energy efficient. Additionally the gas burners heat up the workshop, resulting in a warm work environment for the workers.

An FEM-model capable of simulating induction heating of a steel plate was setup in COMSOL Multiphysics. The FEM-model was validated by comparing simulations to experiments conducted using an induction cable and power supply at Bladt Industries. The experiments were conducted both on a single steel plate with varying distance between the coil and steel plate, and on two plates with varying gap distances, and lastly with a bigger coil geometry on two steel plates.

The temperatures of the simulations are on average 16.96 °C higher than the average temperatures of the three corresponding types of experiment setups. The differences span from 6.22 °C to 35.08 °C. All simulations reach higher average temperatures than the corresponding experiments. The "single plate" simulations are generally less accurate than the "two plate" simulations, while the simulation with a bigger coil geometry is the most accurate of the seven comparisons. Therefore the model might give a more accurate result in the final simulation of a larger weld geometry, however this is inconclusive since only one experiment was conducted with the large coil.

The comparisons made between simulations and experiments show that, while not spot on, partly due to not using variable material properties, the model can be used to give a good estimate of how quickly a given coil setup heats a steel object. Additionally, the model can be used to get an estimate of the energy efficiency of using induction heating as a preheating solution on circular welds.

Having validated the model, a simulation could be run on parameters corresponding to the preheating of circular welds at Bladt Industries. This included a plate thickness of 90 mm, the weld geometry and translational motion of the plate at one meter per minute. Having to simulate several rotations of the sizeable geometry of a monopile section, it was chosen to compute most of the simulation in 2D. As such, the simulation begins in 3D, simulating movement of the coil over the weld geometry. A temperature plane of the cross section of the plates at the end of the model farthest from the coil, where the influence of the electromagnetic field is minimal, is transferred to a 2D FEM-model. Here the conduction, convection and thermal radiation can be computed between each heat instance, which is applied as a cross sectional instantaneous heat input. This process happens repeatedly for three full revolutions until the plate reaches a temperature of at least 100 °C, measured 75 mm from the welding

gap, at any point on the circumference of the monopile. Three full revolutions equates to a preheating time of 75.4 minutes, which is 45 minutes quicker than the preheating duration when using gas burners.

	Energy consumption	Energy cost	CO₂e
Induction heating	2.91 $\frac{\text{kWh}}{\text{m}}$	3.14 $\frac{\text{DKK}}{\text{m}}$	0.360 $\frac{\text{kg CO}_2\text{e}}{\text{m}}$
Heating blanket	5.4 $\frac{\text{kWh}}{\text{m}}$	5.83 $\frac{\text{DKK}}{\text{m}}$	0.675 $\frac{\text{kg CO}_2\text{e}}{\text{m}}$
Gas heating	38.5 $\frac{\text{kWh}}{\text{m}}$	17.07 $\frac{\text{DKK}}{\text{m}}$	9.360 $\frac{\text{kg CO}_2\text{e}}{\text{m}}$

Table 7.1: Comparison of energy consumption, cost and CO₂e emissions of the different preheating methods.

From table 7.1 it is calculated that the energy consumption of gas heating is about 13 times higher than induction heating. The energy cost of gas heating is about 5 times higher than induction heating. The CO₂e emissions of gas heating is about 26 times that of induction heating. The energy consumption, energy cost and CO₂e emissions of induction heating, are all about 46% less compared to using heating blankets. The results should be interpreted as estimates, due to the margin of error in the model.

More accurate results would have been achieved using variable material properties. However, to run a simulation using variable material properties, the model would have to be built using the *frequency transient* study step, which computes the electromagnetic field distribution and heat transfer over time simultaneously, instead of each after the other. This increases the computational time by more than tenfold compared to using constant material properties. Because the computational time plays a role, both in the time available for this project, and in the potential future use of such an FEM-model, the constant material property model was chosen.

In conclusion, a model that simulates induction was built using COMSOL Multiphysics. This model was validated by conducting a series of experiments in collaboration with Bladt Industries. From this validation it was concluded that the margin of error in the model was acceptable. Because of this, the applications of the model were expanded to simulate the preheating of a larger steel plate resembling a section of a monopile. From this simulation, the energy consumption of induction preheating was compared with gas and resistance heating. The finds were that induction uses only 8% of the energy gas uses, and 54% of the energy used by resistance heating.

8. Further Perspectives

This chapter will discuss possible future work regarding the subject of this project, both in terms of further experimenting to get deeper knowledge of influencing parameters, and further development of the FEM-model. Finally how a possible product or solution could be implemented.

8.1 Experiments and Models

If further experiments and modelling were to be done, it could be promising to look at different coil geometries, the number of turns, the amount of coils. It could also be relevant to experiment with different thicknesses in the steel plates, in order to verify the models ability to simulate the induction heating of larger steel plates. If the setup of the experiment is altered, there would also be more data to validate the model, thereby increasing the accuracy of the model. This could also mean that the technology could be implemented in more applications than preheating, such as annealing.

Looking at the heated area, e.g. figure 5.25, it is clear that most of the energy is accumulated in and around the gap. To get a more even heat distribution a new coil geometry could be implemented. A rectangular flat coil or two small coils next to each other could possibly distribute the energy in a more efficient manner.

8.1.1 Preheating Model

The preheating model reaches the desired temperature after about 75 minutes using two induction coils. It would be interesting to see if this can be done even more efficiently, both in terms of time and energy. Decreasing the distance between the coil and the conductor, will increase the coils power, due to impedance matching in the power supply. The rotational speed of the monopile sections could be increased during the preheating process. This will hinder the spikes of high temperatures, as the heating curve will be more level. On the other hand, too fast of a rotation will cause too much cooling. To find the optimal rotation speed, the object, coil and power levels will have to be known. The model could also be used to optimise the number of coils around the monopile. These suggestions needs testing and experiments to validate them, and can lay ground for a future project.

The model itself could also be optimised to work using *frequency transient* instead of simulating in a *frequency domain* study. This would require a more powerful computer or significantly more time to compute these steps.

Another way to optimise the model is to include the heat input from the weld. This heat input would make further heating from induction less necessary.

When building this extended model, the weld would have to be taken into account, as the proximity effect would diminish after the first weld. Further additions could be to improve and verify the model with various ambient temperatures, humidity and forced convection due to wind.

8.2 Applications

Bladt Industries can not apply these results directly to the preheating of a circular weld. As it stands, there are no induction heating products designed for the scale of monopile sections. Instead, a new product would have to be designed specifically for the size of these cylinders, which would require a sizeable investment. Alternatively, a mounting system for the induction cable they currently own could be designed.

A new product could utilise an optimised power supply that would enable the possibility of using one or more coils depending on what is optimal. In future work, it could be interesting to compare one against two or more coils for use in the preheating process, to see which solution is most energy efficient, which solution would require the smallest investment, and which would be the easiest to utilise in the daily use for a company like Bladt. Along with this product, a mounting system could be developed that can hold the coil(s) in position along the monopile segments.

A problem with the power supply is that it makes a lot of noise when converting the AC power to a higher frequency. Therefore, an area of further development could be to design a silent setup. This would also make it more pleasant for the workers using the technology.

The comparisons of induction and heating blankets show induction heating consuming less energy for round, rotating monopiles. It could therefore be interesting to test whether induction could also be implemented to replace heating blankets in stationary situations.

This project has not taken the many other applications of induction heating into account, and which applications it is already being used in. Further work could be an analysis of the different applications, their efficiency and possible ways of implementing them.

9. Project Management

The group behind this project, consists of six individuals who have worked as a group to answer the statement of intent:

How is an FEM-model set up in COMSOL Multiphysics, which accurately simulates induction heating of steel plates with thick section weld geometries?

The group had no experience with FEM-simulation nor preheating a circular weld, hence everybody was at square one this August and it has been an interesting process of moving from complete beginners to having an understanding of FEM and preheating.

Management

The management of the group has been split evenly between the six members, this was done by taking turns in leading the group one week at a time. Knowing that every member had, more or less, the same base line in regards to knowledge of preheating thick section weld geometries, the leader's role was to keep the group moving forward. The leader's role was not as much to *lead* the group (necessarily) in the right direction, as much as to keep the group on track and progressing. Taking turns in leading, has helped to keep the members on an equal level, as well as developed leadership in every member. One downside of having a leader role, could be that less responsibility is felt by the individual when they are not the leader. Instead the individual places some of that responsibility on the current leader. For example, if the group is talking about something not relevant to the project, they may feel warranted to continue for a longer amount of time, as the responsibility of keeping the group on track is placed on the leader. However, due to different leading philosophies, the given leader did not always step in, instead leaving trust and responsibility in the group members' ability to keep productive. When everyone leaves the responsibility to someone else, it is suddenly nobody's responsibility. As such, the group could have benefited from a more direct definition on who the responsibility lies on - either on the leader, or on the individual member.

Log

In addition to this, the leader of the week kept a short log of what the group was working on each day. Having a designated leader at all times (regardless of the members taking turns) meant that "someone" took responsibility at all times. Besides the log, every member has noted their hours and activities throughout the project. This was done both to give the group an idea of how long each task has taken, to know the duration in the process, and to visualise to Bladt - or another interested party - how many hours have gone into making the model. The amount of time spent might seem like relatively much, as

the group members had to attain experience with COMSOL and Bladt's processes. A skilled engineer, with prior welding experience and knowledge of FEM-modelling may have spent significantly less time to obtain the same results. That being said, the whole point of the problem-based learning method at Aalborg University, is to learn and study programmes and subjects that might not be implemented in the standard courses - by meeting these real-life problems and scenarios. Spending time understanding a new technology, process or programme is therefore, in its own way, time well spent - despite many hours of studying without visual progress in the project.

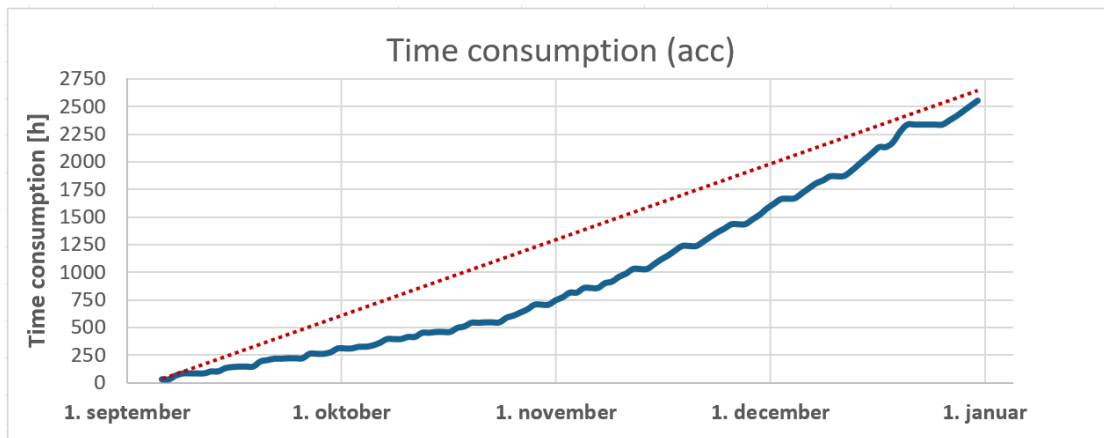


Figure 9.1: Spending a low amount of hours in the beginning of project and catching up in the last months of the project.

The hours spent were not evenly distributed across the semester due to the courses being placed in the beginning of the semester, see figure 9.1. The last two months were without courses and therefore the main part of the time was spent here. This has led to an eager to get fully into the project without distractions from other courses and hand-ins.

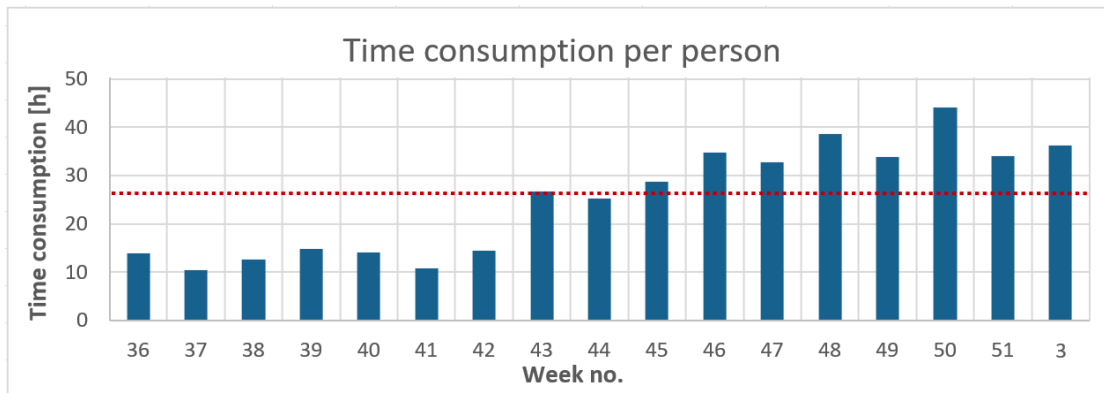


Figure 9.2: Hours per person per week. The red dotted line is minimum number of hours (27.7 hours) per week to reach 450 hours per person.

As seen on figure 9.2 the majority of hours was spent in the last half of the project, as mentioned due to courses.

Apart from providing a guideline to the group, the graph can also provide a guide to how much a project like this would cost to a company, as well as to give a detailed view of how the hours are spent. As earlier mentioned some hours have gone into getting familiar with new software and processing methods (manufacturing of monopiles). Therefore, the amount of hours cannot simply be multiplied by the salary per hour of an engineer to get a price of the project.

In an upcoming project, the hours registered as *Writing* in the following graph (figure 9.3) should be distributed to the actual chapter it was spent on. Unfortunately this was not done in this project. However the graph still provides an outline of how the hours were spent.

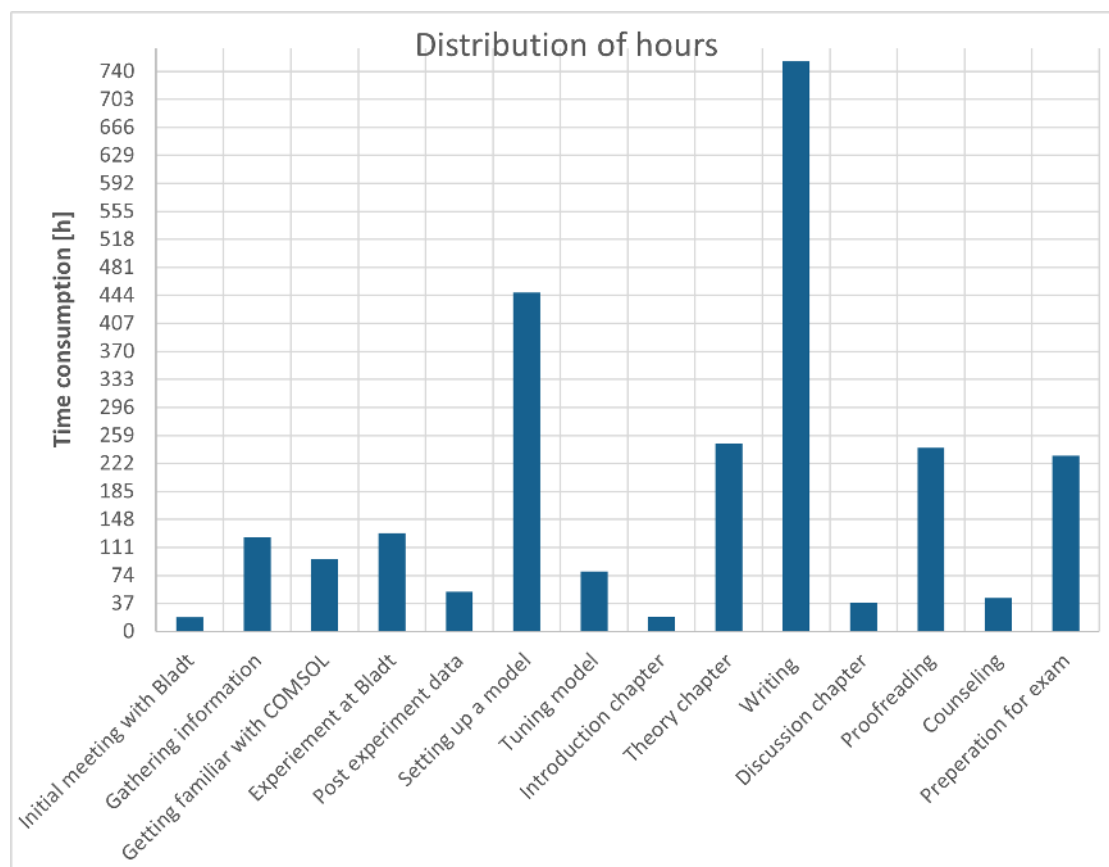


Figure 9.3: How hours were distributed across this paper. On the y-axis each interval is one working week.

The hours in figure 9.3 adds up to 96% of the total amount of hours spent, the last 4% were spent on miscellaneous tasks. The total amount of hours spent accumulates to 2634 hours, which is 439 hours per person ($\frac{2634\text{ h}}{6\text{ person}} = 439 \frac{\text{h}}{\text{person}}$). This is 11.9 weeks per person solely spent on the project, including four days of preparation for exam as well as one day of exam. Outside of the project, time have been spent on courses and homework, which justifies the amount of hours spent on the project per week.

Group Structure and Dynamics

The group was combined of two halves of prior groups which meant that the dynamics of the two had to be adjusted to one another. This was initially done by conducting a set of mutual rules that every member agreed on. The first three statements in the rules are as follows:

- *Every member is on time and well prepared*
- *Every member has to give constructive criticism*
- *It is expected by the group, that the hours put into the project corresponds to 15 ECTS (which is 450 hours per person)*

The rules of the group are based on trust and the members have lived up to this responsibility. It has therefore not been necessary to bring this contract into play. It may also be noted that all the rules are not easily measured, but are more a desired attitude of each member.

In addition to the rules of the group, it was decided that the project should be written in English. As none of the members have English as their first language, this has been a challenge in the beginning of the process. However, it is safe to say that every member has adopted to writing in English and has the idea that this project could not have been written as well in Danish.

If the desired amount of hours (450 hours) and the actual amount (375 hours) are compared, it is clear that this goal is not entirely obtained. This is no surprise as calculations have been done to get an estimate of the hours spent. However, there will be some work after the hand-in which is not accommodated for in this calculation.

COVID-19 and Group Effectivity

As much as we would like *not* to address this issue, it is necessary and has affected this project. Apart from the obvious impacts that everyone has experienced, the group has been directly affected by COVID-19. On several occasions the group has worked from home via MS Teams, lastly were the two weeks before hand-in solely online due to COVID-19. This has had some negative consequences on the group work. If one positive thing is to be mentioned as a consequence of COVID-19 and working from home, it must be that the members have not disturbed each other as much as we would have on campus.

On that note it may be mentioned that the group has had a nice and relaxed relationship, where it sometimes has been a bit too relaxed and fun, in these instances the leader has (in most cases) stepped in and guided the group back on track.

Summary

It has been a common understanding that each member was allowed to be heard and everyone has always had the opportunity to bring questions and express criticism in a proper and constructive manner. This has led to a safe learning space where every member feels confident to speak out.

It was prioritised to do social activities outside working hours. Most members have participated in these activities, some more than others. If the whole group could have been gathered at social events more often, it may have influenced the group in positive way, which may have led to an even better functioning group. However the group has been working well as a team and has not had major difficulties.

Bibliography

- [1] Ian Tiseo. *Global historical CO₂ emissions from fossil fuels and industry 1750-2020*.
<https://www.statista.com/statistics/264699/worldwide-co2-emissions/>
Sidst besøgt 13-10-2021.
- [2] iea.org. *Offshore Wind Outlook 2019*.
<https://www.iea.org/reports/offshore-wind-outlook-2019>
Sidst besøgt 20-12-2021.
- [3] International Energy Agency. *Renewables 2020*.
<https://www.iea.org/reports/renewables-2020/wind>
Sidst besøgt 13-10-2021.
- [4] International Energy Agency. *Offshore wind outlook*.
<https://iea.blob.core.windows.net/assets/2e7ec2d6-7cf1-4636-b92c-046ae16f4448/OffshoreWind-Launch-Presentation1.pdf>
Sidst besøgt 13-10-2021.
- [5] Madhumitha Jaganmohan. *Worldwide capacity of offshore wind power 2009-2020*.
<https://www.statista.com/statistics/476327/global-capacity-of-offshore-wind-energy/>
Sidst besøgt 18-10-2021.
- [6] Carol S. Lenox Morgan S. Browning. "Contribution of offshore wind to the power grid: U.S. air quality implications". In: *Elsevier* 276.115474 (2020), pp. 1–5. doi: <https://doi.org/10.1016/j.apenergy.2020.115474>.
- [7] Bladt Industries. *About Bladt*.
<https://www.bladt.dk/about-bladt.aspx>
Sidst besøgt 30-09-2021.
- [8] Bladt Industries. *Offshore Fundamenter*.
<https://www.bladt.dk/galleri/offshore-fundamenter.aspx>
Sidst besøgt 20-10-2021.
- [9] Steelwind Nordenham. *Beyond XXL Slim Monopiles for Deep-Water Wind Farms*.
<https://www.offshorewind.biz/2020/05/11/beyond-xxl-slim-monopiles-for-deep-water-wind-farms/>
Sidst besøgt 30-09-2021.
- [10] Sindo Kou. *A criterion for cracking during solidification*. Acta Materialia, 2015, pp. 366–374. ISBN: 1359-6454.
- [11] Lippold John C. *Welding metallurgy and weldability*. Wiley, 2015 - 2015, pp. 213–254. ISBN: 1-118-96031-9.

BIBLIOGRAPHY

- [12] EUROPEAN STANDARD. *Welding Recommendations for welding of metallic materials Part 2: Arc welding of ferritic steels.* This British Standard, 2003, pp. 15–32.
- [13] Steven Klimowicz. *Hydrogen mitigation in submerged arc welding.* <https://ui.adsabs.harvard.edu/abs/2014PhDT.....5K/abstract> Sidst besøgt 29-10-2021.
- [14] Rob Colman. *Welding preheat practices: choose the right tool for your job.* <https://www.canadianmetalworking.com/canadianfabricatingandwelding/article/welding/welding-preheat-practices-choose-the-right-tool-for-your-job> Sidst besøgt 20-10-2021.
- [15] Aleksandr Aliferov Sergio Lupi Michele Forzan. *Induction and Direct Resistance Heating.* Springer, 2015, pp. 2–10. ISBN: 978-3-319-03478-2.
- [16] Energinet. *Miljøredegørelse 2020.* <https://energinet.dk/E1/Gron-el/Deklarationer> Sidst besøgt 20-10-2021.
- [17] Dr. Thomas Lauf. *Emissionsbilanz erneuerbarer Energieträger.* https://www.umweltbundesamt.de/sites/default/files/medien/1410/publikationen/2019-11-07_cc-37-2019_emissionsbilanz-erneuerbarer-energien_2018.pdf Sidst besøgt 14-12-2021.
- [18] CROFT PRODUCTIONS. *NATURAL GAS COMPOSITION.* <https://www.croftsystems.net/oil-gas-blog/natural-gas-composition/> Sidst besøgt 20-10-2021.
- [19] Energinet. *Gasdata.* <https://energinet.dk/Gas/Gasdata/Braendvaerdier> Sidst besøgt 27-10-2021.
- [20] Nis Hansen. *Mail correspondence.*
- [21] SEAS-NVE. *Gas Priser.* <https://seas-nve.dk/erhverv/naturgas/vejledende-og-historiske-naturgaspriser/> Sidst besøgt 23-11-2021.
- [22] Miller. *Miller web.* <https://www.millerwelds.com/> Sidst besøgt 23-11-2021.
- [23] Miller Electric Mfg. Co. *Weld Preheating and Stress Relieving.* <https://www.millerwelds.com/equipment/induction-heating/induction-heat-systems-m90100#!/?product-options-title=proheat-35-460-575-v-907689> Sidst besøgt 20-12-2021.

BIBLIOGRAPHY

- [24] MakeItFrom.com. *EN 1.0038 (S235JR) Non-Alloy Steel*.
<https://www.makeitfrom.com/material-properties/EN-1.0038-S235JR-Non-Alloy-Steel>
Sidst besøgt 9-12-2021.
- [25] Wayne Rowlands Raymond A Serway John W Jewett. *Physics for global scientists and engineers, Volume 1*. Cengage, 2017, pp. 588–607. ISBN: 9780170355513.
- [26] Philip Kosky. *Exploring Engineering*. Elsevier Inc., 2013, pp. 259–281. ISBN: 978-0-12-415891-7.
- [27] The Engineering ToolBox. *Emissivity Coefficient Materials*.
https://www.engineeringtoolbox.com/emissivity-coefficients-d_447.html
Sidst besøgt 25-10-2021.
- [28] Britannica. *Lenz's law*.
<https://www.britannica.com/science/Lenzs-law>
Sidst besøgt 1-12-2021.
- [29] Semiatin S. L. Zinn S. *Elements of Induction Heating : Design, Control, and Applications*. A S M International, 1988, pp. 9–10. ISBN: 9781615031986.
- [30] Raymond L. Cook Valery Rudnev Don Loveless. *Handbook of induction*. Taylor and Francis Group, 2017, pp. 55–61. ISBN: 978-1-1387-4874-3.
- [31] Raymond L. Cook Valery Rudnev Don Loveless. *Handbook of induction*. Taylor and Francis Group, 2017, p. 75. ISBN: 978-1-1387-4874-3.
- [32] matweb.com. *Ovako S355JR EN10025-2:2004 Steel*.
https://www.engineeringtoolbox.com/permeability-d_1923.html
Sidst besøgt 19-12-2021.
- [33] Raymond L. Cook Valery Rudnev Don Loveless. *Handbook of induction*. Taylor and Francis Group, 2017, pp. 53–55. ISBN: 978-1-1387-4874-3.
- [34] Lupi S. *Induction and Direct Resistance Heating*. Springer, 2015, pp. 8–10. ISBN: 978-3-319-03479-9.
- [35] Raymond L. Cook Valery Rudnev Don Loveless. *Handbook of induction*. Taylor and Francis Group, 2017, pp. 60–66. ISBN: 978-1-1387-4874-3.
- [36] Jiao. “Intensive Study of Skin Effect in Eddy Current Testing With Pancake Coil”. In: *IEEE Transactions on Magnetics* 53.7 (2017), pp. 1–8. DOI: 10.1109/TMAG.2017.2669181.
- [37] Raymond L. Cook Valery Rudnev Don Loveless. *Handbook of induction*. Taylor and Francis Group, 2017, pp. 66–69. ISBN: 978-1-1387-4874-3.
- [38] David J. Griffiths. *Introduction to electrodynamics*. Cambridge University Press, 2017, pp. 317–355. ISBN: 978-1-108-42041-9.

BIBLIOGRAPHY

- [39] Alexander Fufaev. *The 4 Maxwell's Equations: Important Basics You Need to Know.*
<https://en.universaldenker.org/lessons/11>
Sidst besøgt 23-11-2021.
- [40] Dennis G. Zill. *Advanced engineering mathematics*. Jones and Bartlett Learning, 2016, pp. 878–906. ISBN: 978-1-284-10590-2.
- [41] Hongbao Dong. Yao Zhao. Hua Yuan. Xiaocai Hu. Zhen Yang. "A Simplified Calculation Method of Heat SourceModel for Induction Heating". In: MDPI (2019), pp. 4–5. doi: 10.3390/ma12182938.
- [42] Raymond L. Cook Valery Rudnev Don Loveless. *Handbook of induction*. Taylor and Francis Group, 2017, pp. 103–111. ISBN: 978-1-387-4874-3.
- [43] Raymond L. Cook Valery Rudnev Don Loveless. *Handbook of induction*. Taylor and Francis Group, 2017, pp. 119–126. ISBN: 978-1-387-4874-3.
- [44] COMSOL Multiphysics 5.6. *Effective Nonlinear Magnetic Curves Calculator*.
https://www.comsol.com/model/download/732881/applications.effective_nonlinear_magnetic_curves.pdf
Sidst besøgt 29-11-2021.
- [45] Michael Flankl. "Electrodynamic Energy Harvesting from Moving Conductive Surfaces". In: ETH Zurich (2018), pp. 12–16. doi: <http://dx.doi.org/10.3929/ethz-b-000337918>.
- [46] Joostdevree.nl. *S355 European Standard Steel*.
https://www.joostdevree.nl/bouwkunde2/jpgs/staal_23_standaarden_s355_european_standard_steel.pdf
Sidst besøgt 1-12-2021.
- [47] matweb.com. *Ovako S355JR EN10025-2:2004 Steel*.
<http://www.matweb.com/search/datasheet.aspx?matguid=e4faa7b4b78745bd861741a3154e9e8e&ckck=1>
Sidst besøgt 16-12-2021.
- [48] Lupi S. *Induction and Direct Resistance Heating*. Springer, 2015, pp. 670–672. ISBN: 978-3-319-03479-9.
- [49] omega.com. *Temperature Measurement in Electromagnetic Environments*.
<https://www.omega.com/en-us/resources/temperature-measurement-in-electromagnetic-environments>
Sidst besøgt 15-12-2021.

Appendix

A. Meeting with Bladt 15-09-2021

The following are the notes from the initial meeting with Bladt Industries.

Møde med Bladt d. 15. september 2021

- Relativ lav forvarmning 50-100 grader celsius
 - Sikrer langsom afkøling → sikrer hydrogen kommer ud af fugen
- Hydrogenrevner → suger fugt til sig, hydrogenrevner er de yppigste fejl
- Øvre grænse, "inter-pas" temperatur, varmen slukkes/skrues ned ved øvre grænse
- Nis: "interessant med induktion, gas er ikke optimalt"
- Lindøværft med XL og XXL monopiles, 10,5 – 13 m i diameter
- Arbejder ikke med laser, kun pulversvejsning
- Op til 130 mm plader
- Nis: "evt hybrid, men pulver kan noget som laser ikke kan"
- Plader i forlængelse af hinanden, kaldet "loosing"
 - Forvarmes med elektriske bælter
- Termomekanisk stål (relativ koldvalset, ca 800 grader i stedet for 900)
- Kulstof 0,07%
- Fejlene ses ved ultralyd til sidst i processen
 - Slagge, indtrængningsfejl, centerrevner
- 500-800 mm/min (op til 1000 mm/min) både rundsvejsning og lige svejsning
- Varmtid med måtter, lige såm (ca to timer) rundsøm med gas (ca 1 time)
 - Kræver meget interaktion
- Svejsning 6-8 timer ved langsømme
- Fordel at pladen er varm udover lige i svejsesømmen
- Eftervarme er no-go, alt for dyrt. God teori, svært at efterprøve
- Vibrationsmod spændinger (rystelser)
- Gasopvarmning er et problem ved rundsøm, stort varmespild, bl.a. ved vedligeholdelsesvarme
- Bælter 2,7 kW
- Induktion 35 kW i stålet
- Frekvens er relevant: 13,7 kHz
- Kræver stor omlægning hvis temperatur over 200 grader
- Pris i indkøb og effektivitet, manglende erfaring med induktionsopvarmning
- Brænder 2 liter/kop
- Op til 35 svejsninger i samme såm

B. Experiment

Experiment journal from experiments performed at Bladt Industries the 3rd and 5th of November.

B.1 Purpose of Experiment

The purpose of the experiment is to compare COMSOL simulations to the data from the experiment. The results will be used to calibrate simulations. The simulation and experiment can be transferred to a full size monopile.

B.2 Approach

The experiments are conducted over two days at Bladt Industries. At day one the effect of the distance between two plates, and the distance between coil and plate is evaluated. At day two the focus is to see how edges affect the magnetic fields and temperature.

B.3 Equipment

B.3.1 Thermal Camera

The thermal camera used in the experiment is a Keysight U5850A Thermal Imager. Capable of measuring temperatures between 0 to 1200 °C. The camera was calibrated upon manufacturing the 1st of July 2015. The camera was tested the 8th of November 2021 against an oven at 250 °C were the camera showed 250 °C. See appendix F.

B.3.2 Thermocouples

Thermocouples are used to measure the exact surface temperature at different locations.

B.3.3 Induction Cable and Power Source

The induction heater in the experiment is a Miller ProHeat 35. The Miller ProHeat 35 is a water cooled induction heater, capable of heating subjects up to 788 °C.

B.3.4 Miscellaneous

Miscellaneous covers steel plates, cable ties, supports for various equipment.

B.3.5 Bill of Materials

Amount	Material
2	Steel plate. 1000 mm · 2000 mm · 2 mm
1	Thermal camera
1	Induction cable and power source
2	Supports
1	Plywood board, 1220 mm · 1220 mm · 12 mm
n	Cable ties
8	Thermocouples
n	Spacers (different thicknesses)

Table B.1: Bill of materials.

C. Experiments at Bladt

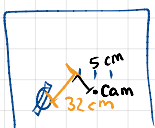
On the following pages, are the notes from the two days of experimenting at Bladt Industries.

Forsøg hos Bladt

0. forsøg - Vand OK

Afst. 42 mm ^(2x21 mm). Foto af spoledimensioner
Terhel har

T_{start}: 19.1 °C Cam
18.8 °C termopar
18 °C Miller



Test til 25 °C. (fordi Miller kum er indstillet til 70 °C)

Succes. Del opvarmes -

Terhel har foto.

- Varm ring
- Kold midte
- Ingen varme, hvor singel-kabel forlader spolen nedenom

1. forsøg

Afst. $2 \times 21 \text{ mm} = 42 \text{ mm}$

Nu er Miller sat til 200 °C

Venter til afkøling

Centrum

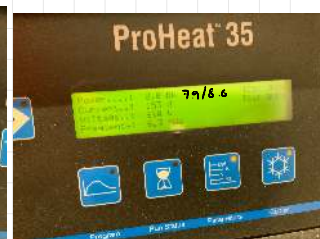
To : Cam 23.0 / 25.0 max (som er i ringen)
Par 24.02 °C
Miller 21 °C

Klokken 10:58



Effekt max 33-35, når den
ligger rigtigt (shal kunne afsætte
i stål). Ellers lavere

Sluk
v. max 200 °C



START

10:58

SLUT

11:05

7 min 20 sek

Termopar delvist mislykket

Plade arbejder ↑



SPOLEN

OBS! termocam kører
på sommertid
i dette forsøg

2. forsøg Skifter placé

Ny placé på plads.



Markeringer på gulv

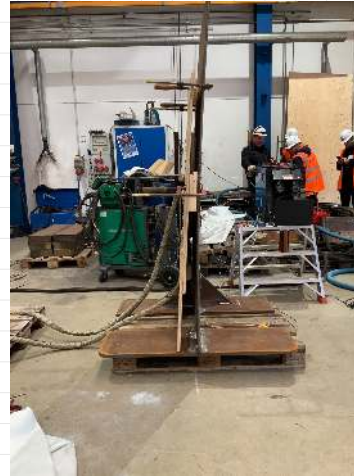
Afstand 47 mm (+6 mm)

T_{START} CAM 19,7 °C
PAR 18,7 °C
MILLER 18 °C



11:57 } 7 min 20 sek
↓
12:05 } (slut over 8 kW)
men intet foto...

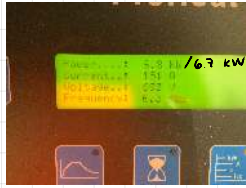
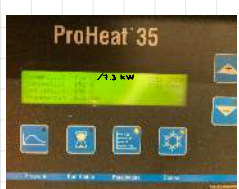
Inde forstør på T
forside og bagside



3. forsøg Ny placé, kølet med vand 15 mininden

Afstand øget: 53 mm

T_{START}: PAR — 22 °C
CAM — 23,0 °C
MILLER - 23°C



START
12:31

SLUT
12:40

10 m 13 sek



4. forsøg

Afstand: 70 mm
Luftkølet
Varmest
i midten

T_{START}: CAM - 25.6 °C
MILLER - 23 °C
PAR - 26.8 °C



Med kridt:

$50^{\circ}\text{C} = 1:16$

$75^{\circ}\text{C} =$

$150^{\circ}\text{C} = 160^{\circ}\text{C}$ (8:12 min)

$175^{\circ}\text{C} = 177^{\circ}\text{C}$ (9:08 min)

$200^{\circ}\text{C} = 226^{\circ}\text{C}$ (13:10 min)

Termopar grøn blev løs
- derfor ujægne målinger



10 min 57 sek

5. forsøg

Vandluulet
Derefter 20 min hvile indendørs

T_{START} ca. 16 °C

Afstand: 42 mm



KRIDT

95: 83 °C

150: 153 °C

200: 223 °C

9 min 8 sek
til 223 °C

6. forsøg

Afstand:

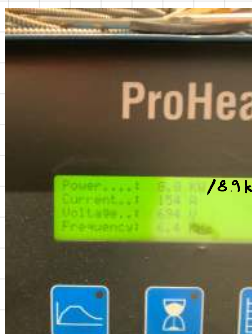
Vandluulet, hullet kørt

24 mm (ikke retsindes)
HELT TÆT

6 min 20 sek
til 200 °C cam

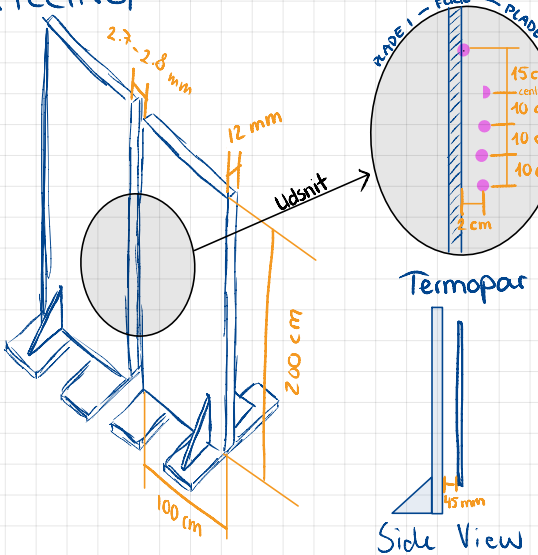
14:51

14:58



FORSØG DAG 2

OPSTILLING:



7. forsøg

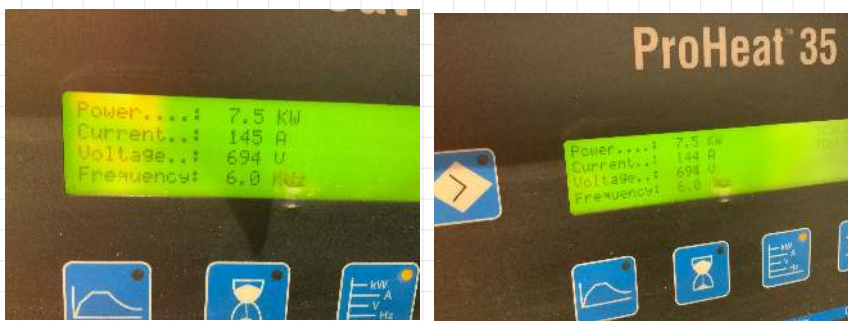
19.3 °C Cam

20.3 °C Par

21 °C Miller



$S_{\min} 57 \text{ sek til } T_{\max} = 300^\circ\text{C}$



8. ~~for~~ ~~s49~~

15.6 °C Par
16.3 °C Cam
16 °C Miller



Kl. 10:31

Kl. 10:35

Nedkøling
er optaget
indtil 50 °C

9. forsøg

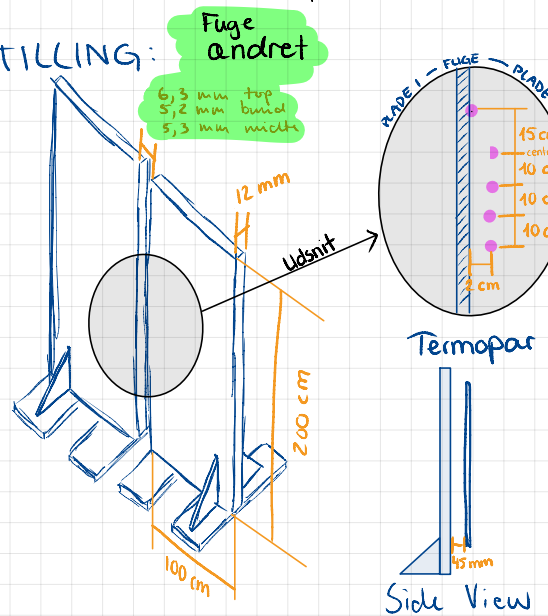
(Morten vejl. er her)

Samme afstand til spole

Lufthullet til 50 °C

Derefter Vandhullet og aftørret

OPSTILLING:



Tstart :

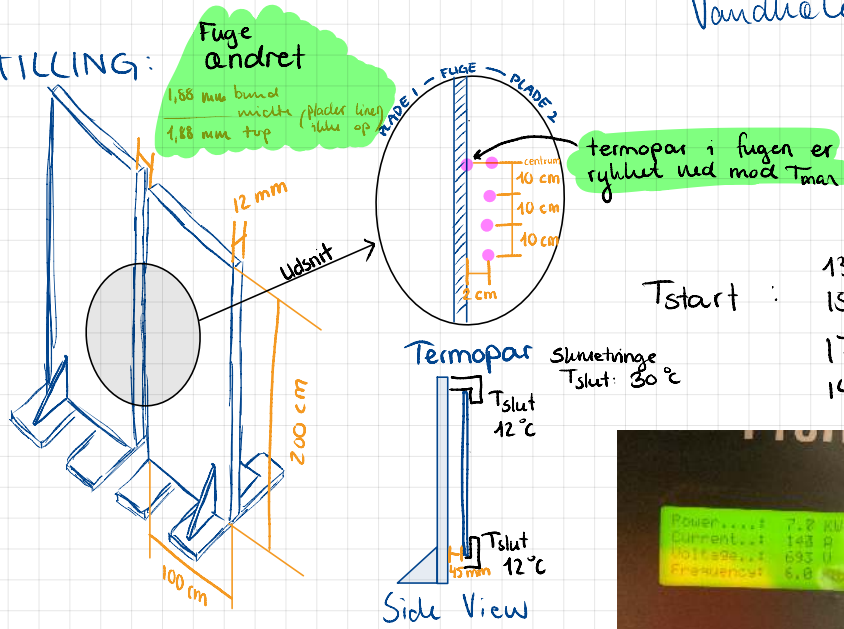
16,2 °C Cam
18,7 °C par
18 °C Miller



5 min 27 sek

10. forsøg

OPSTILLING:



Vandhullet til 8-12 °C

Tstart :

13,2 °C cam
15,1 °C par
17 °C Miller
14 °C Amran



12:24

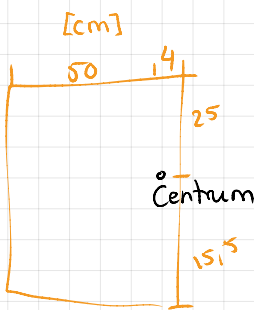


12:28

Luftholing - log under pause

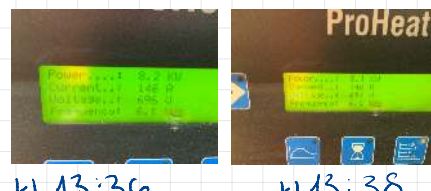
4 min 20 sek til 300 °C

11. forsøg Nærforsøg - samme afstand mellem plader som før uden yderligere hølning



Afstand på
kamera indstillet
til 3 meter

Tstart : Camera : 27 °C (max 28 °C)
Termopar : 27,6 °C (centrum på plader)
Miller : 24 °C



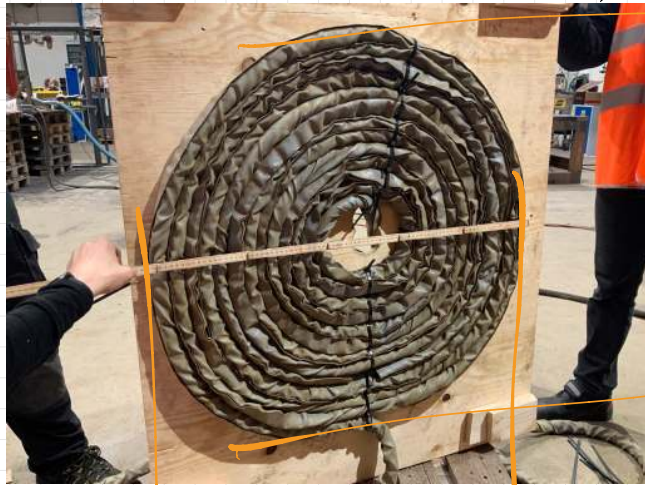
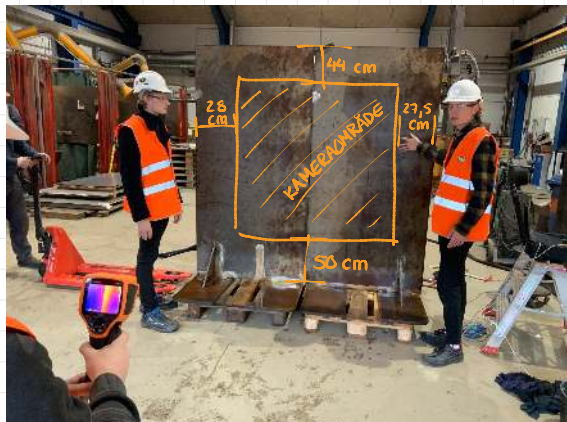
Varmeste sted på
kabel : 53 °C



12. forsøg Flere vindinger

Vandkolet

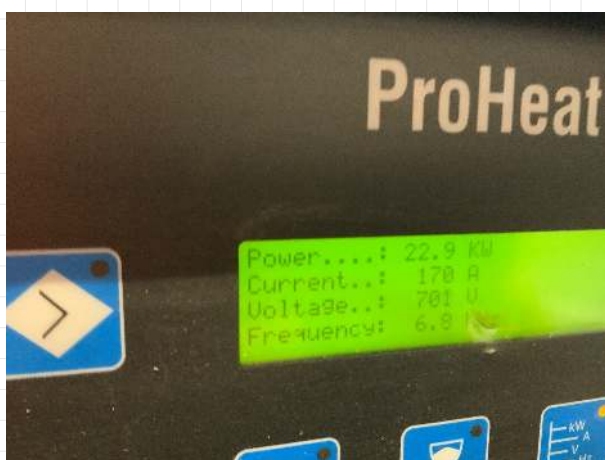
3 m kamera,
indstillet til 1 meter



85
cm

85
cm

Tstart : Cam : 14,2 °C centrum venstre
Miller : 17 °C



kl 14:07



kl 14:08

59 sek til 350 °C

13. forsøg

Færre vindinger
Afstand mellem plader (1 stk masonit / 2,5 mm)

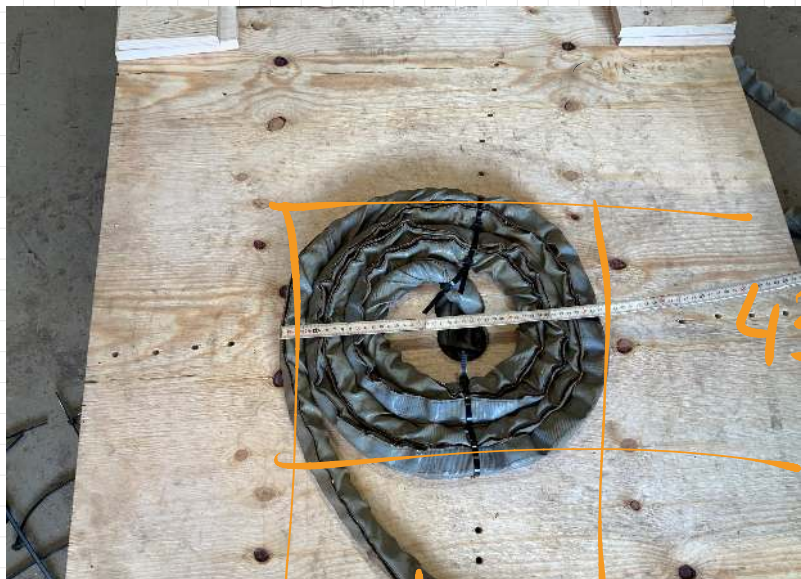
Afstand plade
spole:
43 mm

Vandmølet

Cam: 2 m, indstillet til 2 m



14,5 °C Cam
TSTART: Miller ej påsat



43 cm

Efterslæn
Værer
veget
denne gang



K1 14:21



14:28

7 min 24 sek

D. Ratio - from pixels to mm during experiments

A	B	C	D	E	F	G								
1		True Size	Camera	Aspect Ratio										
2		mm	Calculation*	px	Ratio [mm/px]	Calculation								
3														
4	Width	1447,80 =(200,28-27,5-28)*10		320	4,52 =C4/E4									
5	Height	1060,00 =(200-44-50)*10		240	4,42 =C5/E5									
		*Based on measurements from experiment 12 (see below). Gap: 28 mm. Distance to camera: 3 m		*Based on thermal photo properties below		<u>4,47</u> =AVERAGE(F4:F5)								
				<table border="1"> <tr> <td>Image</td></tr> <tr> <td>Image ID</td></tr> <tr> <td>Dimensions 320 x 240</td></tr> <tr> <td>Width 320 pixels</td></tr> <tr> <td>Height 240 pixels</td></tr> <tr> <td>Horizontal resolution 96 dpi</td></tr> <tr> <td>Vertical resolution 96 dpi</td></tr> <tr> <td>Bit depth 24</td></tr> <tr> <td>Compression JPEG</td></tr> </table>	Image	Image ID	Dimensions 320 x 240	Width 320 pixels	Height 240 pixels	Horizontal resolution 96 dpi	Vertical resolution 96 dpi	Bit depth 24	Compression JPEG	
Image														
Image ID														
Dimensions 320 x 240														
Width 320 pixels														
Height 240 pixels														
Horizontal resolution 96 dpi														
Vertical resolution 96 dpi														
Bit depth 24														
Compression JPEG														

Figure D.1: Excel-calculation of aspect ratio. Essential pictures included within.

E. Results

The data in the following two tables (table E.1 and table E.2) are loaded from the thermal camera, using *KeySight TrueIR Analysis and Reporting Tool*. The starting temperature of 30 °C is chosen to have an equal T₀ of all experiments. The steel plates were cooled between experiments, it was not possible to reach the exact same temperature each time due to the time available at Bladt. The power, current, voltage and frequency output was controlled by the Miller Proheat 35 and is varied accordingly to how much material available.

Variable	Experiment #	Power	Current	Voltage	Frequency	Distance wood-steel	Distance coil-steel	30 °C	200 °C	30 to 200 °C
Coil-steel distance	1	8 kW	154 A	695 V	6.4 kHz	41.7 mm	19.7 mm	photo 11.5	photo 72	423.5 sec
	2	8 kW	153 A	693 V	6.3 kHz	47 mm	25 mm	photo 4	photo 65	423.5 sec
	3	7.1 kW	152 A	693 V	6.3 kHz	53 mm	31 mm	photo 2	photo 87	595 sec
	4	6.8 kW	150 A	691 V	6.3 kHz	70 mm	48 mm	photo 8	photo 100	644 sec
	5	8.3 kW	153 A	695 V	6.3 kHz	42.3 mm	20.3 mm	photo 4.5	photo 65	423.5 sec
	6	9.5 kW	154 A	695 V	6.4 kHz	24 mm	2 mm	photo 1	photo 54	371 sec

Table E.1: Experiments from day one sorted after coil-steel distance.

Variable	Experiment #	Power	Current	Voltage	Frequency	Gap	Turns	30 °C	200 °C	300 °C	30 to 200 °C	30 to 300 °C
Gap	7	7.5 kW	145 A	694 V	6 kHz	2.8 mm	8.5	photo 1	photo 24	photo 51	161 sec	350 sec
	8	7.8 kW	146 A	694 V	6.1 kHz	2.8 mm	8.5	photo 0.5	photo 19	photo 41	129.5 sec	283.5 sec
	9	7.8 kW	147 A	694 V	6.1 kHz	5.6 mm	8.5	photo 1.5	photo 20	photo 43	129.5 sec	290.5 sec
	10	7.7 kW	144 A	693 V	6 kHz	1.88 mm	8.5	photo 1	photo 12	photo 30.5	77 sec	206.5 sec
Close ups	11	8.1 kW	146 A	696 V	6.1 kHz	1.88 mm	8.5	photo 0	photo 7.5	photo 20	52.5 sec	140 sec
Turns in coil	12	22.9 kW	170 A	701 V	6.8 kHz	2.8 mm	12.5	photo 0.2	photo 3.5	photo 7	23.1 sec	47.6 sec
	7	7.5 kW	145 A	694 V	6 kHz	2.8 mm	8.5	photo 1	photo 25	photo 51	168 sec	350 sec
	8	7.8 kW	146 A	694 V	6.1 kHz	2.8 mm	8.5	photo 0.5	photo 19	photo 41	129.5 sec	283.5 sec
	13	6.2 kW	200 A	673 V	8.5 kHz	2.8 mm	4.5	photo 5.5	photo 32	photo 65	185.5 sec	416.5 sec

Table E.2: Note that experiment #7 and #8 are used both in the experiment where the gap and turns are varied. as they use a number of coils between experiment #12 and #13 and have the same gap as #12 and #13.

F. Test of Thermal Camera

An oven was set to 250.0 °C and a small piece of iron, approximately 30 mm · 100 mm · 150 mm, was heated until it was warm throughout the entire plate. The thermal camera measured 249.8 °C, and was accepted as a valid thermometer.

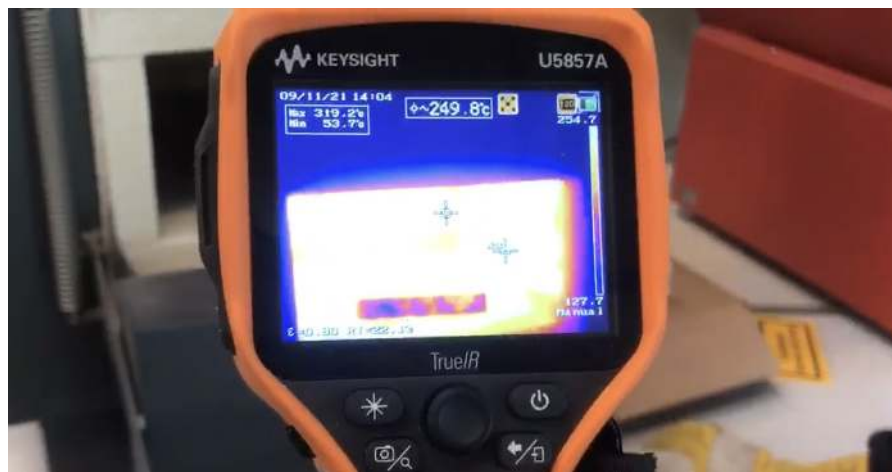


Figure F.1: Thermal camera measuring 249.8 °C.

The T_{\max} of 319.2 °C in the photo is the camera measuring the heater in the oven, which turns on as the oven door opens.

G. Progress of Simulations

This appendix shows the step-by-step progress of building a working method and accurate model. The group had no experience with COMSOL Multiphysics beforehand, and had only been briefly introduced to the Finite Element Method in the semester.

G.1 Introduction to COMSOL

As an introduction to COMSOL Multiphysics, the group completed some of the relevant tutorials included with COMSOL. Additionally, the group had a meeting with the supervisor where the group was shown an example on how to build a model.

G.2 Simple Heat Source Model

The group set up a model of a steel plate using the built-in materials. Using a *heat source boundary*, the plate was heated with no loss to the surroundings. The purpose was to simulate heat transfer and to see which power was necessary to keep the plate below 200 °C. Afterwards, a model was set up, with a high initial temperature to test the cooling of the plate, using a heat flux set up as convection and *surface-to-ambient radiation*.

G.3 Early Induction Heating Model

The next step was to build a model which could use both magnetic fields and heat transfer in solids, to simulate induction heating. A simple pancake coil with a square cross section was designed in SolidWorks and imported to COMSOL. A small steel plate and a surrounding air domain was built. The physics were set to magnetic fields, heat transfer in solids, and *electromagnetic heating* as the multiphysics. One of the first difficulties was to figure out which study steps would work with induction heating. The study step, *Coil Geometry Analysis* was most obvious, but for the frequency, there were a few different options, as you could either use *frequency transient* or frequency domain. First, it was attempted to combine frequency domain with the stationary study step, however this didn't work as there was no movement of the coil and no cooling physics in this early model. Instead, the frequency domain was combined with a time dependent study step.

The next issue appeared when defining the coil. When defining a coil in COMSOL, you pick an input boundary and an output boundary on the coil. However, it was not possible to choose the output boundary. It took a while before

the group found that you had to exactly line up the input and output boundaries of the coil, with a boundary of the air domain, before you were allowed to choose an output boundary. In order to line these boundaries up exactly, the *Remove Details* geometry function was used.

The next problems were to assign the physics, magnetic fields and heat transfer in solids and their dependants, to the right study steps, and to set up the *solver configurations*. After this, the first successful induction heating simulations were produced. However, since these were done before conducting experiments at Bladt, the model used the built-in material properties for steel, and the dimensions of the plate and coil were arbitrary.

G.4 Material Properties and Frequency Transient

After having done the experiments, the dimensions were updated to match the experiments. In COMSOL's 3D models it is not possible to define the power of the coil directly. Instead you have to define either the current or the voltage, which indirectly decides the power delivered to the coil, which you can evaluate in the derived values after running the frequency domain study step. This means that calibrating the power of the coil takes a while, because you have to run part of the simulation every time you change the current. Additionally the mesh of both the coil and plate influenced the power of the coil, which meant that you could not find a system as to which current resulted in a specific power.

The plates' material properties were manually set to those of S235. Finding the right material properties was one of the most difficult aspects of setting up the model. Constant parameters are relatively easy to find, but variables dependent on temperature or the magnetic field, like electrical resistivity and permeability, require more effort to set up correctly in COMSOL and sometimes required deeper theoretical knowledge. The electrical resistivity could be defined, using the *linearized resistivity* property group, where you define a reference electrical resistivity, a reference temperature, and a temperature coefficient. The most difficult material property was the relative permeability of S235. The relative permeability is entered as a constant, so instead a B-H curve was used, which varies with magnetic field strength and intensity. However, in the *frequency domain* it is necessary to use what is called an effective B-H curve which is essentially a B-H curve transformed to a parabola. To transform a B-H curve into an effective B-H curve, an application in COMSOL called '*effective nonlinear magnetic curves*' was used. When using these variable material properties it is necessary to use the *frequency transient* study step, which combines the frequency and time domains, such that the electromagnetic field and temperature changes can effect each other over time. This was not possible us-

ing the *frequency domain* and time dependent study steps, because these were computed separately, one after the other. It turned out that the *frequency transient* method with variable parameters, took far longer to compute, even when using a 64 core CPU with over 350 GB of memory. The group computed a couple of coarse mesh *frequency transient* simulations which were compared to equal simulations using constant material properties, which showed that the *frequency transient* model resulted in temperatures slightly closer to the experiments. However, the constant material parameter model gave a decent estimate, and could be computed with finer meshes, in far less time. As such, the group decided to continue, using constant material properties to save computational time, given the time restraints of the project.

G.5 Validation of Model

Now it was time to validate the model, by comparing simulations to the experiments. The group chose three experiments from the single plate experiments, three from the two-plate experiments, and one experiment with a larger coil diameter. The models were calibrated to match the conditions of the experiments and the results were compared to the data from the experiments to find the accuracy of the model. Some mesh improvements were made to get more accurate results while also saving computational time. The differences were analysed and potential sources of error were presented. The model was deemed to be within an acceptable range of the data from the experiments.

G.6 Circular Weld

With the model validated, it was time to apply the model to a circular weld. With all experience gained from the previous simulations, this model was made possible. It was decided that the easiest way, was to make the model in two steps. The first step was like all the other induction simulations, but with *translational motion* of the steel plates. The last step was in 2D and only contained heat transfer as the first simulations of simple heat flux. Because the last step was in 2D the computational process was short. Which meant there was a lot of time to test different approaches, like changing the amount of heat inputs (coils).

H. Geometry

On the following pages, are the reference of the geometry for the weld section.

Morten Klemmen Flyger Bach

Fra: Nis Hansen [REDACTED]
Sendt: 15. oktober 2021 14:08
Til: Terkel Føns Dyring
Cc: mp-21-mp-3-2024fib16; Soerensen, Christian Buhl (SGRE OF INO BOP); Morten Kristiansen
Emne: SV: Spørgsmål angående forvarmningsprojekt - 2.024 AAU

Hej Terkel m.fl.
Jeg **svarer** nedenfor.
God weekend.

Med venlig hilsen / Best Regards

Nis Hansen
Responsible Welding Engineer

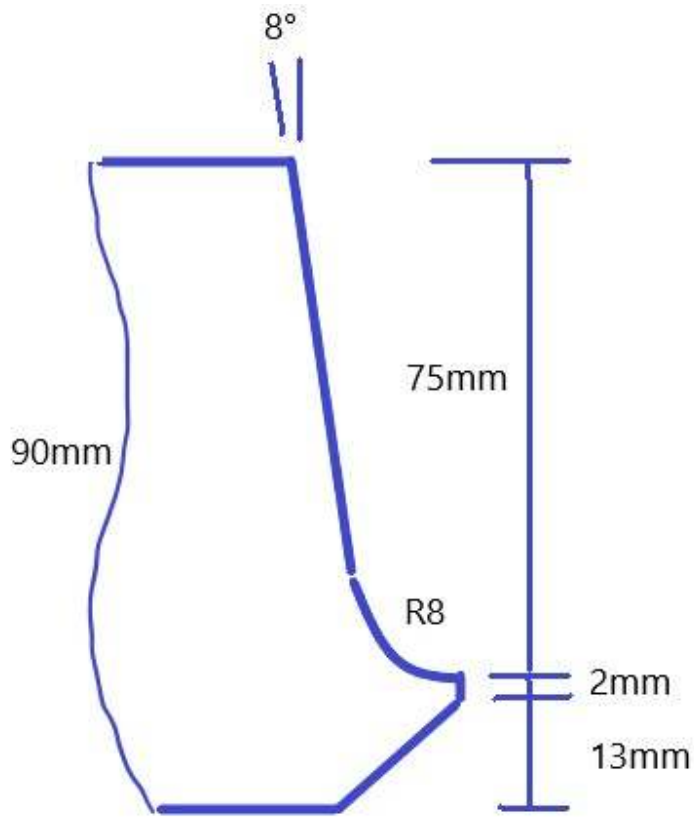


Fra: Terkel Føns Dyring [mailto:tdyrin20@student.aau.dk]
Sendt: 14. oktober 2021 12:55
Til: Nis Hansen [REDACTED]
Cc: mp-21-mp-3-2024fib16 <mp-21-mp-3-2024fib16@student.aau.dk>; Soerensen, Christian Buhl (SGRE OF INO BOP) <CHRISTIAN.SOERENSEN@siemensgamesa.com>; Morten Kristiansen <morten@mp.aau.dk>
Emne: Spørgsmål angående forvarmningsprojekt - 2.024 AAU

Hej Nis,

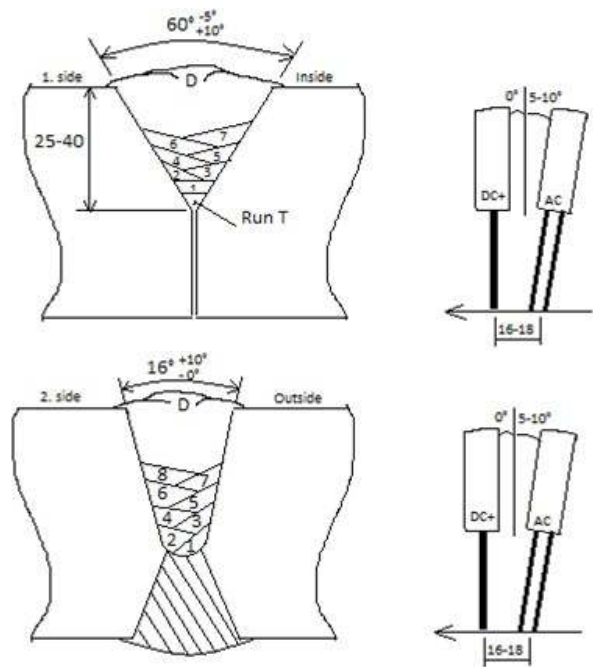
Vi er kommet godt i gang med projektet, derfor har vi nogle opfølgende spørgsmål og nogle data som vi ikke fik fat i sidst vi snakkede sammen.

- De 2.7 kW som varmetæpperne bruger under forvarmningen, er det for alle fire varmetæpper eller per varmetæppe? **De 2,7 kW er pr. varmebælte/tæppe**
- Med hvilke hastigheder roterer de forskellige rørsegmenter under svejsningen af rundsømmene? **800 – 1050mm/min**
- Hvor meget gas bruges under svejsningen af rundsømmet? **Propan eller naturgas**
- Hvilken ståltype anvender i mest? **S355NL/ML**
- En mere præcis geometri på den svejseudskæring i bruger . **Eksempel:**



Plus modpart, naturligvis. Dette er for langsømme.

Og for rundsømme:



- Den tilladte temperaturgradient for stålet. Vi antager, at vi maks. må komme på 650°C, dog kan der være lidt skrappere krav i nogle tilfælde, altså lavere, så som 550-600°C

Hvis det kan lade sig gøre vil vi sætte stor pris på datablade der omhandler jeres svejsning (mere præcist, de dateblade med fremgangsmåden for svejsningsprocessen, med antal svejsninger og skiftende hastigheder du viste til mødet d.15/9) og høre om det er noget vi gerne må inkludere i vores rapport som bilag.

Vi har selvfølgelig forståelse for, hvis det ikke er muligt at finde alle oplysningerne. **Vi kan nok finde noget. Kan vi tage dette senere?**

Vi arbejder på en forsøgsbeskrivelse, der snart vil blive sendt jeres vej. Har I en køreplade eller lignende, med en tykkelse på omkring 10 mm? **Må ikke vi kan skaffe noget 10-12mm plade – angive krav til dimension**

Hilsen,
Amran, Anders, Mads, Morten, Terkel og Viktor.
Gruppe 2.024, AAU

tdyrin20@student.aau.dk



I. Application of EN-1011-2

Step 1: Determine the the carbon equivalent value of the welded steel.

$$CE = C + \frac{Mn}{6} + \frac{Cr + Mo + V}{5} + \frac{Ni + Cu}{15} \quad (I.1)$$

Using this formula the CE value of S355 steel is calculated to 0.65%.

Step 2: Estimate the hydrogen class of the welding of the welding method. For submerged arc welding (SAW) using EM12K flux has a diffusible hydrogen content 3-5 ml and is rated as class D.

Step 3: Determine the weld geometry/type.

The weld geometry used to assemble monopiles is a butt weld. This has influence on the calculation of the combined thickness.

d_1 = average thickness over a length of 75 mm

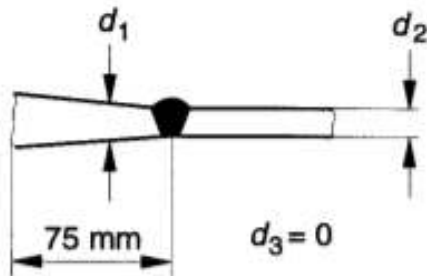


Figure I.1: Determination of combined thickness for butt weld [12].

$$\text{Combined thickness} = d_1 + d_2 + d_3 \quad (I.2)$$

Combined thickness for a two plates with a thickness of 90 mm is therefor 180 mm.

Step 4: Determine the heat input of the welding process.

$$\text{Heat input} = \frac{60 \cdot I U}{\text{Weld speed}} \quad (I.3)$$

Step 5: Read on figure I.2 the correct preheating temperature.

Different heat inputs is shown along the X axis i n $\frac{\text{kJ}}{\text{mm}}$ and the combined thickness along the Y axis in mm.

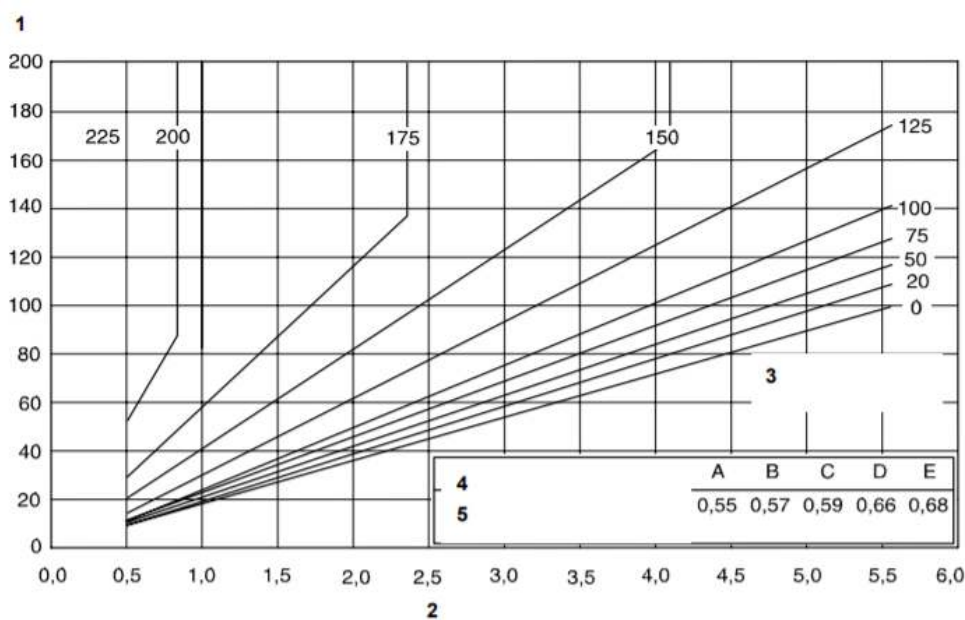


Figure I.2: Conditions for welding steels with defined carbon equivalents [12].

Keys for figure I.2

1. Combined thickness [mm]
2. Heat input [kJ/mm]
3. Minimum preheating temperature [°C]
4. Hydrogen scale
5. Carbon equivalent

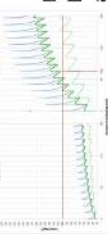
J. Maximum Temperature Under Coil

On the following page, the Excel-sheets used to estimate the maximum temperature under the coil during the sixth heating instance are attached.

from 3D simulation

All other max temps are extracted from 2D simulation									
Heat instance #	Below coil	Slice	t_{min}	T_{max}	$+1\ min$	$+2\ min$	$+3\ min$	$+4\ min$	$+5\ min$
1 -1.00	172,81	0,00	112,34	1,00	82,26	2,00	71,89	3,00	65,89
2 11,57	12,57	138,51	13,57	107,43	14,57	96,18	15,57	89,27	16,57
3 24,13	25,13	156,85	26,13	125,20	27,13	113,56	28,13	101,13	30,13
4 36,70	37,70	171,04	38,70	139,08	39,70	127,38	40,70	119,56	41,70
5 49,27	50,27	182,95	51,27	150,66	52,27	130,70	53,27	110,70	54,27
6 61,83	62,83	192,87	63,83	160,36	64,83	148,37	65,83	140,13	66,83
7 74,40	75,40	201,13	76,40	168,54	77,40	156,45	78,40	148,12	79,40
8 86,97	87,97	208,31	88,97	175,58	89,97	163,38	90,97	154,99	91,97
9 99,53	100,53	214,52	101,53	181,67	102,53	169,39	103,53	160,95	104,53
10 112,10	113,10	219,83	114,10	186,95	115,10	186,95	116,10	166,13	117,10

Estimated maximum temperature below coil after heating instance no. 6 (3 rounds). This round finishes after 75,4 minutes at t=74,4 min



Local maximums (temp) in slice (blue line) from this figure:

Delta temperatures:

Heat instance #	Below coil	Slice	t_{min}	T_{max}	$+1\ min$	$+2\ min$	$+3\ min$	$+4\ min$	$+5\ min$
1 -1,00	1,00	-60,47	1,00	30,08	2,00	-10,36	3,00	-6,01	5,00
2 11,57	13,57	-3,07	13,57	112,25	14,57	-11,25	15,57	-6,92	4,38
3 24,13	25,13	-31,65	27,13	-11,54	28,13	-7,46	29,13	-5,07	3,13
4 36,70	37,70	-31,96	39,70	-11,70	40,70	-7,82	41,70	-5,17	4,26
5 49,27	50,27	-32,30	52,27	-11,84	53,27	-8,11	54,27	-5,25	5,27
6 61,83	62,83	-32,51	63,83	-11,98	64,83	-8,25	65,83	-5,39	6,73
7 74,40	75,40	-32,59	76,40	-12,09	77,40	-8,33	78,40	-5,51	6,86
8 86,97	87,97	-32,73	88,97	-12,19	89,97	-8,39	90,97	-5,61	6,97
9 99,53	100,53	-32,85	101,53	-12,27	102,53	-12,27	103,53	-5,70	6,06
10 112,10	113,10	-32,88	114,10	-12,33	115,10	-12,33	116,10	-8,49	6,14

Local maximums (temp) in slice (blue line) from this figure:

Delta temperatures:

Heat instance #	Below coil	Slice	t_{min}	T_{max}	$+1\ min$	$+2\ min$	$+3\ min$	$+4\ min$	$+5\ min$
1 -1,00	1,00	12,389,095,63	12,389,095,63	=AFRUNDISD2	=AFRUNDISD2	=AFRUNDISD2	=AFRUNDISD2	=AFRUNDISD2	=AFRUNDISD2
2 11,57	13,57	110,912,61,198	112,389,095,63	=AFRUNDISD4	=AFRUNDISD4	=AFRUNDISD4	=AFRUNDISD4	=AFRUNDISD4	=AFRUNDISD4
3 24,13	25,13	125,679,999,99	138,508,170,981	=AFRUNDISD5	=AFRUNDISD5	=AFRUNDISD5	=AFRUNDISD5	=AFRUNDISD5	=AFRUNDISD5
4 36,70	37,70	125,134	125,134	=AFRUNDISD6	=AFRUNDISD6	=AFRUNDISD6	=AFRUNDISD6	=AFRUNDISD6	=AFRUNDISD6
5 49,27	50,27	125,851,115,40	126,851,115,40	=AFRUNDISD7	=AFRUNDISD7	=AFRUNDISD7	=AFRUNDISD7	=AFRUNDISD7	=AFRUNDISD7
6 61,83	62,83	127,058,156,60	127,058,156,60	=AFRUNDISD8	=AFRUNDISD8	=AFRUNDISD8	=AFRUNDISD8	=AFRUNDISD8	=AFRUNDISD8
7 74,40	75,40	127,598,182,95	128,510,060,58	=AFRUNDISD9	=AFRUNDISD9	=AFRUNDISD9	=AFRUNDISD9	=AFRUNDISD9	=AFRUNDISD9
8 86,97	87,97	128,036,42,68	128,036,42,68	=AFRUNDISD10	=AFRUNDISD10	=AFRUNDISD10	=AFRUNDISD10	=AFRUNDISD10	=AFRUNDISD10
9 99,53	100,53	128,532,10,52	128,532,10,52	=AFRUNDISD11	=AFRUNDISD11	=AFRUNDISD11	=AFRUNDISD11	=AFRUNDISD11	=AFRUNDISD11
10 112,10	113,10	128,096,21,61	128,096,21,61	=AFRUNDISD12	=AFRUNDISD12	=AFRUNDISD12	=AFRUNDISD12	=AFRUNDISD12	=AFRUNDISD12

Local maximums (temp) in slice (blue line) from this figure:

Delta temperatures:

Heat instance #	Below coil	Slice	t_{min}	T_{max}	$+1\ min$	$+2\ min$	$+3\ min$	$+4\ min$	$+5\ min$
1 -1,00	1,00	12,389,095,63	12,389,095,63	=AFRUNDISD2	=AFRUNDISD2	=AFRUNDISD2	=AFRUNDISD2	=AFRUNDISD2	=AFRUNDISD2
2 11,57	13,57	110,912,61,198	112,389,095,63	=AFRUNDISD4	=AFRUNDISD4	=AFRUNDISD4	=AFRUNDISD4	=AFRUNDISD4	=AFRUNDISD4
3 24,13	25,13	125,679,999,99	138,508,170,981	=AFRUNDISD5	=AFRUNDISD5	=AFRUNDISD5	=AFRUNDISD5	=AFRUNDISD5	=AFRUNDISD5
4 36,70	37,70	125,134	125,134	=AFRUNDISD6	=AFRUNDISD6	=AFRUNDISD6	=AFRUNDISD6	=AFRUNDISD6	=AFRUNDISD6
5 49,27	50,27	125,851,115,40	126,851,115,40	=AFRUNDISD7	=AFRUNDISD7	=AFRUNDISD7	=AFRUNDISD7	=AFRUNDISD7	=AFRUNDISD7
6 61,83	62,83	127,058,156,60	127,058,156,60	=AFRUNDISD8	=AFRUNDISD8	=AFRUNDISD8	=AFRUNDISD8	=AFRUNDISD8	=AFRUNDISD8
7 74,40	75,40	127,598,182,95	128,510,060,58	=AFRUNDISD9	=AFRUNDISD9	=AFRUNDISD9	=AFRUNDISD9	=AFRUNDISD9	=AFRUNDISD9
8 86,97	87,97	128,036,42,68	128,036,42,68	=AFRUNDISD10	=AFRUNDISD10	=AFRUNDISD10	=AFRUNDISD10	=AFRUNDISD10	=AFRUNDISD10
9 99,53	100,53	128,532,10,52	128,532,10,52	=AFRUNDISD11	=AFRUNDISD11	=AFRUNDISD11	=AFRUNDISD11	=AFRUNDISD11	=AFRUNDISD11
10 112,10	113,10	128,096,21,61	128,096,21,61	=AFRUNDISD12	=AFRUNDISD12	=AFRUNDISD12	=AFRUNDISD12	=AFRUNDISD12	=AFRUNDISD12

Local maximums (temp) in slice (blue line) from this figure:

Delta temperatures:

Methods and Formulas:

Heat instance #

Below coil	T_{max}	Slice	t_{min}	T_{max}	$+1\ min$	$+2\ min$	$+3\ min$	$+4\ min$	$+5\ min$
t, min	t_{min}								
#									

Local maximums (temp) in slice (blue line) from this figure:

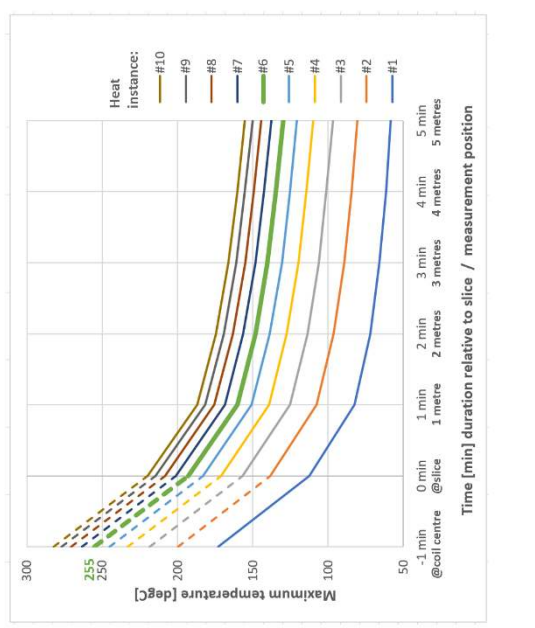
Delta temperatures:

Heat instance #

Below coil	T_{max}	Slice	t_{min}	T_{max}	$+1\ min$	$+2\ min$	$+3\ min$	$+4\ min$	$+5\ min$
t, min	t_{min}								
#									

Local maximums (temp) in slice (blue line) from this figure:

Delta temperatures:



Estimated maximum temperature below coil after heating instance no. 6 (3 rounds). This round finishes after 75,4 minutes at t=74,4 min

ESTIMATED VALUES

Every other value comes from simulation: 2x 12.5 coils

HEATING INSTANCE

Heat instance #

K. Figure 5.32 Full Size

